N,N'-Dimethylsquaramide as a central scaffold for anionophore design

Daniel A. McNaughton,[a] Edward York,[a] Tristan Rawling,[a] and Philip A. Gale.[a*]

[a.] *School of Mathematical and Physical Sciences, Faculty of Science, University of Technology Sydney, Sydney, NSW 2007, Australia*

* E-mail: philip.gale@uts.edu.au

Contents

1. General Remarks

Unless stated otherwise, all chemicals and solvents were purchased from commercial suppliers and used without further purification. Deuterated solvents for NMR were purchased from Cambridge Isotope Laboratories. 1-Palmitoyl-2-oleoyl-*sn*-*glycero*-3-phosphocholine (POPC) was purchased from Avanti Lipids or Corden Pharma. Anhydrous solvents were collected from an Inert Corp PureSolv MD7 solvent purification system. Deionised water was collected from a Merck Millipore Milli-Q™ reference ultrapure water purification system.

NMR spectra (^{1}H NMR, ^{13}C NMR and 2D NOESY NMR) were collected on a Bruker AVIII 500 or a Bruker Avance DPX 400. NMR titrations were performed on a Bruker Avance DPX 400. Chemical shifts (δ) were reported in ppm and calibrated using the residual solvent peak of either DMSO-d_6 or chloroform-*d*. Data was reported with spin multiplicities abbreviated to s = singlet, d = doublet, t = triplet, q = quartet, m = multiplet and br = broad, coupling constant J in Hz, and the relative integral.

Low-resolution mass spectrometry (LR-MS) was performed with a Bruker Amazon SL mass spectrometer using electrospray ionisation or APCI. High-resolution mass spectra (HR-MS) were recorded on a Bruker Apex II Fourier Transform Ion Cyclotron Resonance (FTICR) mass spectrometer with a 7.0 T magnet, fitted with an off-axis analytic electrospray source with quadrupole mass analyser, and are reported as m/z (relative intensity).

The ISE assay experiments were conducted on the Fisherbrand™ Accumet™ Chloride Combination Electrode, and HPTS transport data was collected on an Agilent Cary Eclipse Fluorescence Spectrophotometer equipped with a temperature-controlled multicell holder (25 °C). MTS assay absorbance was measured using a Tecan Infinite M1000 Pro plate reader (CellTiter 96 Aqueous Non-Radioactive Cell Proliferation Assay, Promega).

2. Synthetic Overview

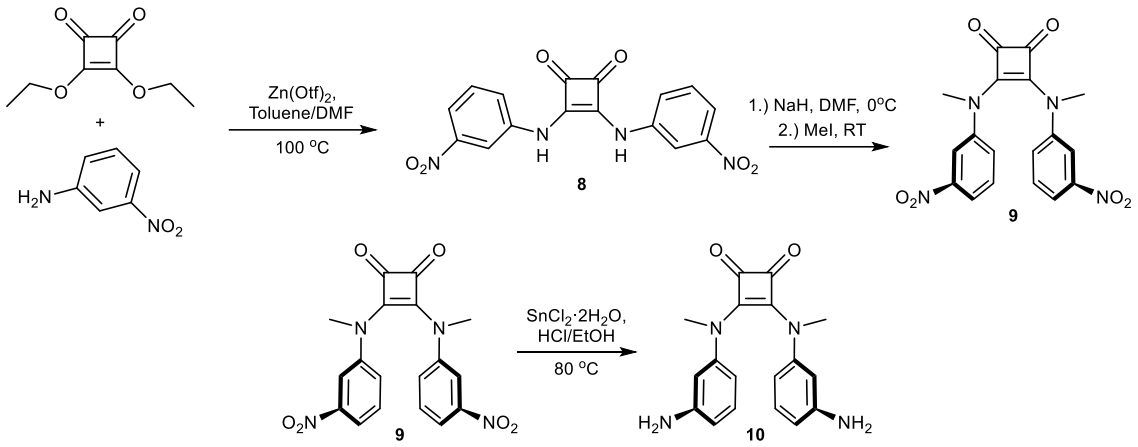

Scheme S1. The synthetic pathway to diamino intermediate compound **10** inspired by Arimura *et. al.*, with alterations.[1]

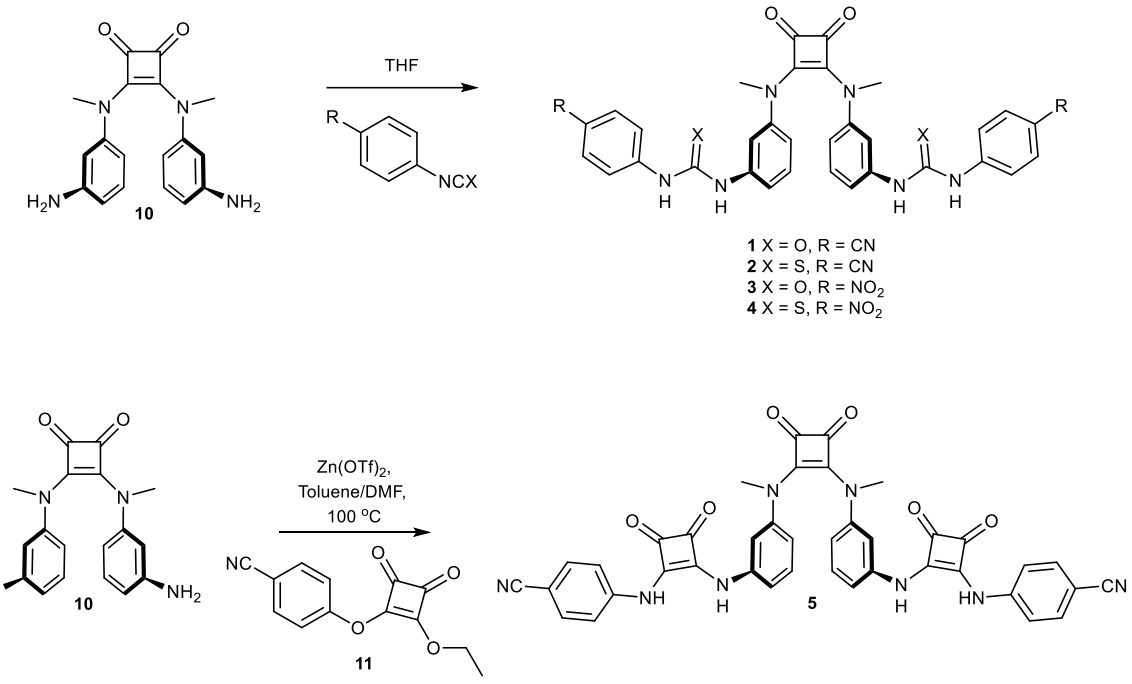

Scheme S2. The general synthesis of bis-(thio)urea compounds **1**–**4** and bis-squaramide compound **5**.

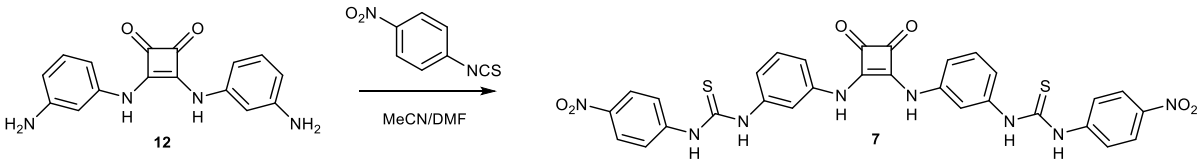

Scheme S3. The synthesis of compound **7** from compound **12**.

3. Synthesis

N-(3-nitrophenyl)squaramide (8)

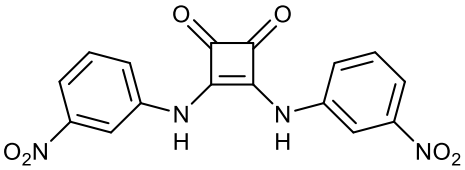

m-nitroaniline (2000 mg, 14.5 mmol) and zinc trifluoromethanesulfonate (877 mg, 2.42 mmol) were dissolved in a mixture of toluene (9.5 mL) and DMF (0.5 mL) before 3,4-diethoxy-3-cyclobutene-1,2-dione (0.65 mL, 4.35 mmol) was added dropwise to the solution. This was heated to 100 °C and left to stir for 3 d. A precipitate formed, which was collected upon cooling and filtered. The precipitate was subsequently washed with DCM (2 x 35 mL) and MeOH (2 x 35 mL) to yield a bright yellow solid (1400 mg, 3.95 mmol, 91%).

^{1}H NMR (400 MHz, DMSO-d_6) δ ppm 10.36 (2 H, b), 8.37 (2 H, s), 7.90 (2 H, d, J 8.1), 7.79 (2 H, d, J 8.1), 7.64 (2 H, t, J 8.2).

LR-MS (ESI$^+$) *m/z* 377.1 [M+Na]$^+$, (ESI$^-$) *m/z* 353.03 [M−H]$^-$

N-(3-nitrophenyl)-*N'*-(methyl)squaramide (9)

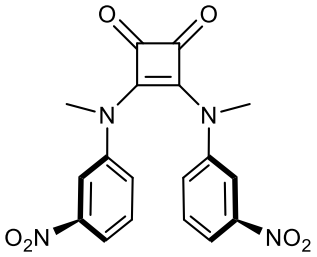

Sodium hydride (60 %, 200 mg, 5 mmol, washed twice with hexane) was suspended in dry DMF (3 mL). This was added dropwise and slowly to a solution of compound **8** (800 mg, 2.26 mmol) dissolved in dry DMF (10 mL), which had been cooled to 0 °C. This was allowed to warm to room temperature and stirred for 10 min before iodomethane (2.5 mL) was added dropwise. The reaction mixture was stirred at RT for 1 d before being poured into an aqueous solution saturated with ammonium chloride. The precipitate was collected by vacuum filtration and washed with methanol to yield compound **9** (580 mg, 1.51 mmol, 67%).

^{1}H NMR (400 MHz, DMSO-d_6) δ ppm 7.62 (2 H, dd, J 6.4, J 2.4), 7.56 (2 H, s), 7.30 (4 H, m), 3.69 (6 H, s)

LR-MS (ESI$^+$) *m/z* 405.07 [M+Na]$^+$.

N-(3-aminophenyl)-*N'*-(methyl)squaramide (10)

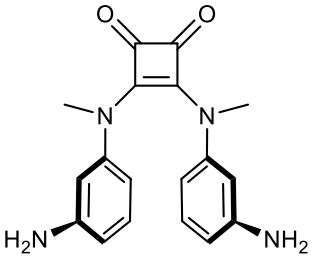

Tin(II) chloride dihydrate (5 g, 22 mmol) was added to conc. HCl (32%, 15 ml) and left to stir for 10 min. Next, compound **9** (800 mg, 2.09 mmol) was added portion-wise, followed by 5 mL of conc. HCl to wash compound off the sides. This was stirred at 50 °C for 1 h before 24 mL of EtOH was added, and the temperature increased to 80 °C. The mixture was stirred for 3 h before the EtOH was removed with a stream of nitrogen to evaporate the EtOH. The remaining solution was poured into 20 mL of water and neutralised using NaOH solution. The resultant precipitate, which contained a large portion of tin hydroxide, was collected on celite via vacuum filtration. This precipitate cake was extracted with EtOAc to give a light green solution, which was then evaporated to leave compound **10** as a light yellow powder. The aqueous layer was also green and was evaporated under nitrogen to also leave a yellow powder (500 mg, 1.55 mmol, 74%).

^{1}H NMR (400 MHz, DMSO-d_6) δ ppm 6.76 (2 H, t, J 7.85), 6.20 (2 H, dd, J 8.15, J 1.89), 6.11 (4 H, m), 5.01 (5 H, s), 3.37 (6 H, s).

LR-MS (ESI$^+$) *m/z* 323.18 [M+H]$^+$, 345.12 [M+Na]$^+$, (ESI$^-$) *m/z* 321.13 [M−H]$^-$.

N-(4-cyanophenylurea)-*N'*-(methyl)squaramide (1)

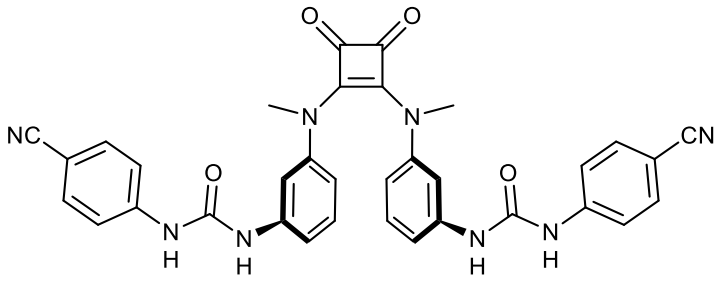

Compound **10** (65 mg, 0.2 mmol) was dissolved in dry DCM (6 mL) and stirred for 5 min. Next, 4-cyanophenyl isocyanate (72 mg, 0.5 mmol) was added portion-wise over 5 min, leaving a brown solution stirred at RT overnight. A precipitate formed; however, the solvent

was evaporated without filtration, and the solids were taken up in 10 mL of MeOH. This was sonicated, filtered, and dried to yield a crystalline yellow solid (70 mg, 0.11 mmol, 57%).

MP = 223–226 °C

^{1}H NMR (400 MHz, DMSO-d_6) δ ppm 8.26 (2 H, s), 7.91 (2 H, s), 6.84 (4 H, m), 6.77 (4 H, m), 6.29 (2H, t, J 2.14), 6.10 (2 H, t, J 8.09), 5.97 (2 H, ddd, J 8.22, 2.10, 0.91), 5.68 (2 H, ddd, J 8.09, 2.30, 0.91), 2.80 (6 H, s); **^{13}C NMR** (101 MHz, DMSO-d_6) δ ppm 186.7, 167.6, 152.3, 144.5, 143.7, 139.9, 133.7, 129.3, 119.7, 118.5, 114.5, 114.2, 110.9, 103.7, 38.3.

LR-MS (ESI$^-$) *m/z* 609.23 [M−H]$^-$; **HR-MS** (ESI$^+$) calcd for $C_{34}H_{26}N_8NaO_4$ [M+Na]$^+$: 633.19692, found *m/z* 633.19597.

N-(4-cyanophenylthiourea)-*N'*-(methyl)squaramide (2)

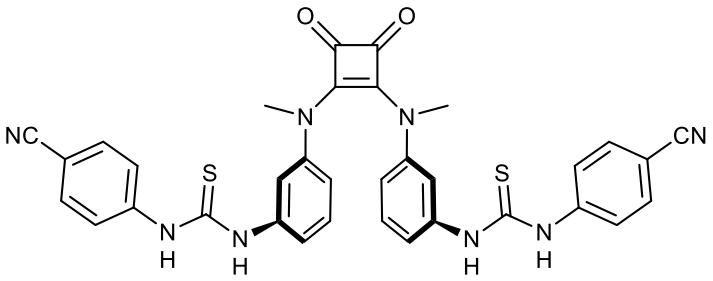

Compound **10** (80 mg, 0.25 mmol) was dissolved in dry THF (5 mL) and stirred for 2 min. Next, 4-cyanophenyl isothiocyanate (100 mg, 0.62 mmol) was dissolved in dry THF (1 mL) and added dropwise. After 1 h, the solution had turned from orange to dark brown and was left to stir overnight at RT. Following this, an additional portion of 4-cyanophenyl isothiocyanate (50 mg) was added to the reaction, which was then heated to 45 °C for 6 h. The reaction was tracked to completion via TLC, following which the solvent was evaporated and the solids washed with diethyl ether (15 mL) and ethyl acetate (5 mL) to yield a light green solid (81 mg, 0.13 mmol, 50%).

MP = 166–169 °C

^{1}H NMR (400 MHz, DMSO-d_6) δ ppm 10.21 (1H, s), 10.05 (2 H, s), 7.75 (8 H, q, J 8.7), 7.21 (2 H, s), 7.04 (4 H, dd, J 14.04, J 6.33), 6.66 (2 H, d, J 7.65), 3.53 (6H, s); **^{13}C NMR** (101 MHz, DMSO-d_6) δ ppm 186.7, 179.2, 167.8, 144.4, 143.2, 139.7, 133.2, 129.1, 122.7, 119.8, 119.5, 117.6, 116.2, 105.8, 38.9.

LR-MS (ESI$^-$) *m/z* 313.89 [M−H]$^-$; **HR-MS** (ESI$^+$) calcd for $C_{34}H_{25}N_8O_2S_2$ [M−H]$^-$: 641.15474, found *m/z* 641.15530.

N-(4-nitrophenylurea)-*N'*-(methyl)squaramide (3)

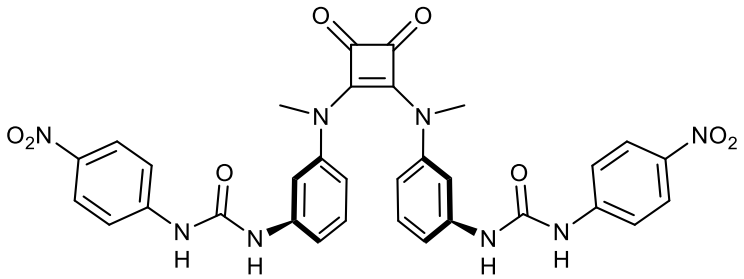

Compound **10** (80 mg, 0.25 mmol) was dissolved in dry THF (4 mL) and stirred for 2 min. Next, 4-nitrophenyl isocyanate (102 mg, 0.62 mmol) was suspended in dry THF (2 mL) and added dropwise. The solution was heated to 50 °C, leading to the immediate precipitation of a bright yellow solid, and left to stir overnight at RT. The reaction was tracked to completion via TLC, after which the solvent was evaporated, and the solids were subjected to hot filtration in MeCN. Collection of the solids and drying yielded a bright yellow solid (113 mg, 0.17 mmol, 70%).

MP = 219–222 °C

^{1}H NMR (400 MHz, DMSO-d_6) δ ppm 9.34 (2 H, s), 8.81 (2 H, s), 8.07 (4 H, d, J 8.7), 7.62 (4 H, d, J 8.8), 7.10 (2 H, s), 6.92 (2 H, d, J 8.0), 6.85 (2 H, d, J 8.3), 6.51 (2 H, d, 8.0), 3.65 (6 H, s); **^{13}C NMR** (101 MHz, DMSO-d_6) δ ppm 186.8, 167.5, 152.1, 146.7, 143.8, 141.3, 139.8, 129.3, 125.4, 117.8, 114.6, 114.4, 111.0, 38.4.

LR-MS (ESI$^+$) *m/z* 673.16 [M+Na]$^+$, (ESI$^-$) *m/z* 649.24 (M−H)$^-$; **HR-MS** (ESI$^+$) calcd for $C_{32}H_{26}N_8NaO_8$ [M+Na]$^+$: 674.17994, found *m/z* 674.18034.

N-(4-nitrophenylthiourea)-*N'*-(methyl)squaramide (4)

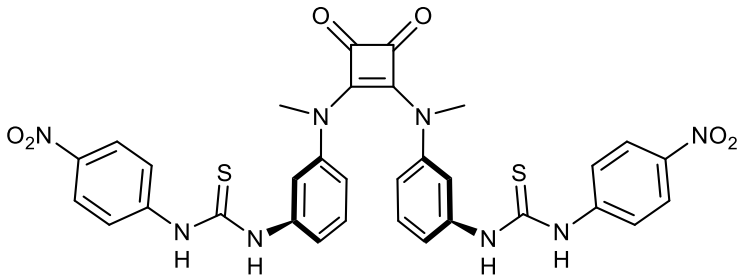

Compound **10** (80 mg, 0.25 mmol) was dissolved in dry THF (4 mL) and stirred for 2 min. Next, 4-nitrophenyl isothiocyanate (112 mg, 0.62 mmol) was dissolved in dry THF (2 mL) and added dropwise. The solution was left to stir overnight at RT. The reaction had not reached completion overnight. Therefore, another portion of 4-nitrophenyl isothiocyanate (50 mg) was

added. Following completion tracked by TLC, the solvent was evaporated, and the remaining solids were washed with 40 mL of ether. Collection of the solids and drying yielded a dark green solid (135 mg, 0.20 mmol, 79%).

MP = 150−153 °C

^{1}H NMR (400 MHz, DMSO-d_6) δ ppm 10.47 (2 H, s), 10.25 (2 H, s), 8.18 (4 H, d, J 8.8), 7.82 (4 H, d, J 9.0), 7.24 (2 H, d, J 2.18), 7.05 (4 H, dt, J 15.8, 8.1), 6.67 (2 H, m), 3.55 (6 H, s) **^{13}C NMR** (101 MHz, DMSO-d_6) δ ppm 183.4, 179.6, 170.2, 163.2, 145.2, 141.5, 125.6, 117.7, 53.1, 42.4, 35.2, 28.9.

LR-MS (ESI$^+$) *m/z* 705.10 [M+Na]$^+$, (ESI$^-$) *m/z* 681.23 (M−H)$^-$; **HR-MS** (ESI$^+$) calcd for $C_{32}H_{26}N_8NaO_6S_2$ [M+Na]$^+$: 705.13089, found *m/z* 705.13048.

N-(4-cyanophenyl)-*N'*-(methyl)squaramide (11)

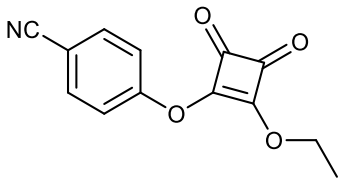

p-Cyanoaniline (500 mg, 4.23 mmol) and zinc trifluoromethanesulfonate (200 mg, 1.05 mmol) were dissolved in EtOH (25 mL) before 3,4-diethoxy-3-cyclobutene-1,2-dione (0.63 mL, 4.23 mmol) was added dropwise to the solution. The mixture was stirred at Rrt overnight, resulting in the formation of a yellow precipitate. This was collected, washed with EtOH and dried to yield a bright yellow product (720 mg, 2.98 mmol, 70 %)

^{1}H NMR (400 MHz, DMSO-d_6) δ ppm 11.08 (1 H, s), 7.83 (2 H, s), 7.58 (2 H, s), 4.82 (2 H, s), 1.46 (3 H, s)

LR-MS (ESI$^+$) *m/z* 265.05 [M+Na]$^+$, (ESI$^-$) *m/z* 241.03 (M−H)$^-$

N-(4-cyanophenylsquaramide)-*N'*-(methyl)squaramide (5)

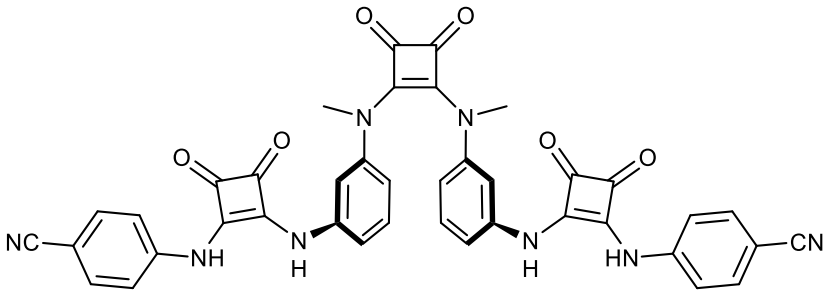

Compound **10** (80 mg, 0.25 mmol) and zinc trifluoromethanesulfonate (272 mg, 0.75 mmol) were dissolved in toluene (5.7 mL) and DMF (0.3 mL). Compound **11** (182 mg, 0.75 mmol) was added portion-wise, and the solution was stirred at reflux for 2 d. The solvent was evaporated, and ethanol was added to the residue. The precipitates were collected via vacuum filtration and dried to yield compound **5** as a brown solid (90 mg, 0.13 mmol, 50%).

MP = +250 °C

^{1}H NMR (400 MHz, DMSO-d_6) δ ppm 10.07 (2 H, s), 9.84 (2 H, s), 7.82 (4 H, d, J 8.6), 7.59 (4 H, d, J 8.4), 7.17 (2 H, s), 6.99 (2 H, t, J 8.0), 6.83 (2 H, d, J 7.6), 6.61 (2 H, d, J 7.5), 3.65 (6 H, s) **^{13}C NMR** (101 MHz, DMSO-d_6) δ ppm 186.9, 182.5, 181.3, 167.5, 166.4, 165.4, 144.6, 143.0, 139.1, 134.2, 130.2, 119.0, 117.8, 115.8, 114.4, 111.0, 105.2, 38.5.

LR-MS (ESI$^+$) *m/z* 737.15 [M+Na]$^+$, (ESI$^-$) *m/z* 713.28 (M−H)$^-$; **HR-MS** (ESI$^+$) calcd for $C_{40}H_{25}N_8O_6$ [M−H]$^-$: 713.19025, found *m/z* 713.19094.

N,N′-(3-aminophenyl)squaramide (12)

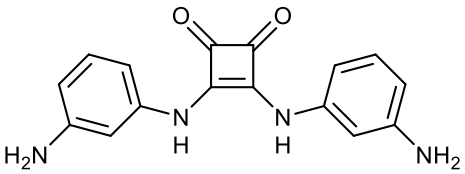

m-Phenylenediamine (1000 mg, 9.26 mmol) and zinc trifluoromethanesulfonate (1500 mg, 4.21 mmol) were dissolved in EtOH (15 mL) before 3,4-diethoxy-3-cyclobutene-1,2-dione (0.6 mL, 4.21 mmol) was added dropwise to the solution. This was stirred at RT for 2 d. A precipitate formed, which was collected upon cooling and filtered. The residue was purified using column chromatography in an eluent mixture of 10% MeOH/1% TEA/DCM to yield a beige solid (843 mg, 2.38 mmol, 57%).

MP = 205−208 °C

^{1}H NMR (400 MHz, DMSO-d_6) δ ppm 9.62 (2 H, s), 6.99 (2 H, t, J 8.0), 6.76 (2 H, dd, J 7.9, 2.2), 6.60 (2 H, t, J 2.2), 6.29 (2 H, dd, J 8.0, 2.0), 5.21 (4 H, s); **^{13}C NMR** (101 MHz, DMSO-d_6) δ ppm 181.7, 166.0, 150.1, 139.7, 130.2, 109.9, 106.6, 104.0.

LR-MS (ESI$^+$) *m/z* 317.12 [M+Na]$^+$, (ESI$^-$) *m/z* 293.11 (M−H)$^-$; **HR-MS** (ESI$^+$) calcd for $C_{16}H_{13}N_4O_2$ [M−H]$^-$: 293.10440, found *m/z* 293.10422.

N,N'-(4-nitrophenylthiourea)-squaramide (7)

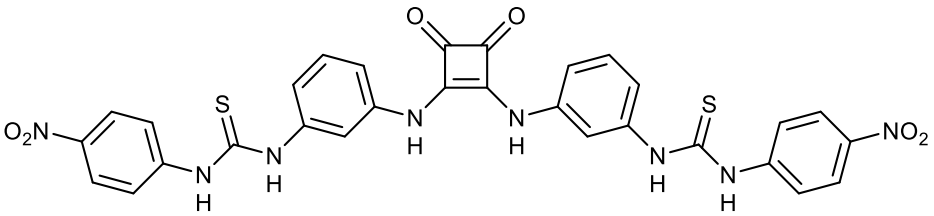

Compound **12** (70 mg, 0.24 mmol) was suspended in dry MeCN (5 mL) and DMF (0.25 mL). 4-nitrophenyl isothiocyanate (107 mg, 0.6 mmol) was dissolved in dry MeCN (2 mL) and added dropwise to the solution, which was stirred under argon at RT for 2 d. A yellow precipitate was collected by filtration and washed with ether and DCM to yield the desired compound as a light brown solid (91 mg, 0.14 mmol, 56%).

MP = 162–164 °C

^{1}H NMR (400 MHz, DMSO-d_6) δ ppm 10.48 (2 H, s), 10.43 (2 H, s) 10.03 (2 H, s), 8.21 (4 H, d, J 9.0), 7.87 (4 H, d, J 9.1), 7.71 (2 H, d, J 2.2), 7.40 (4H, m), 7.18 (2 H, d, 7.8); **^{13}C NMR** (101 MHz, DMSO-d_6) δ ppm 182.0, 179.5, 166.1, 146.7, 142.9, 140.4, 139.2, 130.1, 124.8, 122.3, 118.8, 115.6, 113.8.

LR-MS ((ESI$^-$) *m/z* 653.19 (M−H)$^-$; **HR-MS** (ESI$^+$) calcd for $C_{30}H_{21}N_8O_6S_2$ [M−H]$^-$: 653.10310, found *m/z* 653.10333.

N,N'-((4-trifluoromethyl)phenyl)squaramide (6)

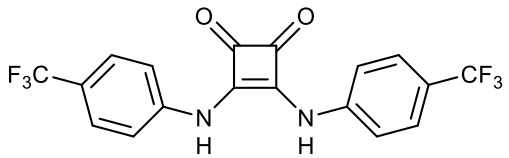

3-Ethoxy-4((4-trifluoromethyl)amino)cyclobutene-1,2-dione (300 mg, 1.05 mmol) and zinc trifluoromethanesulfonate (350 mg, 0.875 mmol) were dissolved in EtOH (10 mL) before (4-trifluoromethyl)aniline (0.15 mL, 1.05 mmol) was added dropwise to the solution. This was stirred at RT for 2 d. A precipitate formed, which was collected upon cooling and filtered. The precipitate was washed with cold EtOH to yield a light yellow solid (380 mg, 0.95 mmol, 90%).

^{1}H NMR (400 MHz, DMSO-d_6) δ ppm 10.24 (2 H, s), 7.73 (4 H, d, J 8.5), 7.63 (2 H, d, J 8.5).

LR-MS (ESI$^+$) *m/z* 423.04 [M+Na]$^+$, (ESI$^-$) *m/z* 399.05 (M−H)$^-$.

4. Characterisation Data

4.1 Spectra

Proton NMR and low-resolution mass spectrometry (LR-MS) are shown for each compound. Carbon NMR and high-resolution mass spectrometry (HR-MS) are shown for novel compounds.

N-(3-nitrophenyl)squaramide (8)

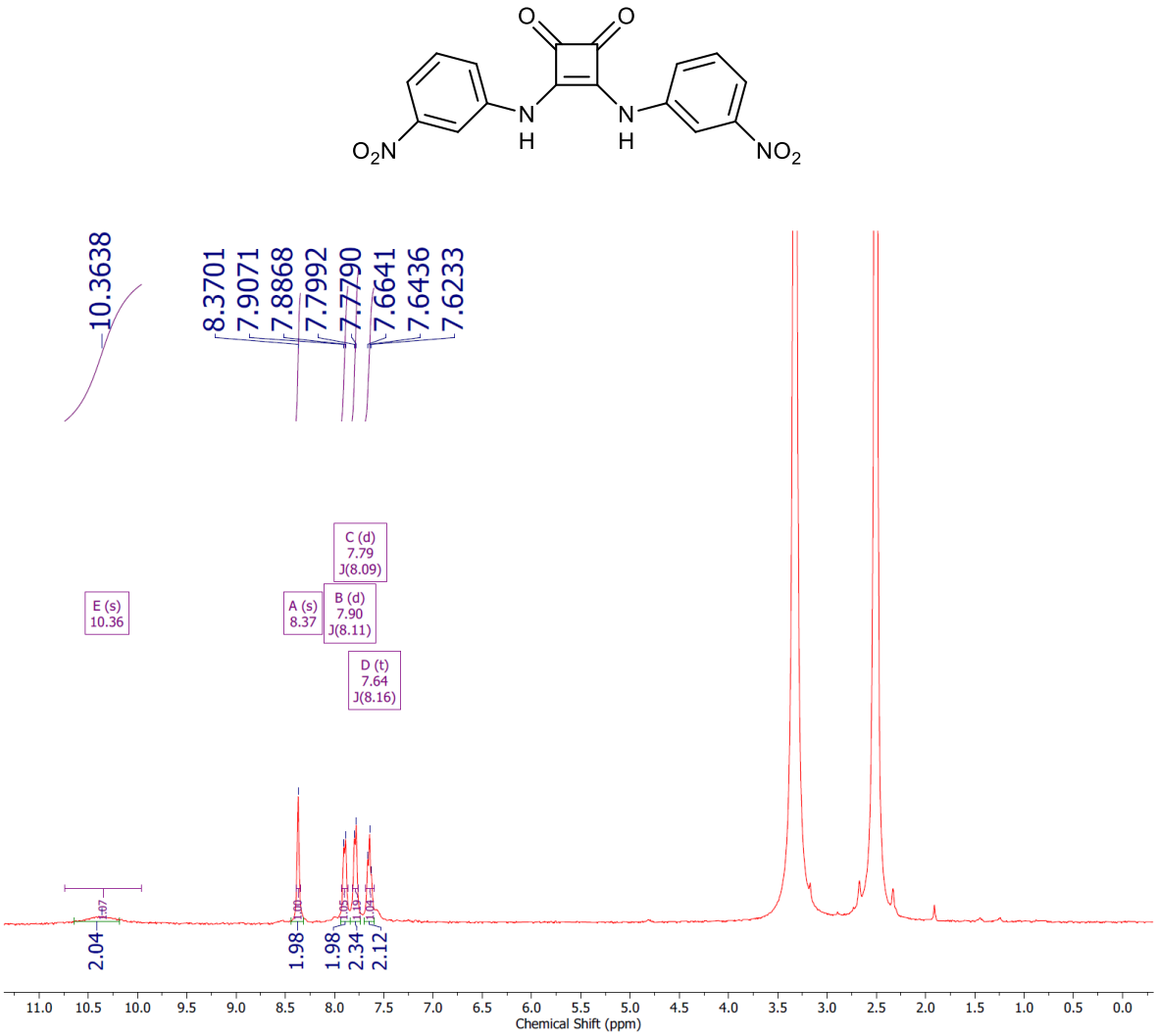

Figure S1. ^{1}H NMR (400 MHz) spectrum of *N*-(3-nitrophenyl)squaramide in DMSO-d_6 at 298 K. Low resolution due to low compound solubility.

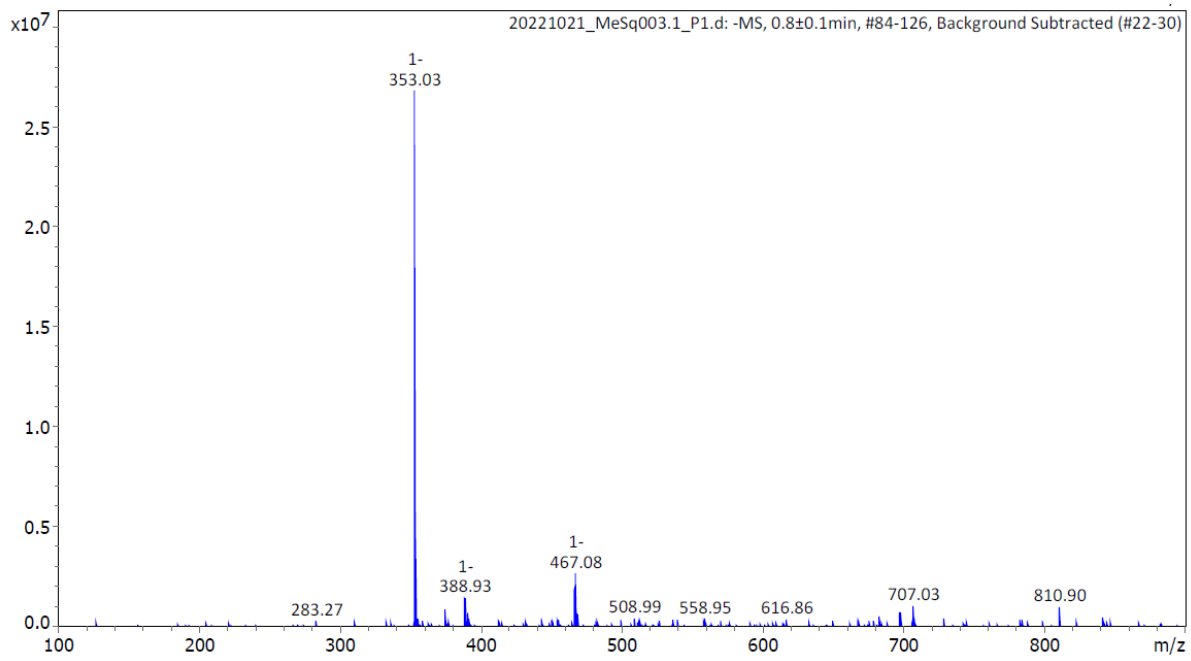

Figure S2. LR-MS (ESI$^+$) spectrum of *N*-(3-nitrophenyl)squaramide.

N-(3-nitrophenyl)-*N'*-(methyl)squaramide (9)

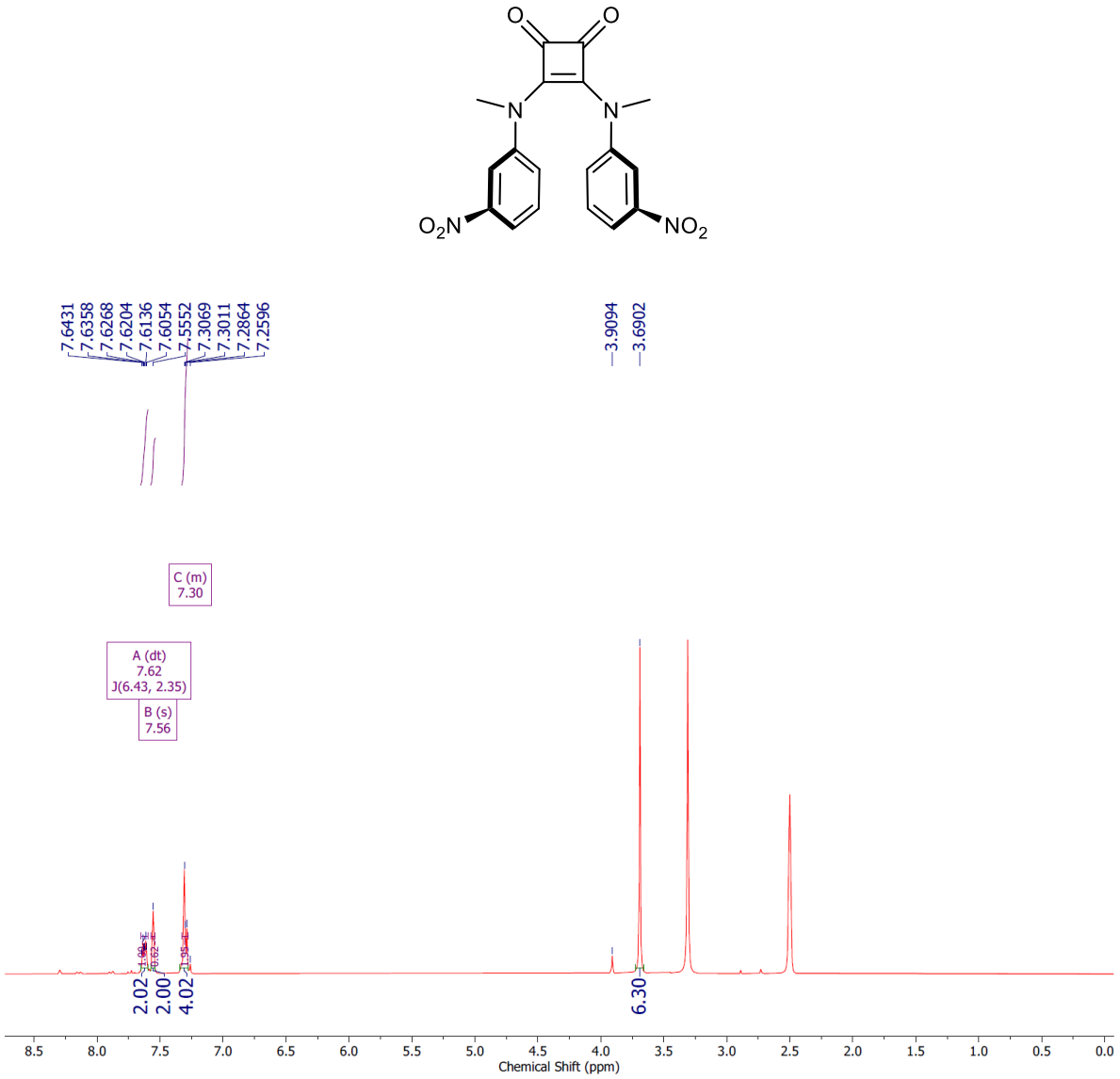

Figure S3. ^{1}H NMR (400 MHz) spectrum of *N*-(3-nitrophenyl)-*N'*-(methyl)squaramide in DMSO-d_6 at 298 K.

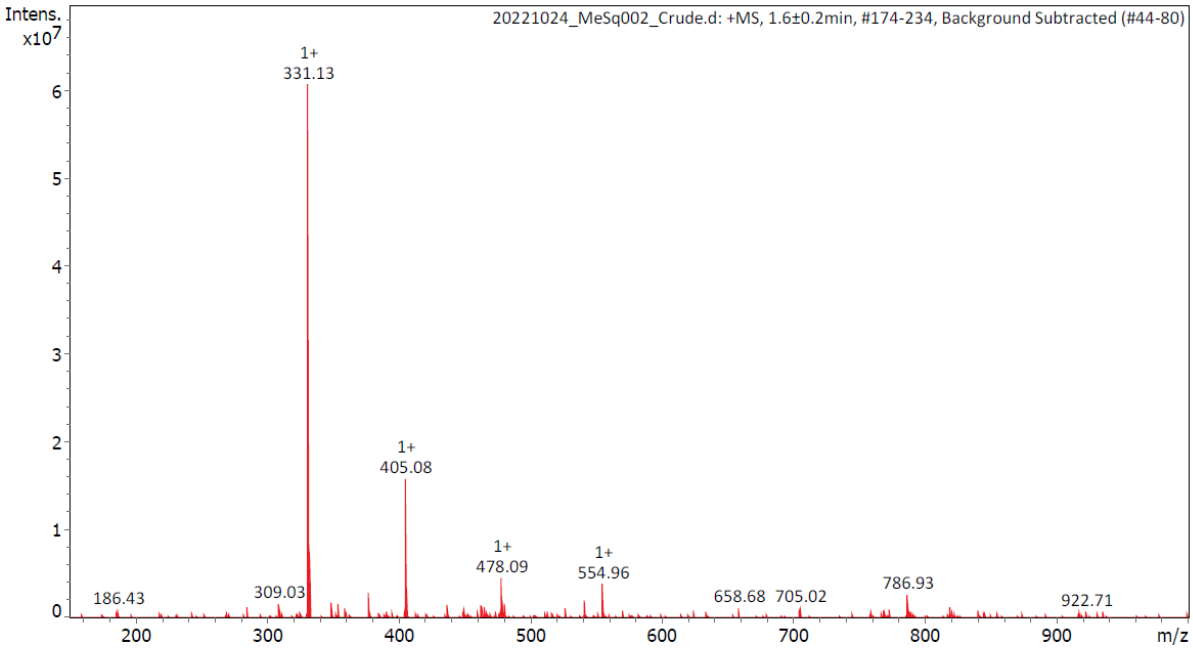

Figure S4. LR-MS (ESI$^+$) spectrum of *N*-(3-nitrophenyl)-*N'*-(methyl)squaramide.

N-(3-aminophenyl)-*N'*-(methyl)squaramide (10)

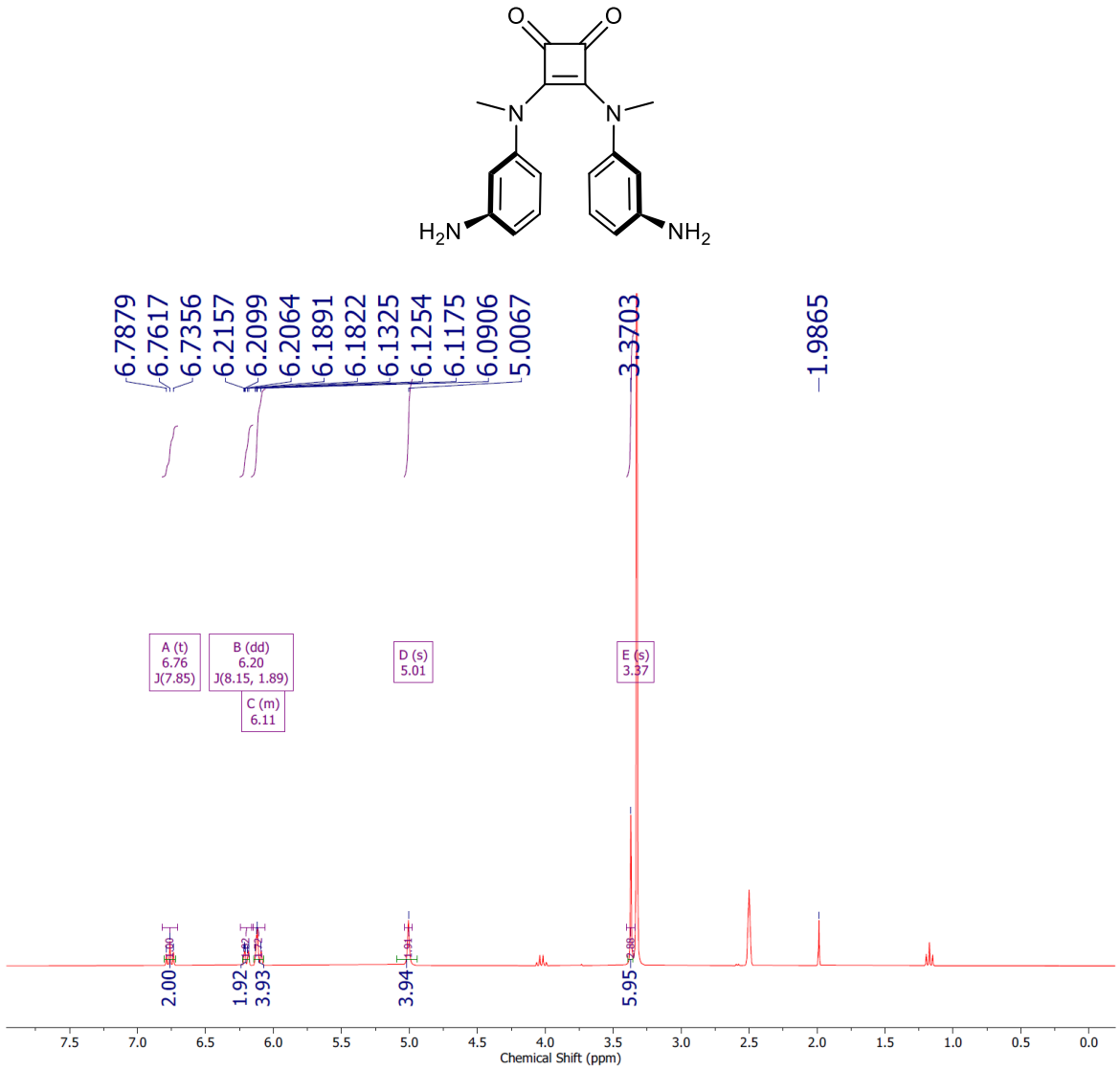

Figure S5. ^{1}H NMR (400 MHz) spectrum of *N*-(3-aminophenyl)-*N'*-(methyl)squaramide in DMSO-d_6 at 298 K.

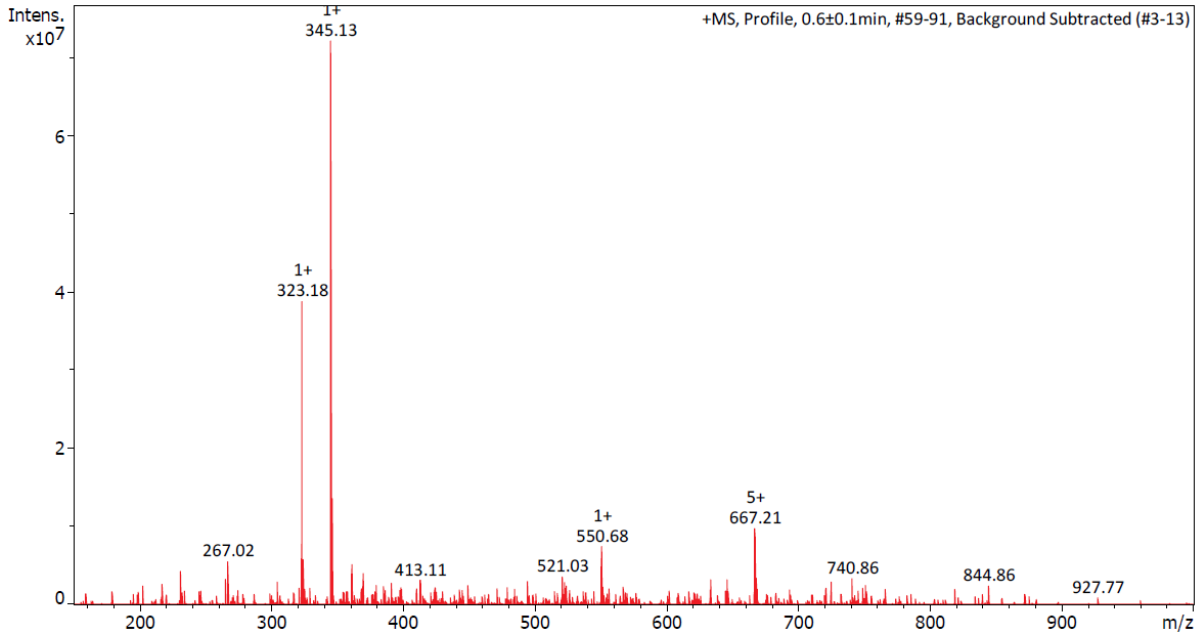

Figure S6. LR-MS (ESI$^+$) spectrum of *N*-(3-aminophenyl)-*N'*-(methyl)squaramide.

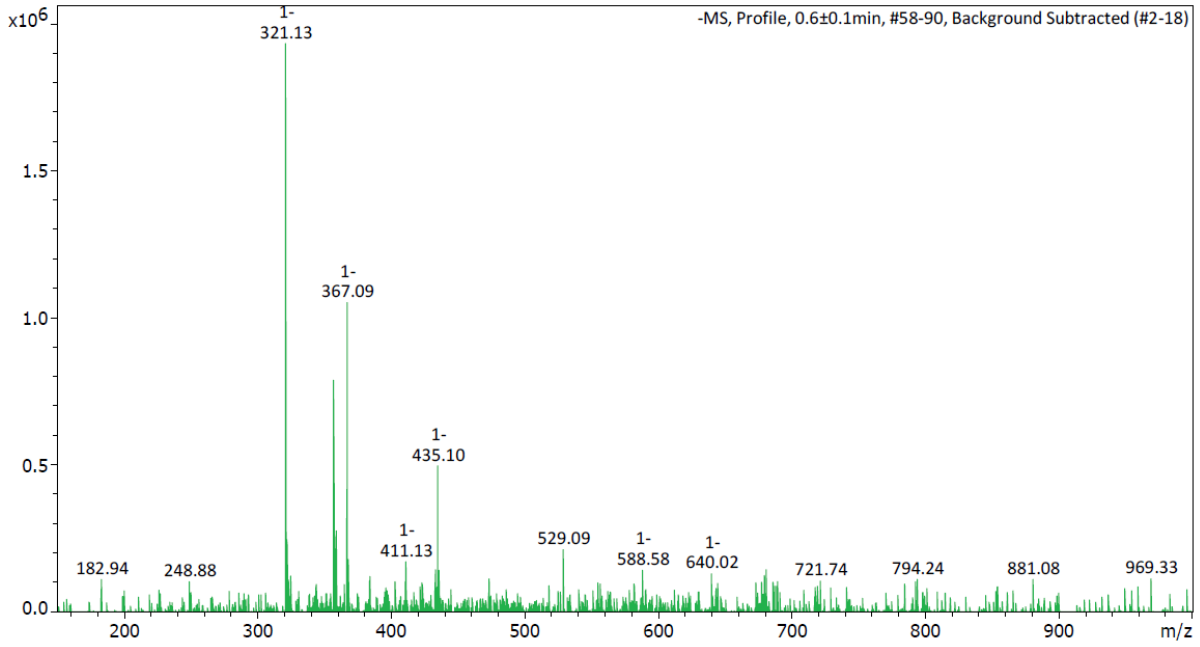

Figure S7. LR-MS (ESI$^-$) spectrum of *N*-(3-aminophenyl)-*N'*-(methyl)squaramide.

N-(4-cyanophenylurea)-*N'*-(methyl)squaramide (1)

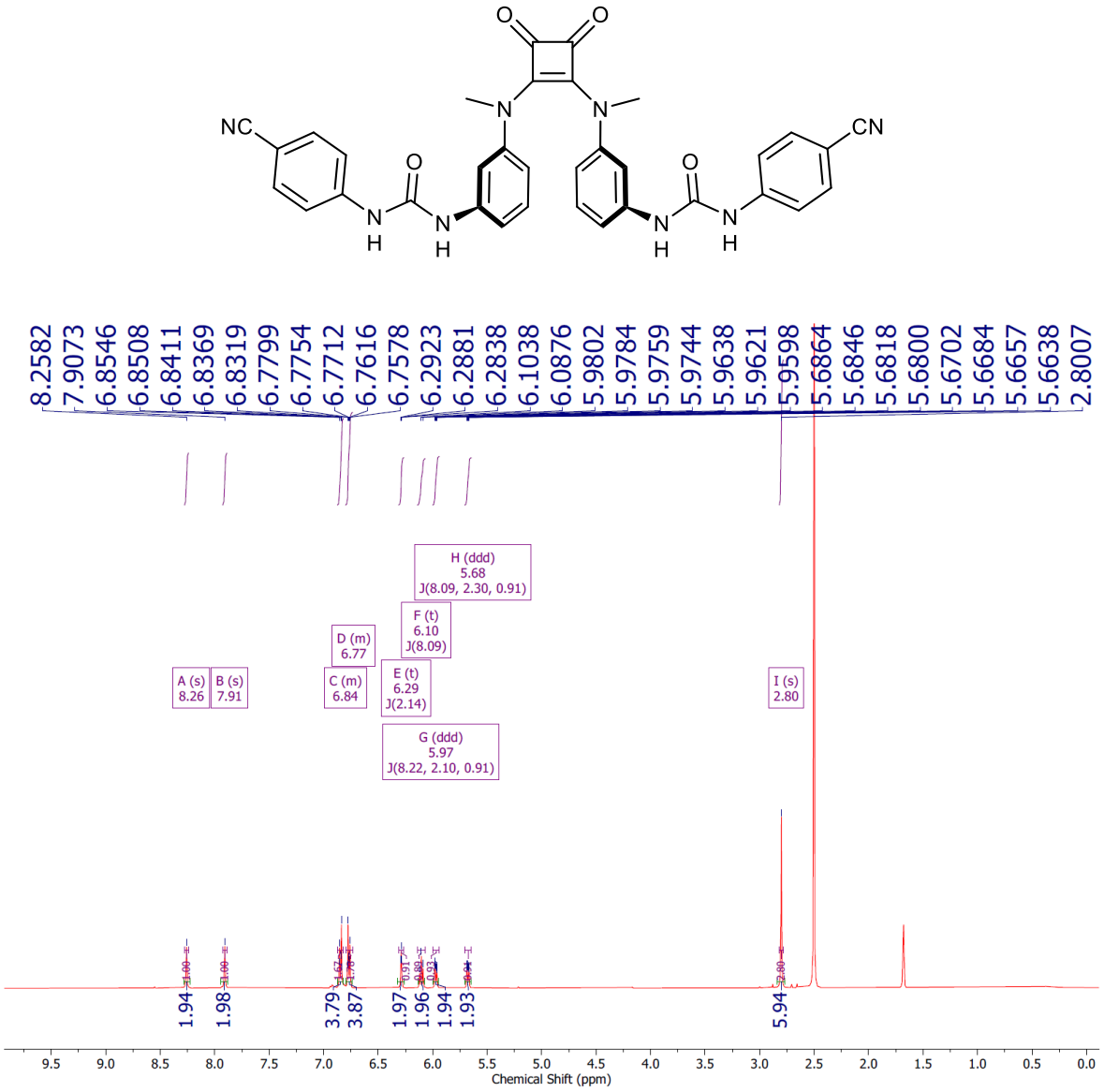

Figure S8. ^{1}H NMR (500 MHz) spectrum of *N*-(4-cyanophenylurea)-*N'*-(methyl)squaramide in DMSO-d_6 at 298 K.

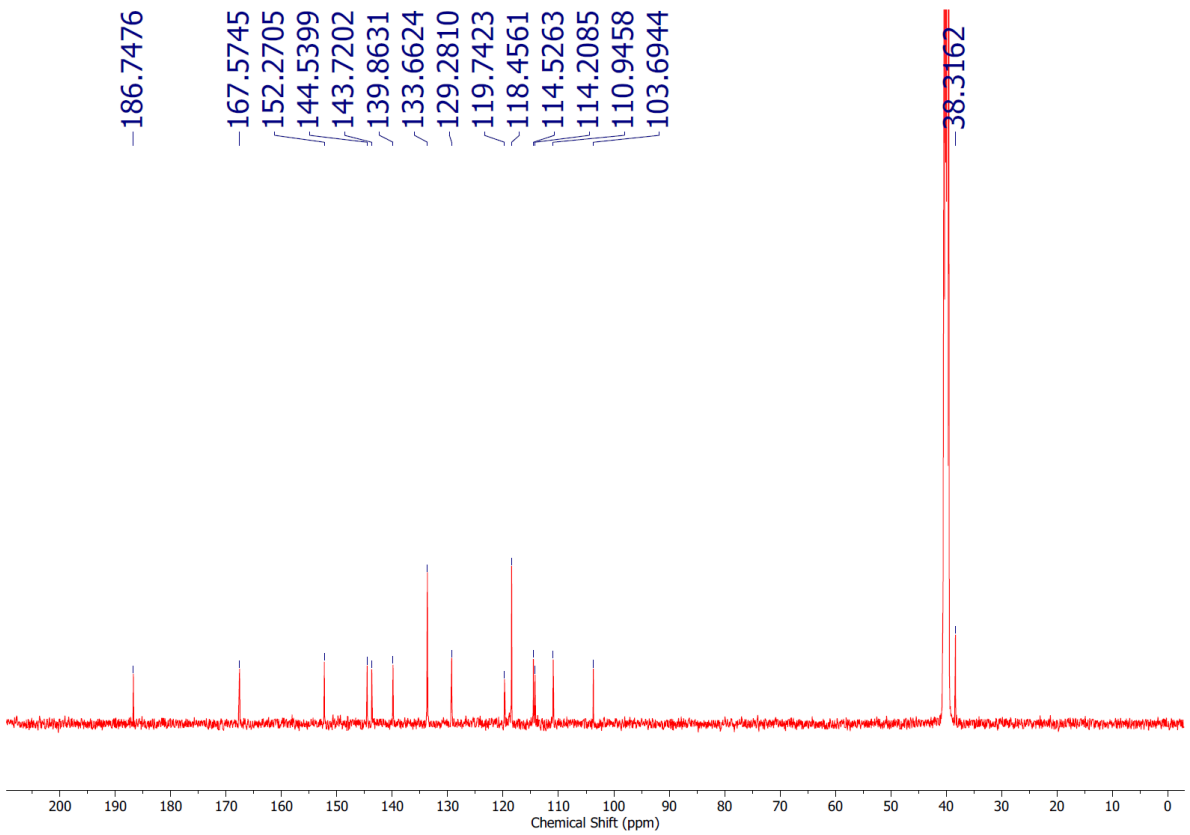

Figure S9. ^{13}C NMR (101 MHz) spectrum of *N*-(4-cyanophenylurea)-*N'*-(methyl)squaramide in DMSO-d_6 at 298 K.

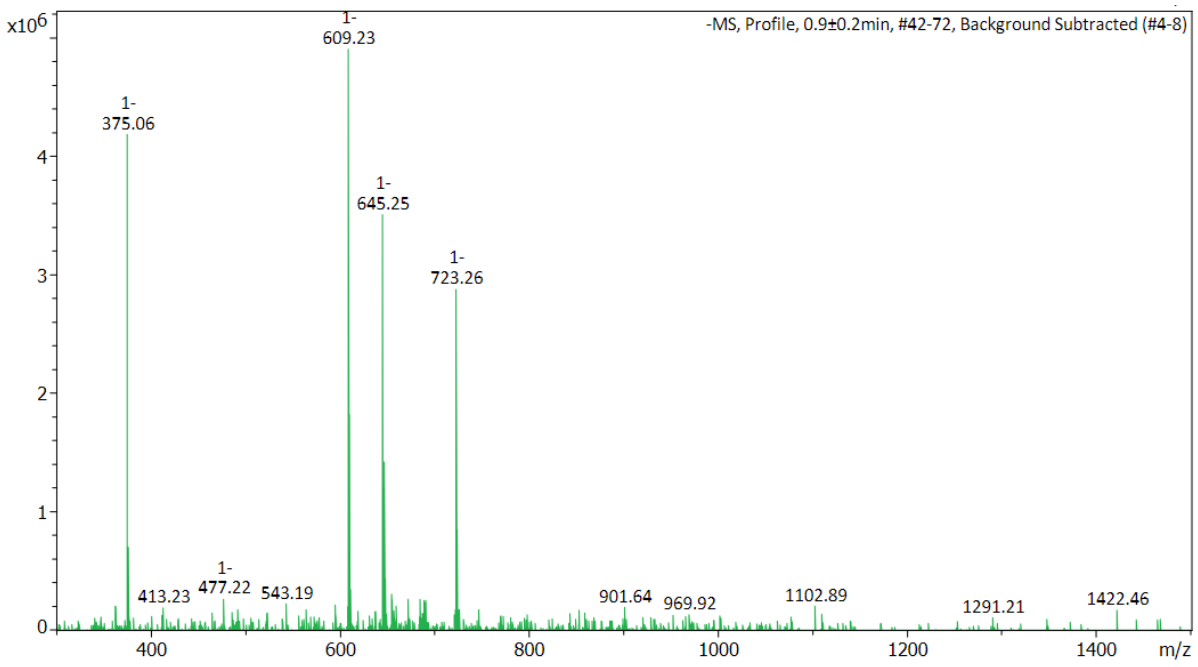

Figure S10. LR-MS (ESI$^-$) spectrum of *N*-(4-cyanophenylurea)-*N'*-(methyl)squaramide.

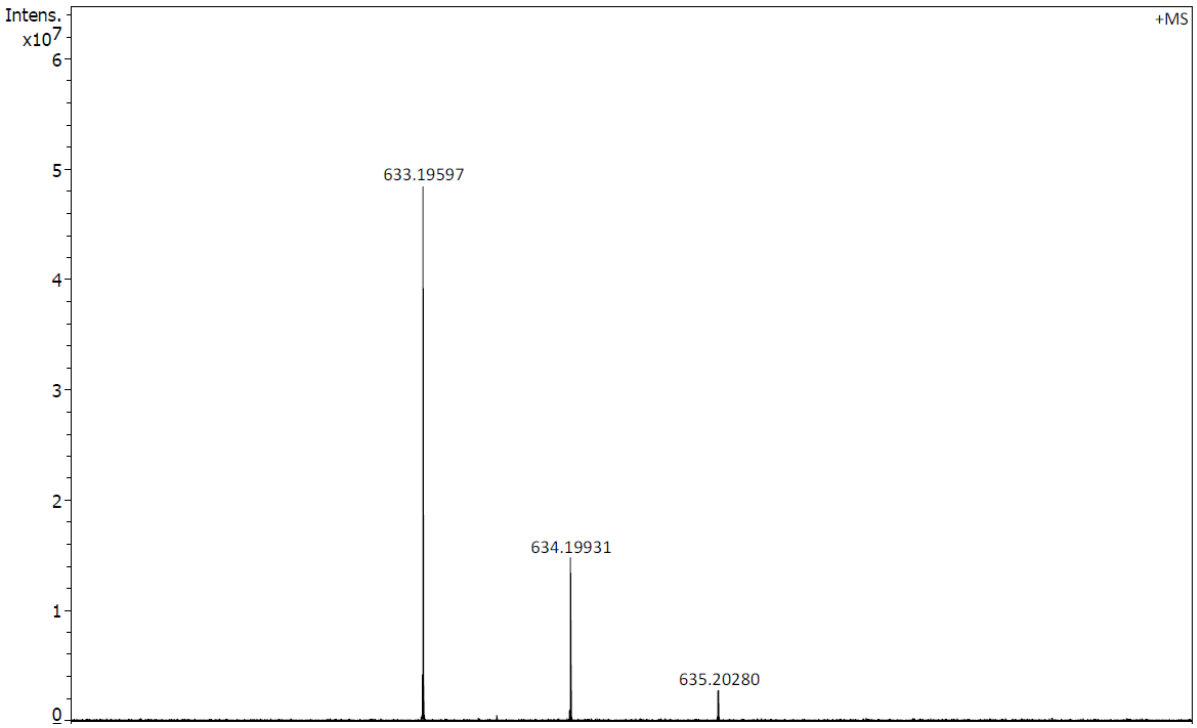

Figure S11. HR-MS (ESI$^+$) spectrum of *N*-(4-cyanophenylurea)-*N'*-(methyl)squaramide.

N-(4-cyanophenylthiourea)-*N*′-(methyl)squaramide (2)

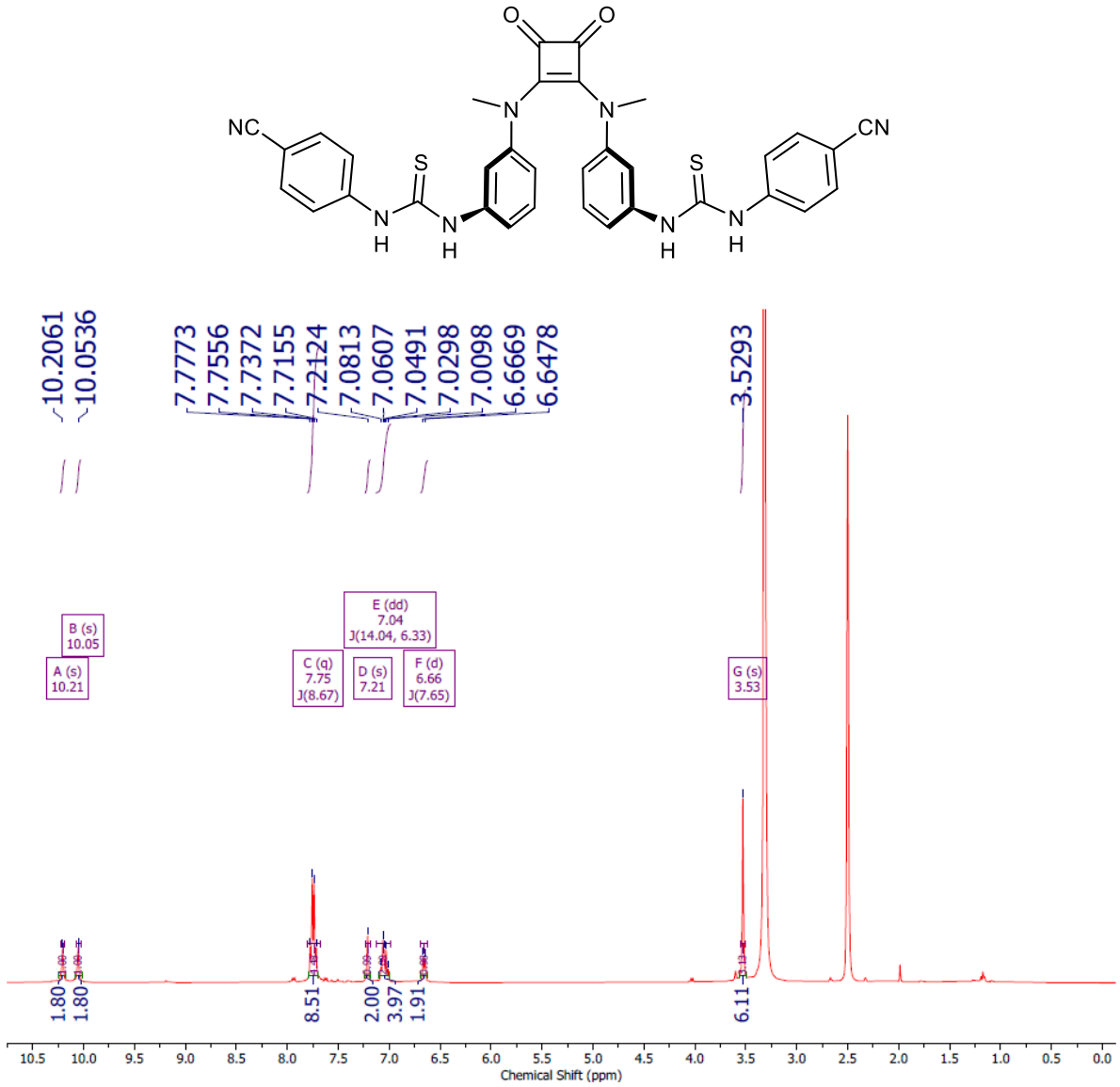

Figure S12. ^{1}H NMR (500 MHz) spectrum of *N*-(4-cyanophenylthiourea)-*N*′-(methyl)squaramide in DMSO-d_6 at 298 K.

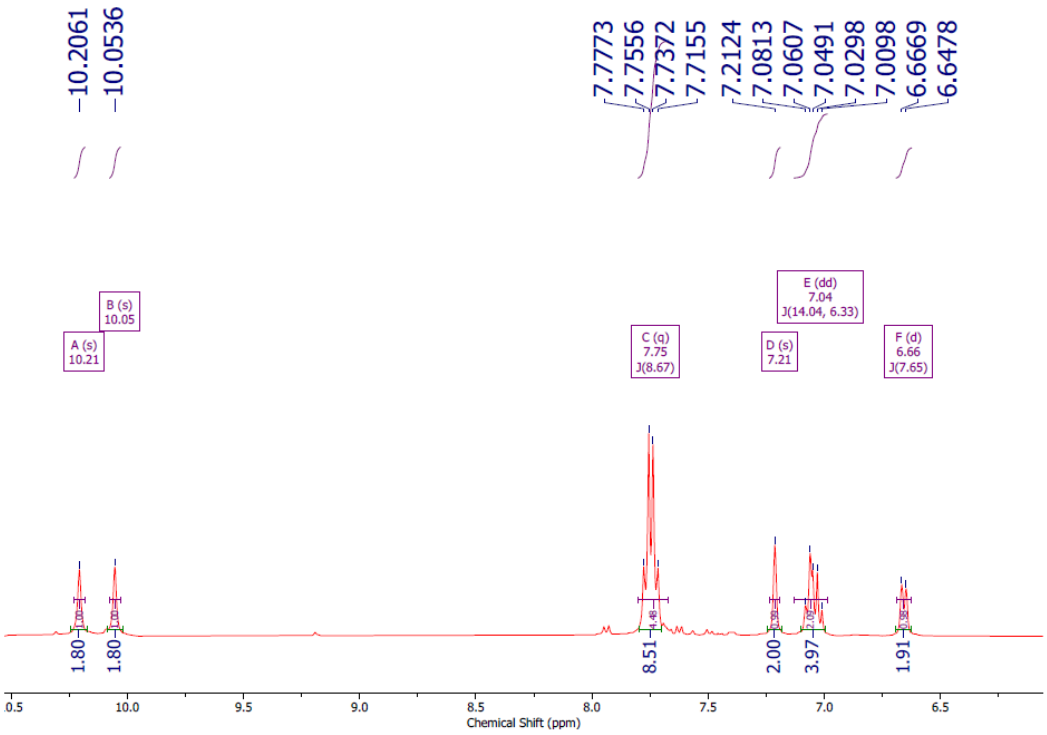

Figure S13. Zoomed ^{1}H NMR (500 MHz) spectrum of *N*-(4-cyanophenylthiourea)-*N'*-(methyl)squaramide in DMSO-d_6 at 298 K.

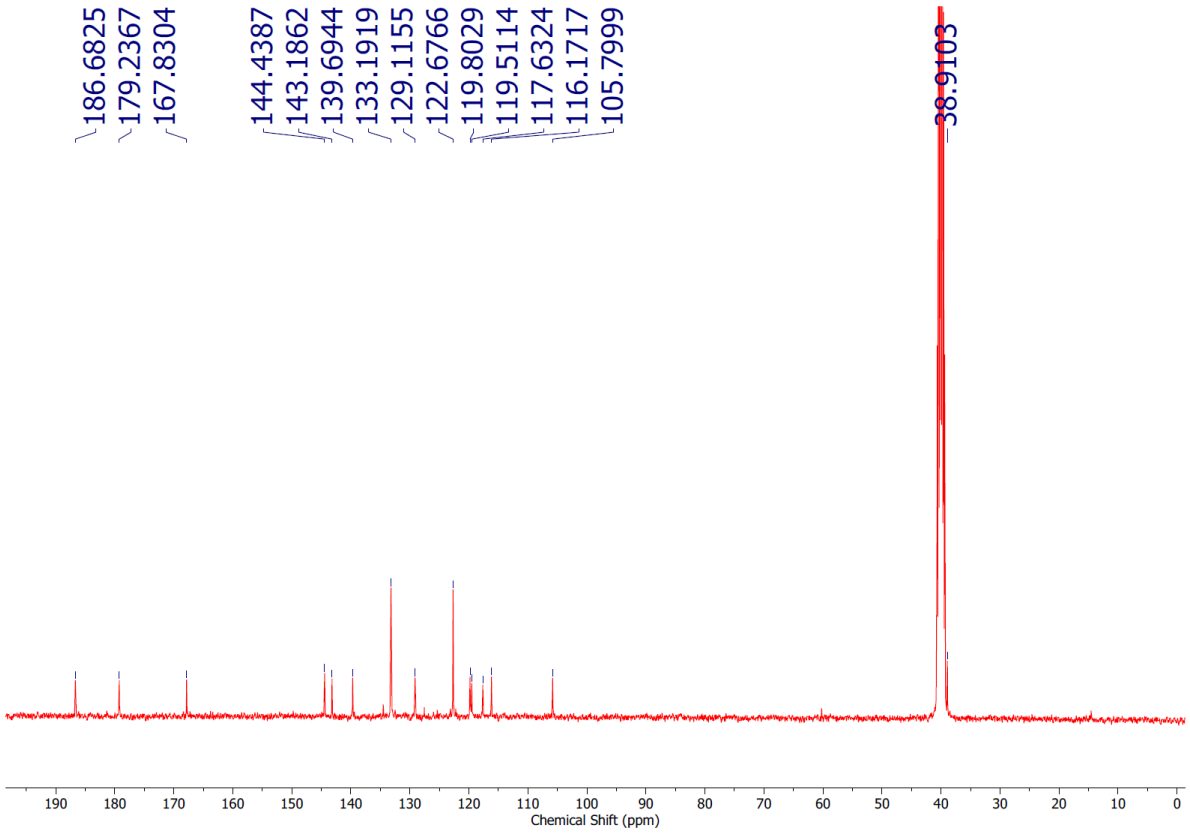

Figure S**14**. ^{13}C NMR (101 MHz) spectrum of *N*-(4-cyanophenylthiourea)-*N'*-(methyl)squaramide in DMSO-d_6 at 298 K.

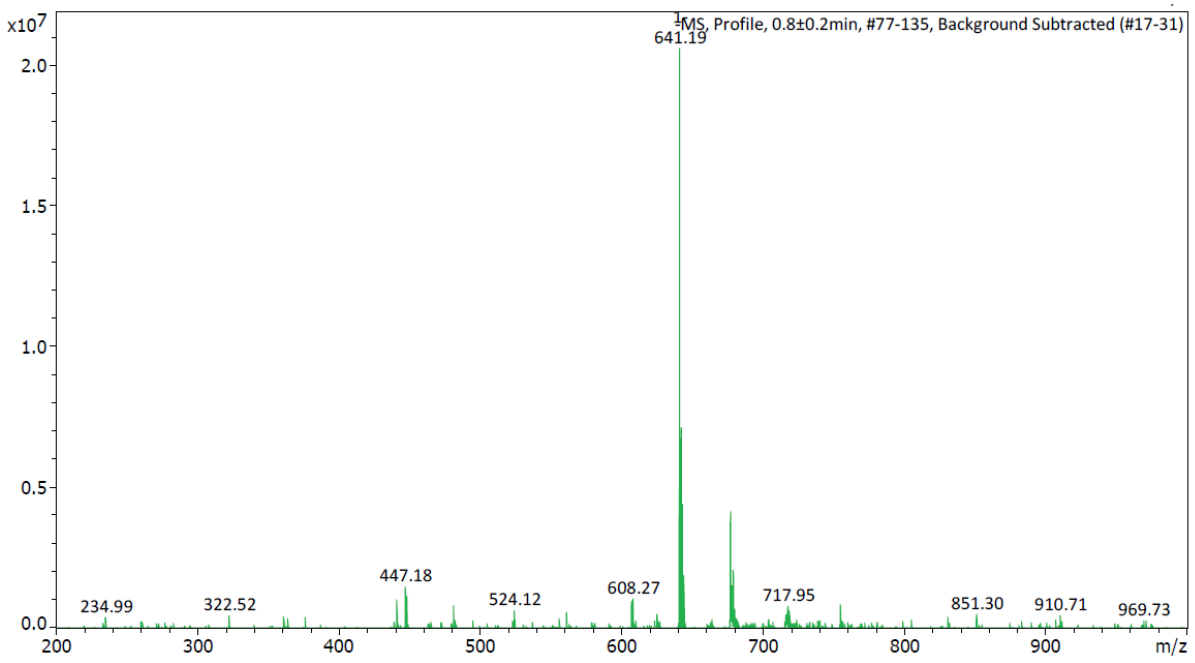

Figure S15. LR-MS (ESI⁻) spectrum of *N*-(4-cyanophenylthiourea)-*N'*-(methyl)squaramide.

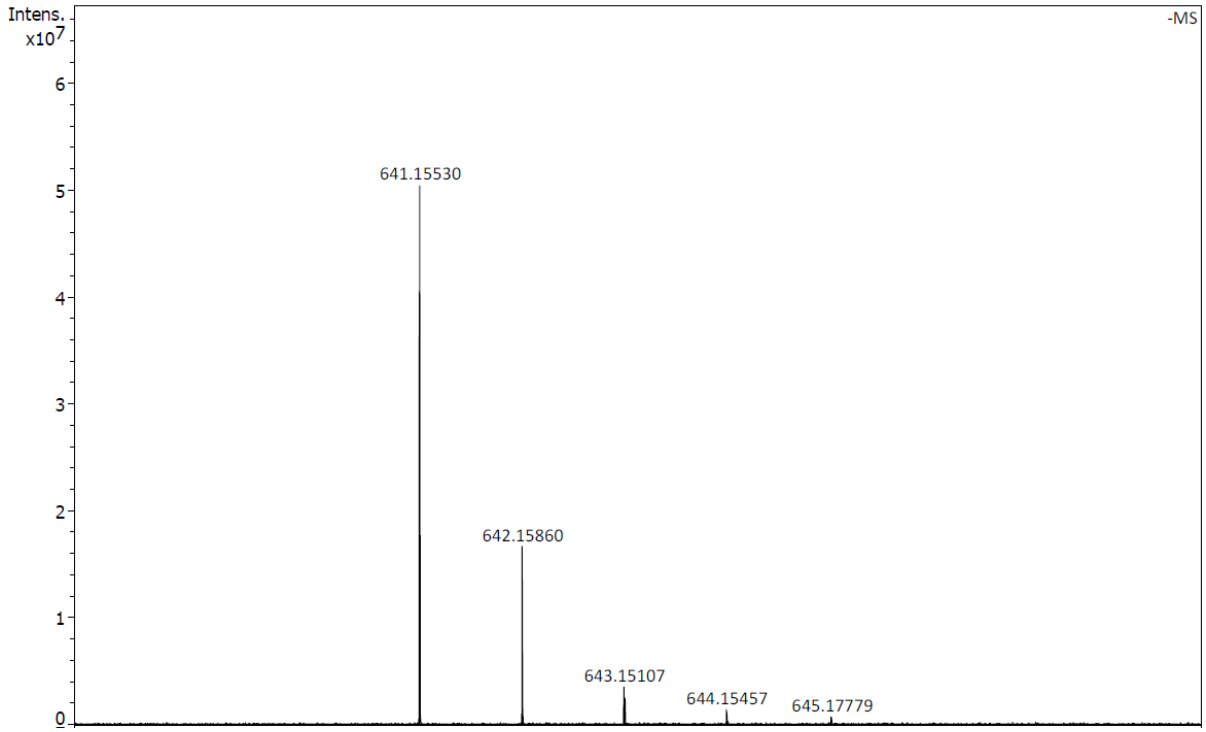

Figure S16. HR-MS (ESI⁻) spectrum of *N*-(4-cyanophenylthiourea)-*N'*-(methyl)squaramide.

N-(4-nitrophenylurea)-*N'*-(methyl)squaramide (3)

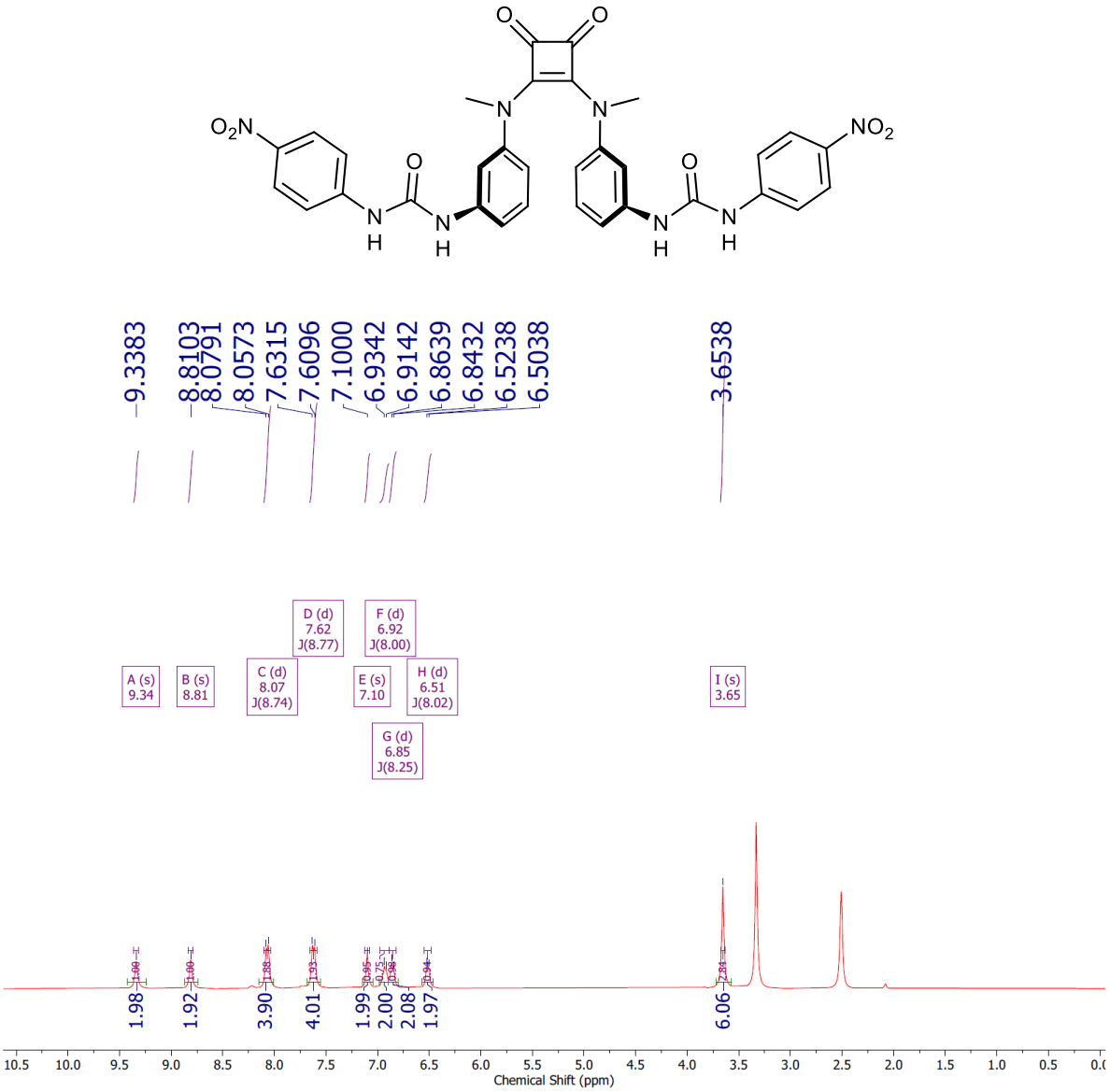

Figure S17. ^{1}H NMR (500 MHz) spectrum of *N*-(4-nitrophenylurea)-*N'*-(methyl)squaramide in DMSO-d_6 at 298 K.

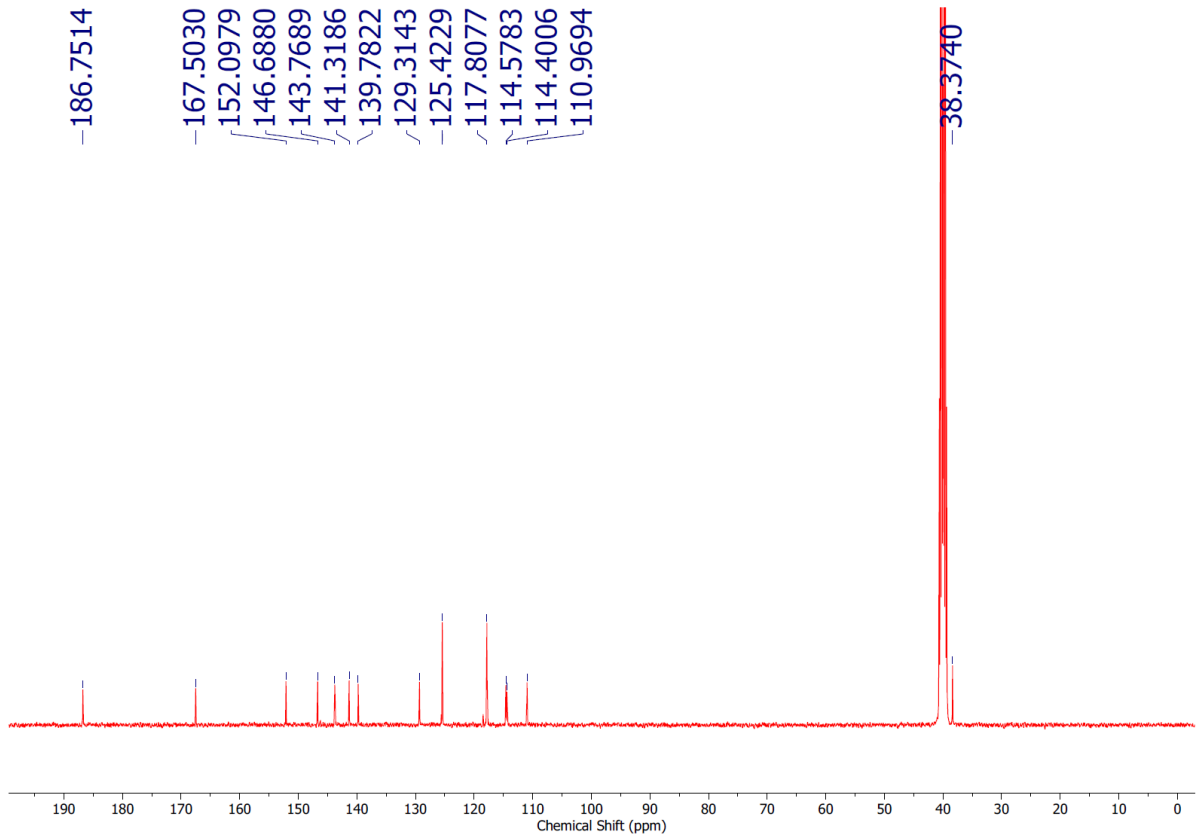

Figure S18. ^{13}C NMR (101 MHz) spectrum of *N*-(4-nitrophenylurea)-*N'*-(methyl)squaramide in DMSO-d_6 at 298 K.

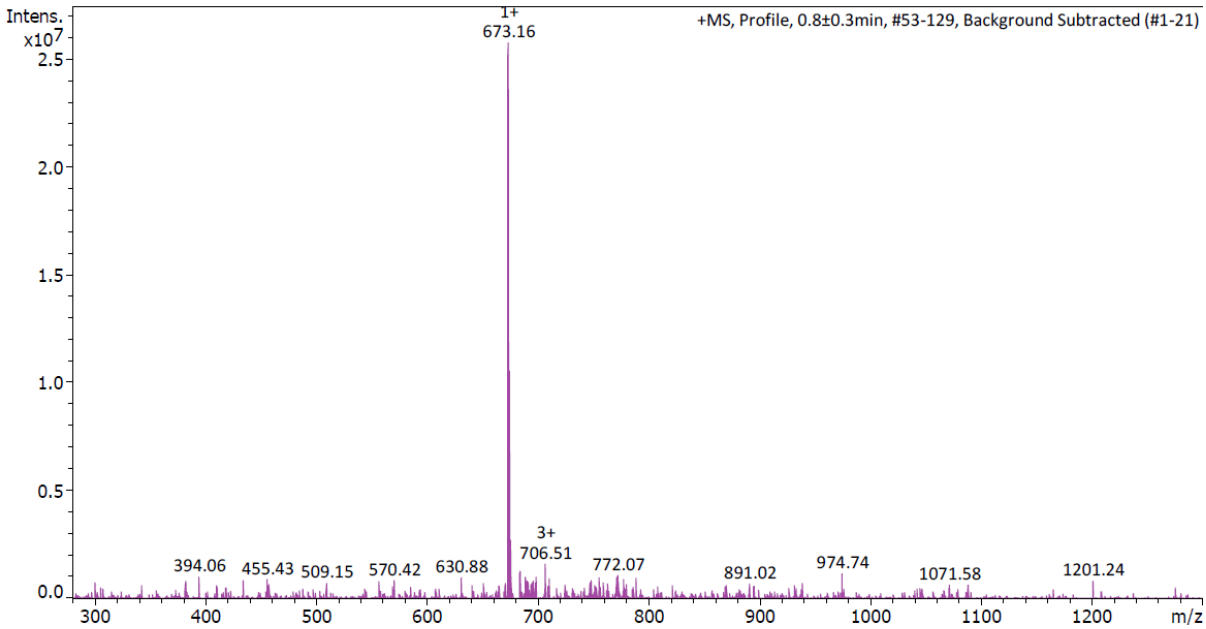

Figure S19. LR-MS (ESI$^+$) spectrum of *N*-(4-nitrophenylurea)-*N'*-(methyl)squaramide.

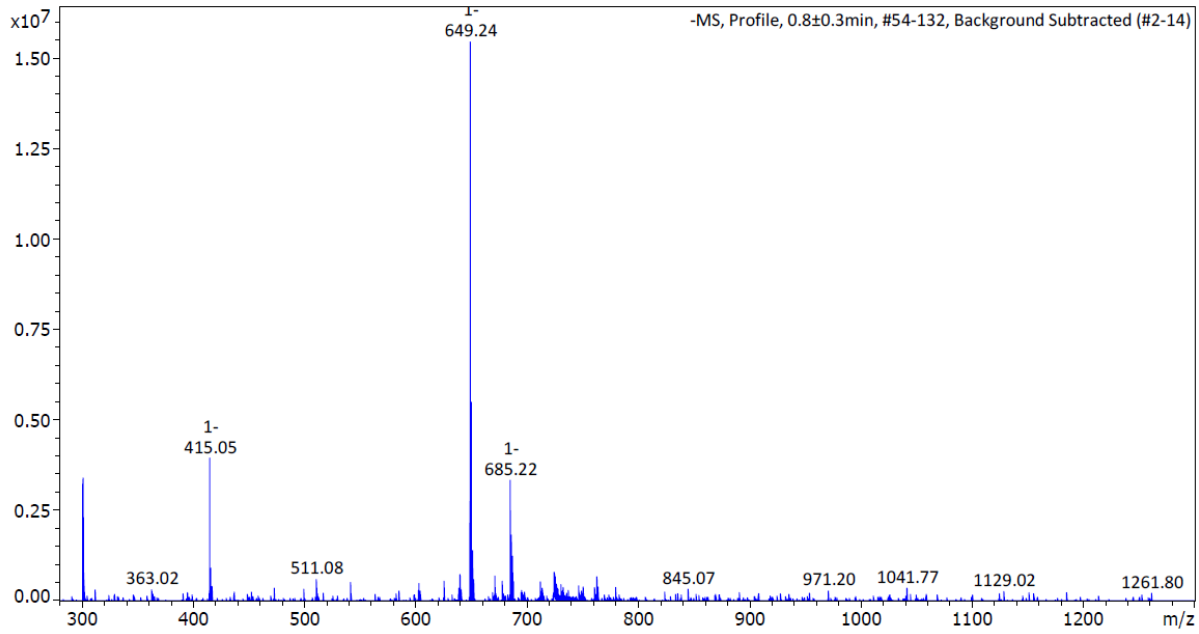

Figure S20. LR-MS (ESI⁻) spectrum of *N*-(4-nitrophenylurea)-*N'*-(methyl)squaramide.

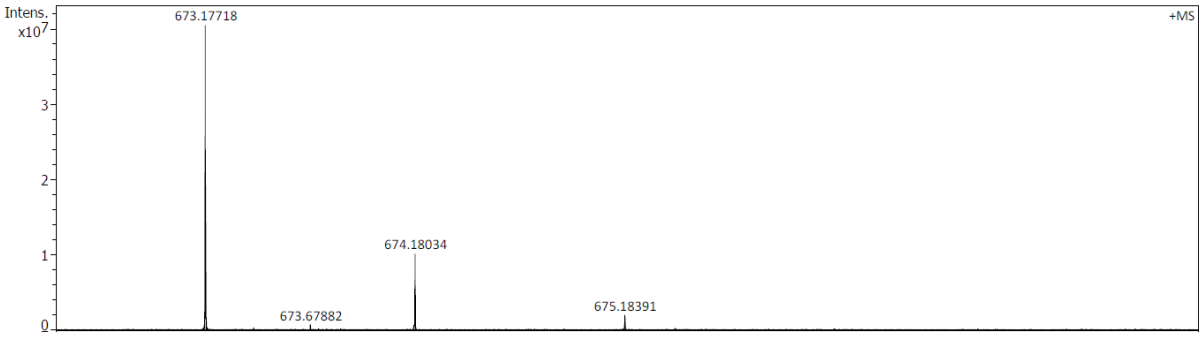

Figure S21. HR-MS (ESI⁺) spectrum of *N*-(4-nitrophenylurea)-*N'*-(methyl)squaramide.

N-(4-nitrophenylthiourea)-*N'*-(methyl)squaramide (4)

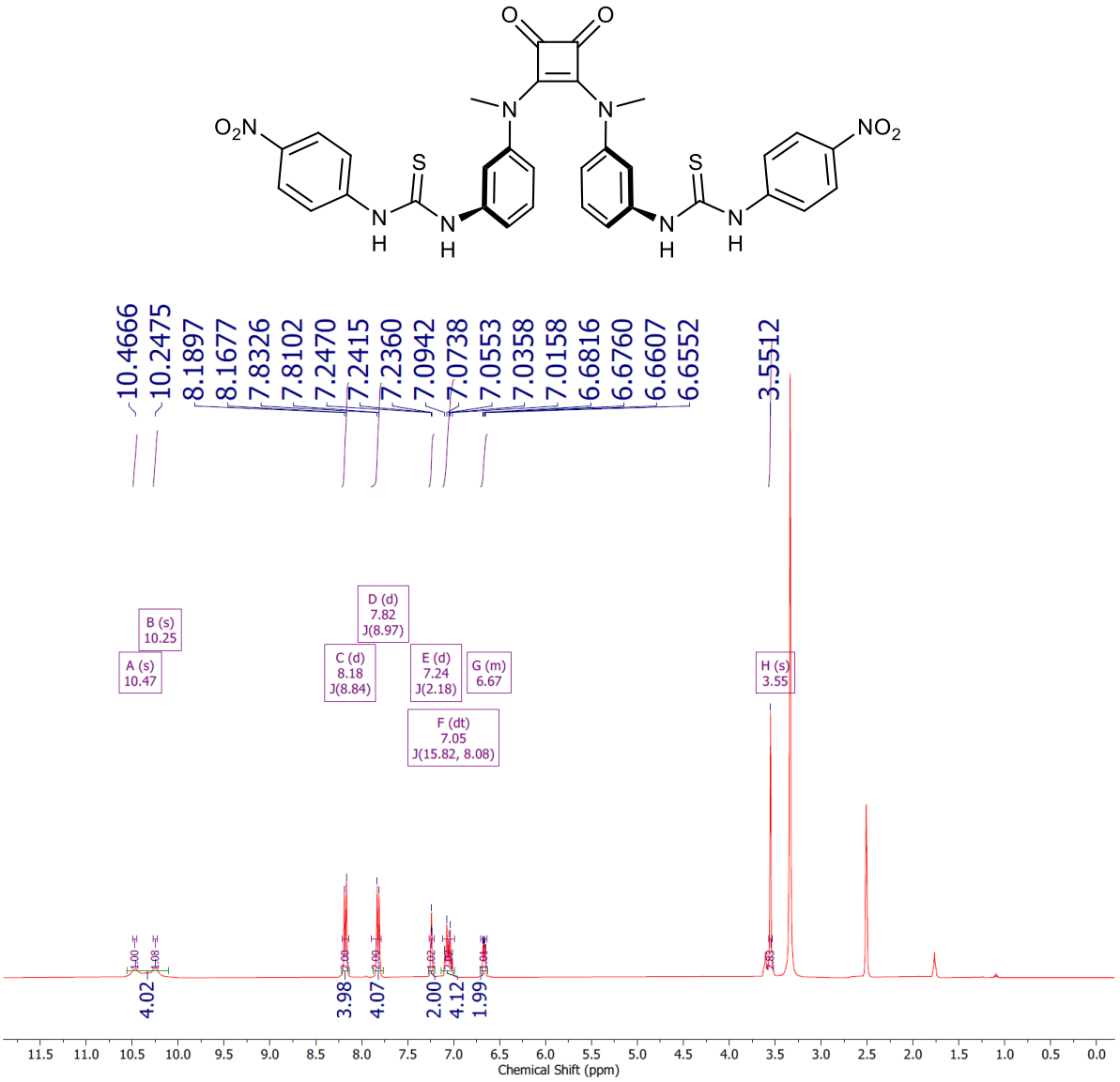

Figure S22. ^{1}H NMR (500 MHz) spectrum of *N*-(4-nitrophenylthiourea)-*N'*-(methyl)squaramide in DMSO-d_6 at 298 K. THF solvent peaks present in spectrum.

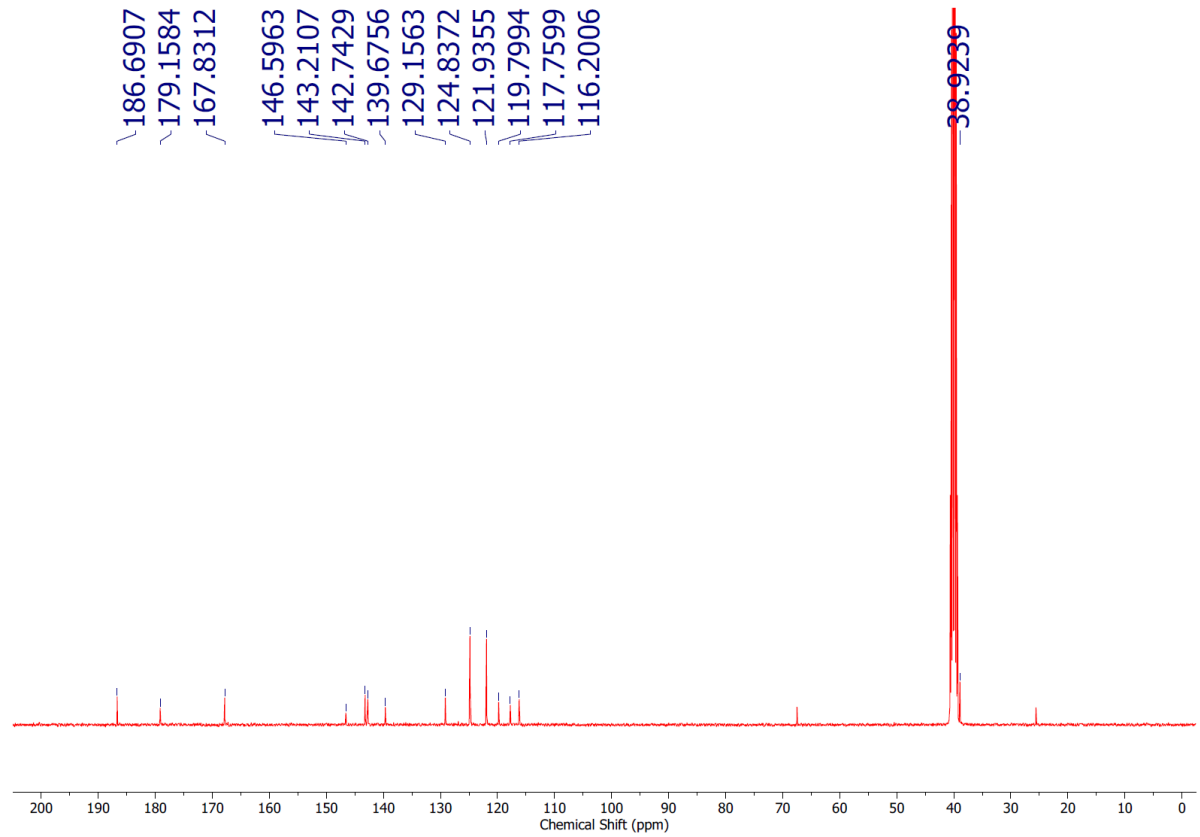

Figure S23. ^{13}C NMR (101 MHz) spectrum of *N*-(4-nitrophenylthiourea)-*N'*-(methyl)squaramide in DMSO-d_6 at 298 K. THF solvent peaks present in spectrum.

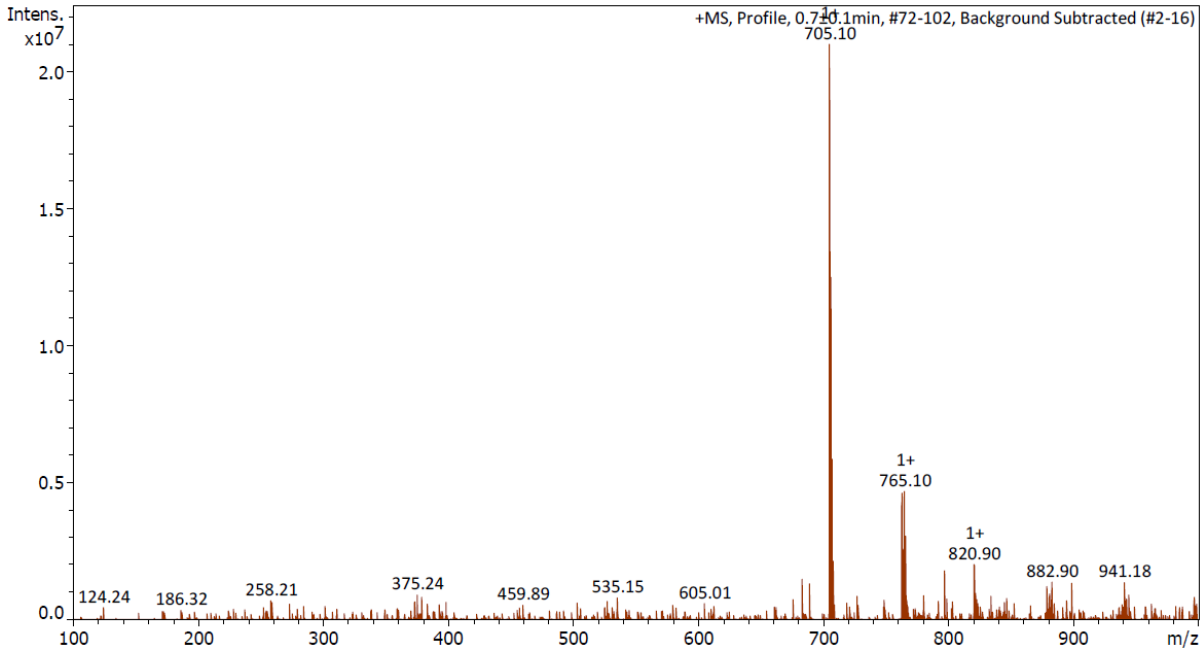

Figure S24. LR-MS (ESI$^+$) spectrum of *N*-(4-nitrophenylthiourea)-*N'*-(methyl)squaramide.

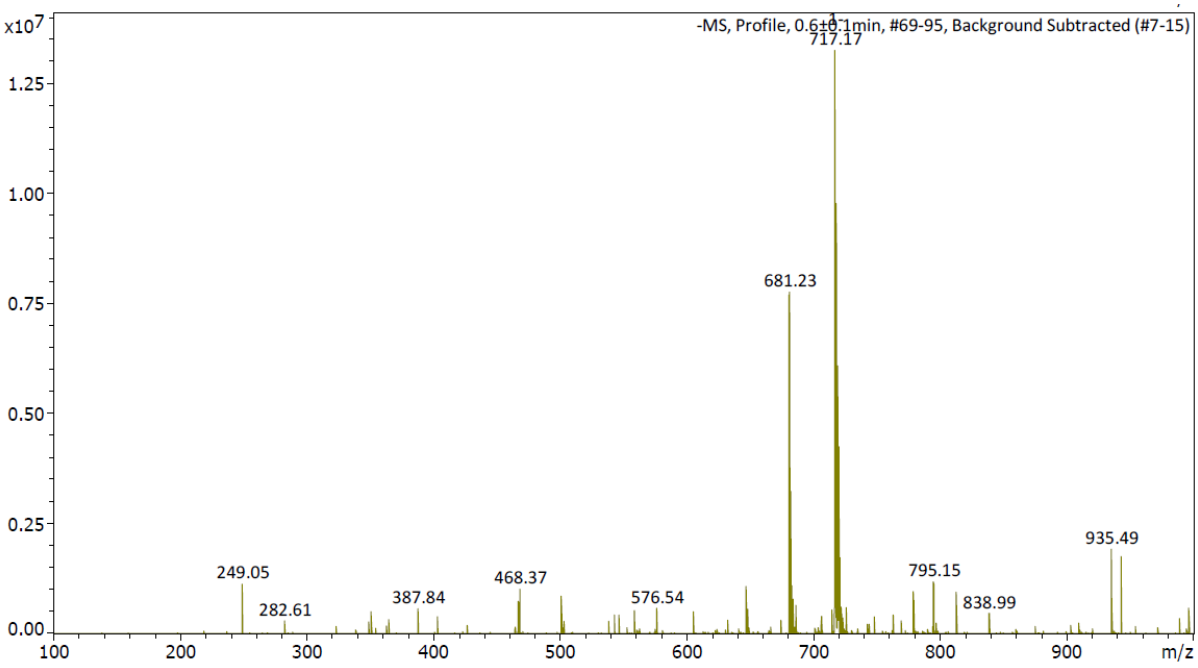

Figure S25. LR-MS (ESI$^-$) spectrum of *N*-(4-nitrophenylthiourea)-*N'*-(methyl)squaramide.

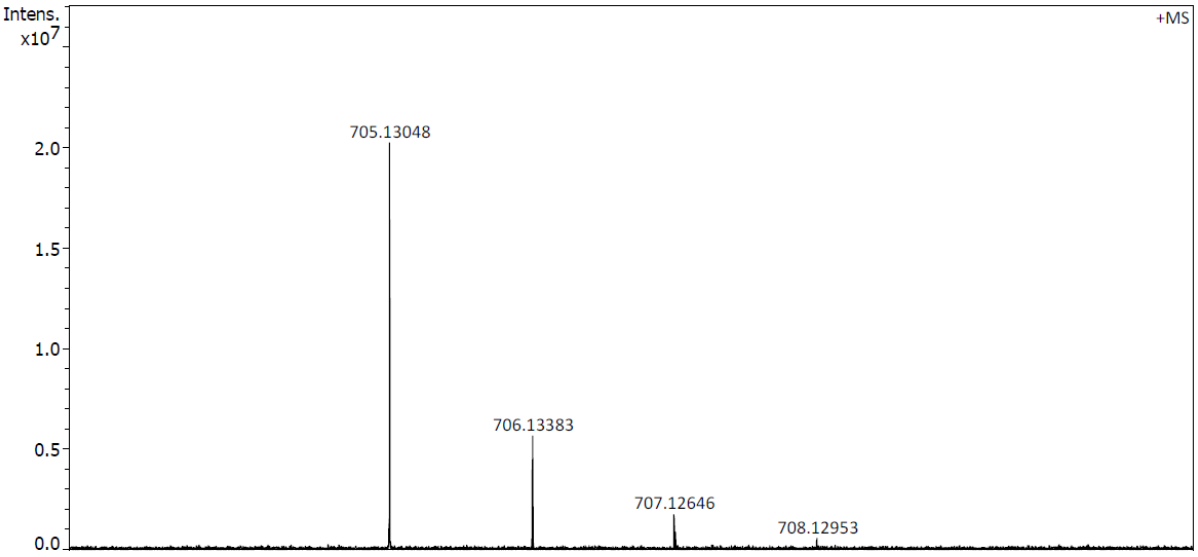

Figure S26. HR-MS (ESI$^+$) spectrum of *N*-(4-nitrophenylurea)-*N'*-(methyl)squaramide.

N-(4-cyanophenyl)-*N'*-(ethoxy)squaramide (11)

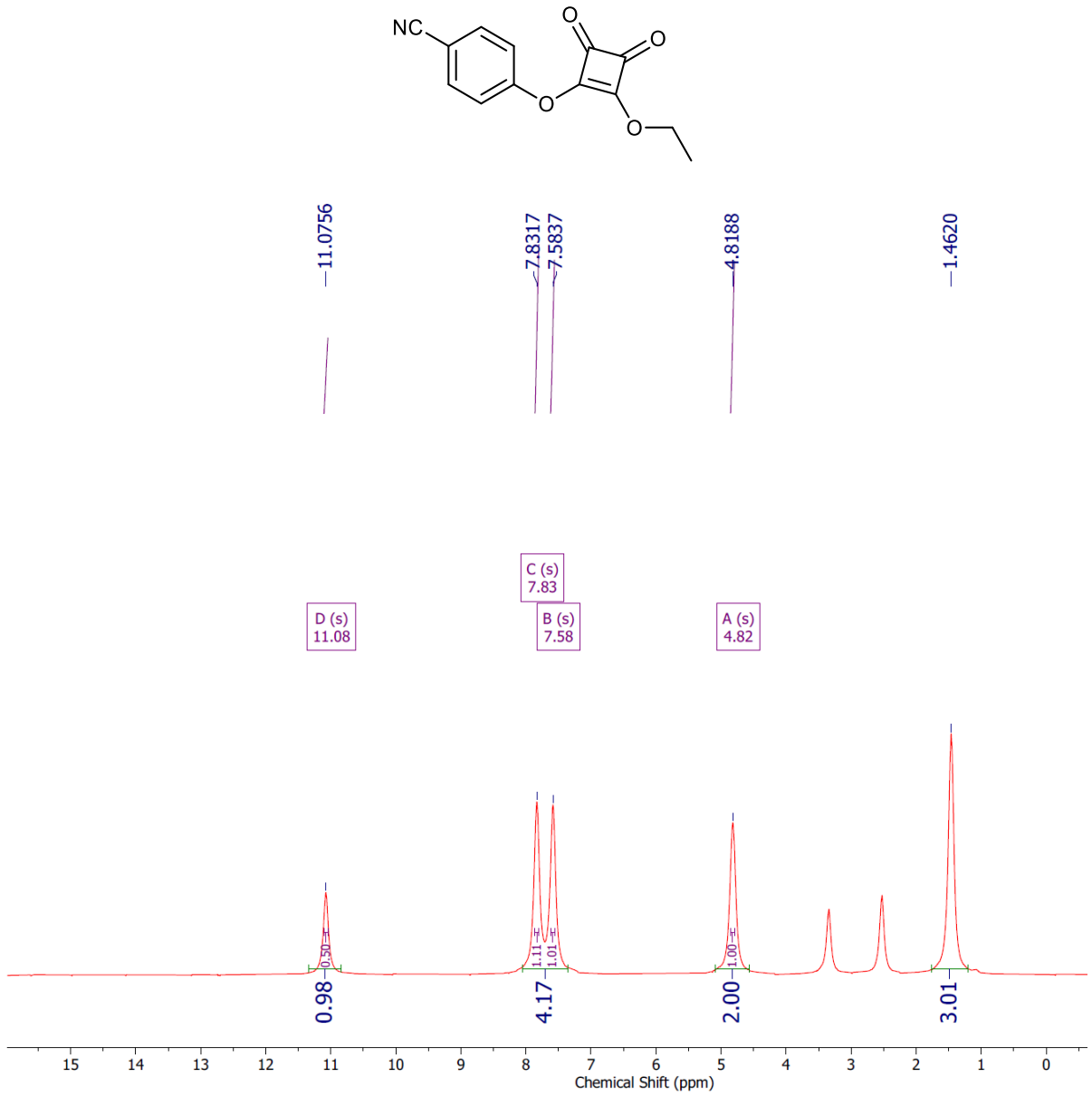

Figure S27. ^{1}H NMR (400 MHz) spectrum of *N*-(4-cyanophenyl)-*N'* (ethoxy)squaramide in DMSO-d_6 at 298 K.

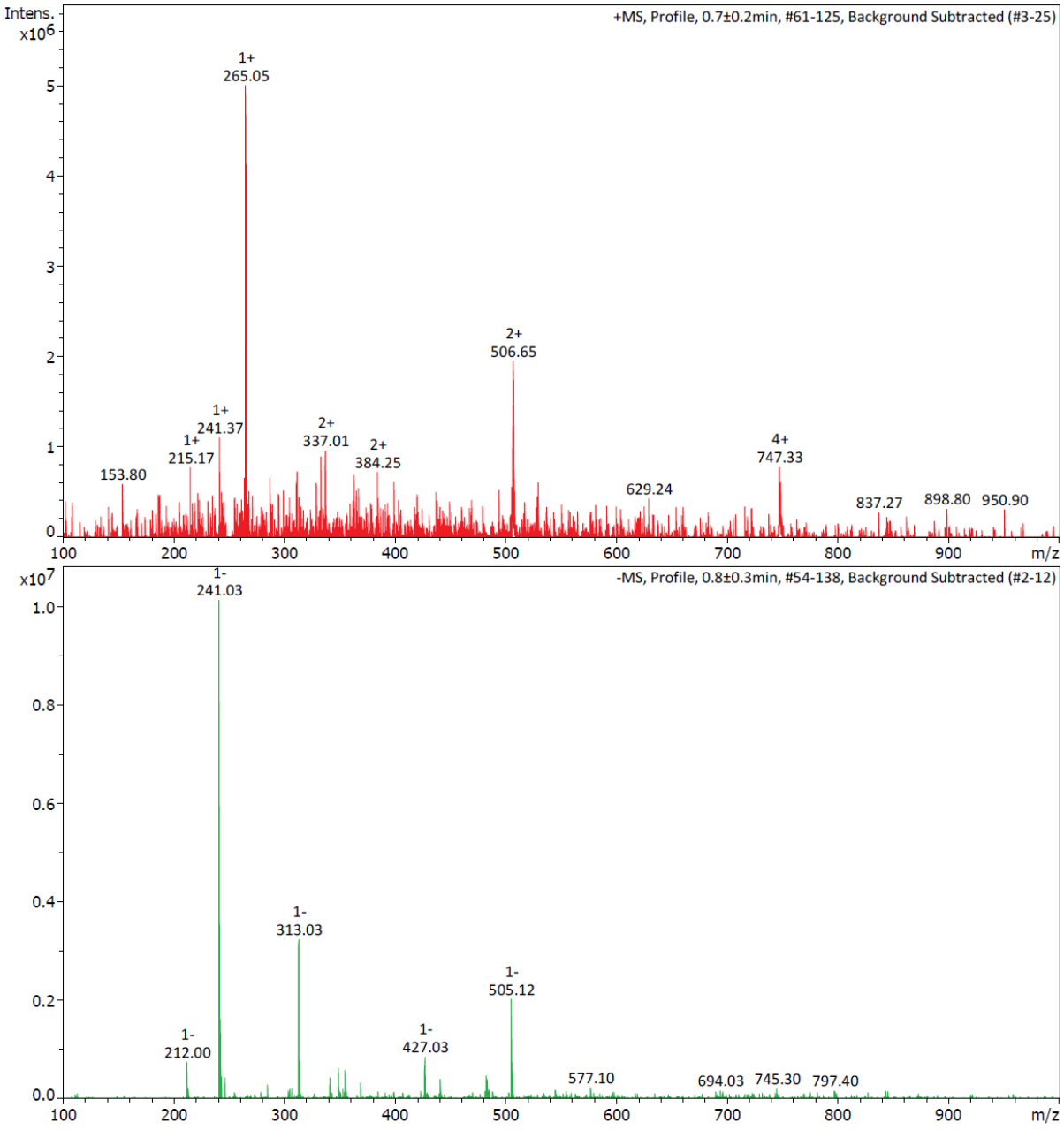

Figure S28. LR-MS (ESI^+ and ESI^-) spectrum of *N*-(4-cyanophenylsquaramide)-*N'*(methyl)squaramide.

N-(4-cyanophenylsquaramide)-*N*′-(methyl)squaramide (5)

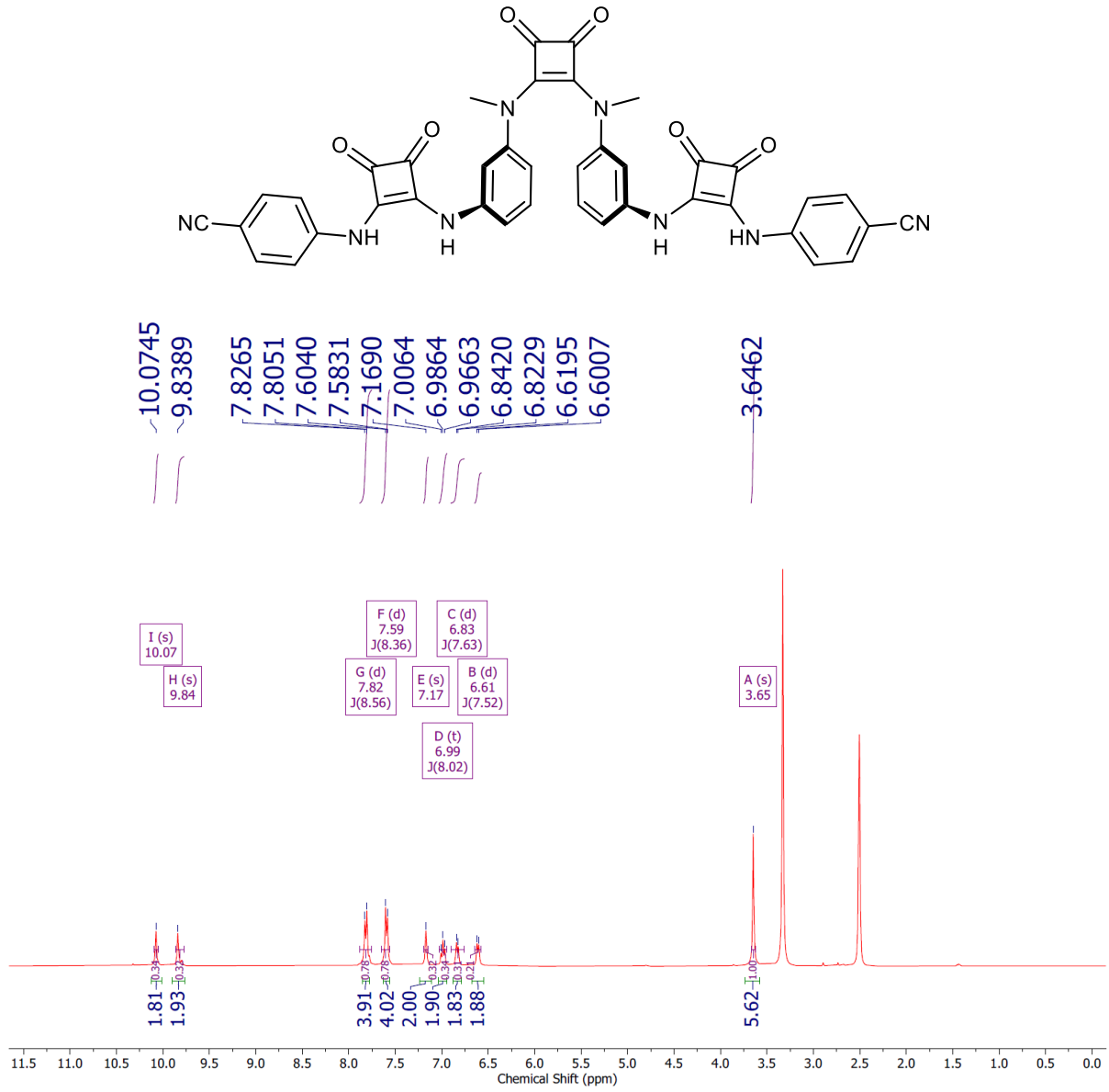

Figure S29. ^{1}H NMR (400 MHz) spectrum of *N*-(4-cyanophenylsquaramide)-*N*′-(methyl)squaramide in DMSO-d_6 at 298 K.

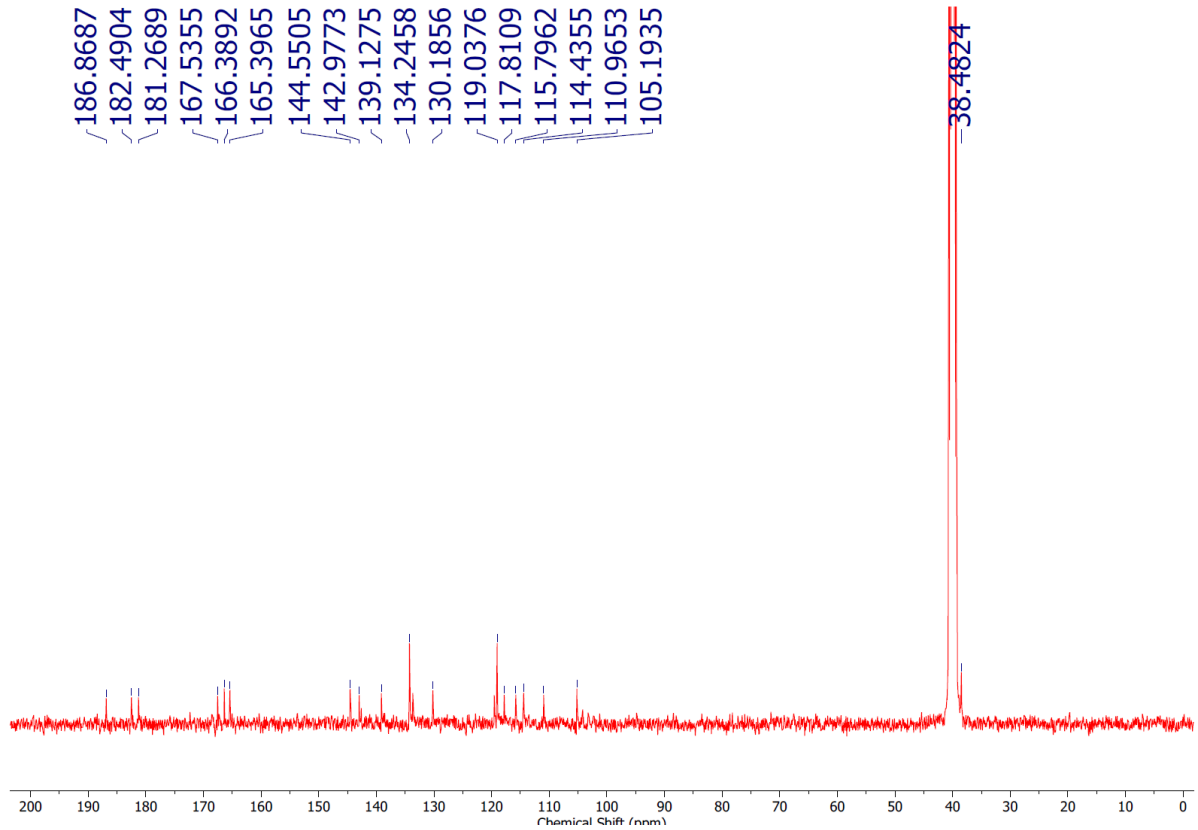

Figure S30. ^{13}C NMR (101 MHz) spectrum of *N*-(4-cyanophenylsquaramide)-*N'*(methyl)squaramide in DMSO-d_6 at 298 K. High noise-to-signal ratio due to very low solubility of compound/ tendency of the compound to precipitate over the timescale of a ^{13}C experiment.

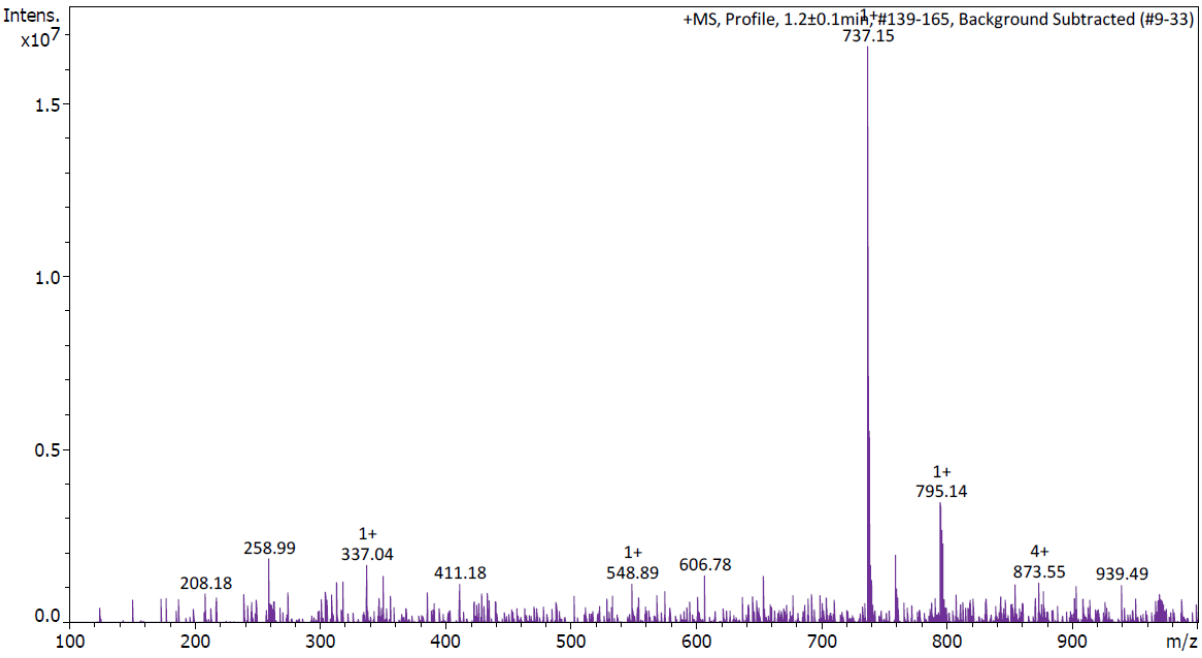

Figure S31. LR-MS (ESI$^+$) spectrum of *N*-(4-cyanophenylsquaramide)-*N'*(methyl)squaramide.

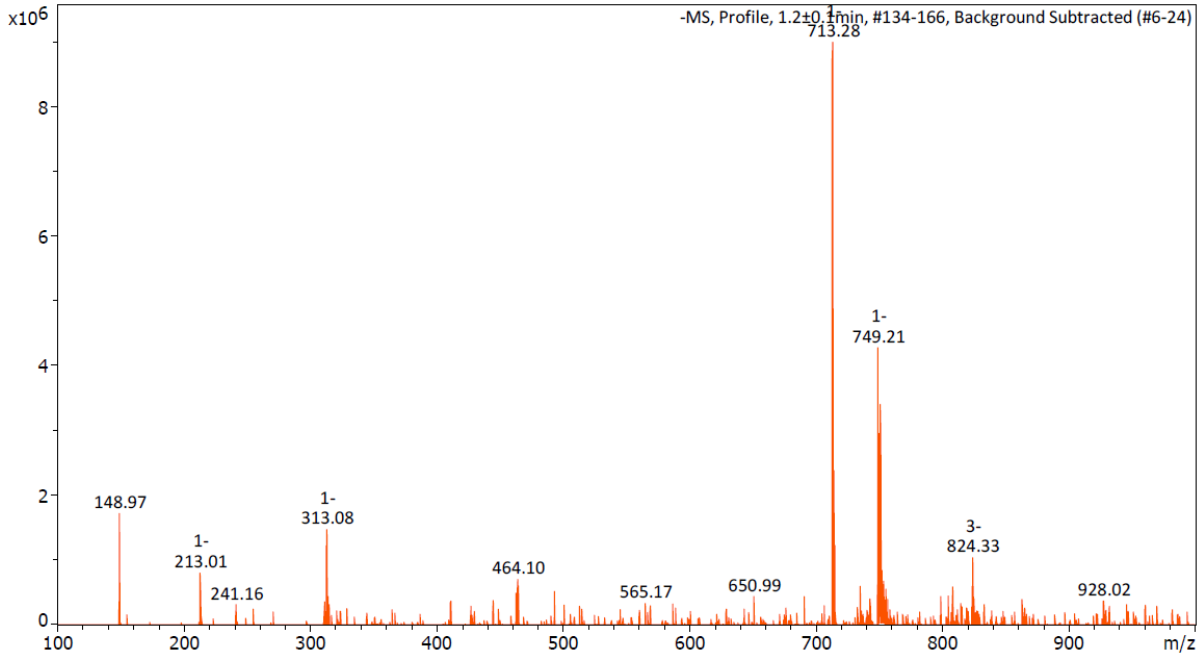

Figure S32. LR-MS (ESI⁻) spectrum of *N*-(4-cyanophenylsquaramide)-*N'* (methyl)squaramide.

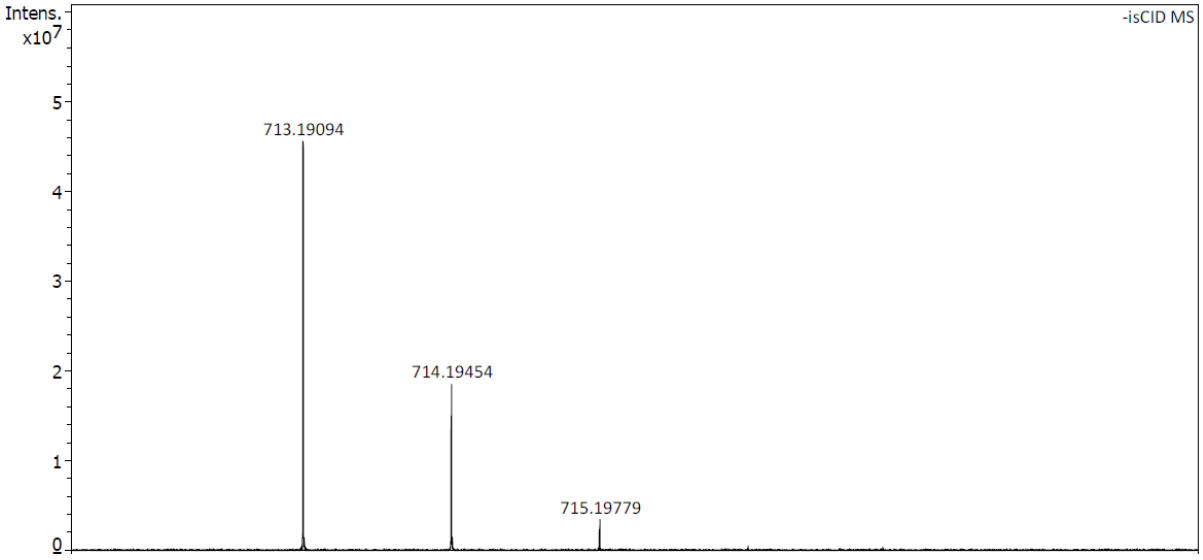

Figure S33. HR-MS (ESI⁻) spectrum of *N*-(4-nitrophenylurea)-*N'*-(methyl)squaramide.

N,N'-(3-aminophenyl)squaramide (12)

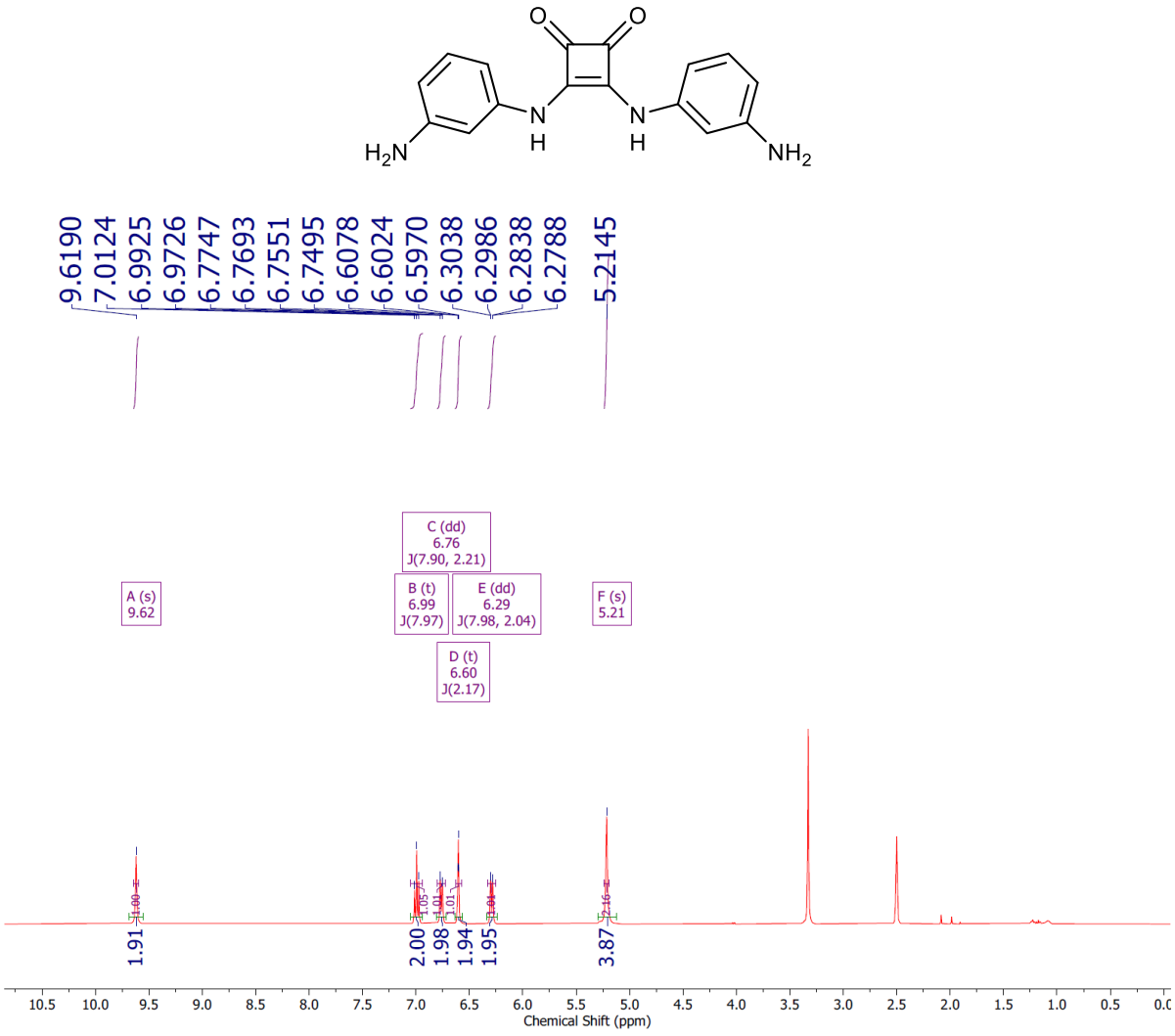

Figure S34. ^{1}H NMR (400 MHz) spectrum of *N,N'*-(3-aminophenyl)squaramide in DMSO-d_6 at 298 K.

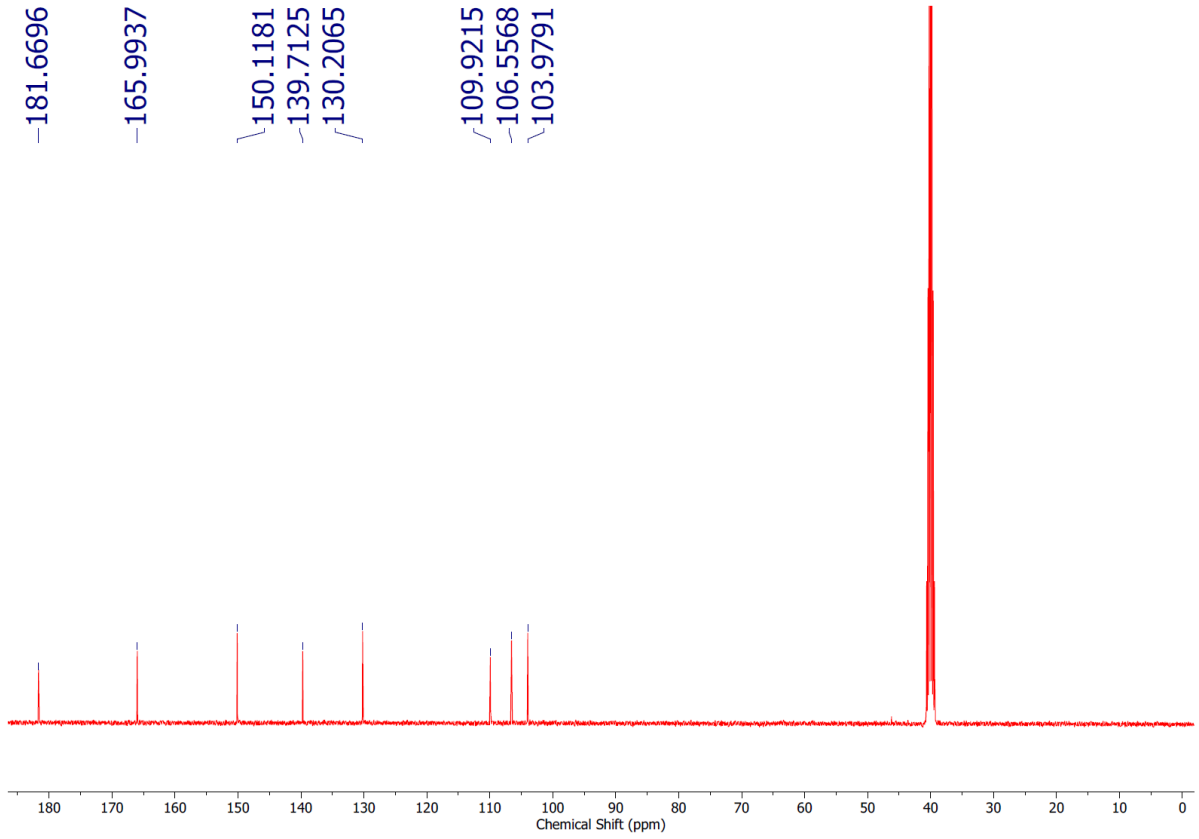

Figure S35. ^{13}C NMR (101 MHz) spectrum of *N,N'*-(3-aminophenyl)squaramide in DMSO-d_6 at 298 K.

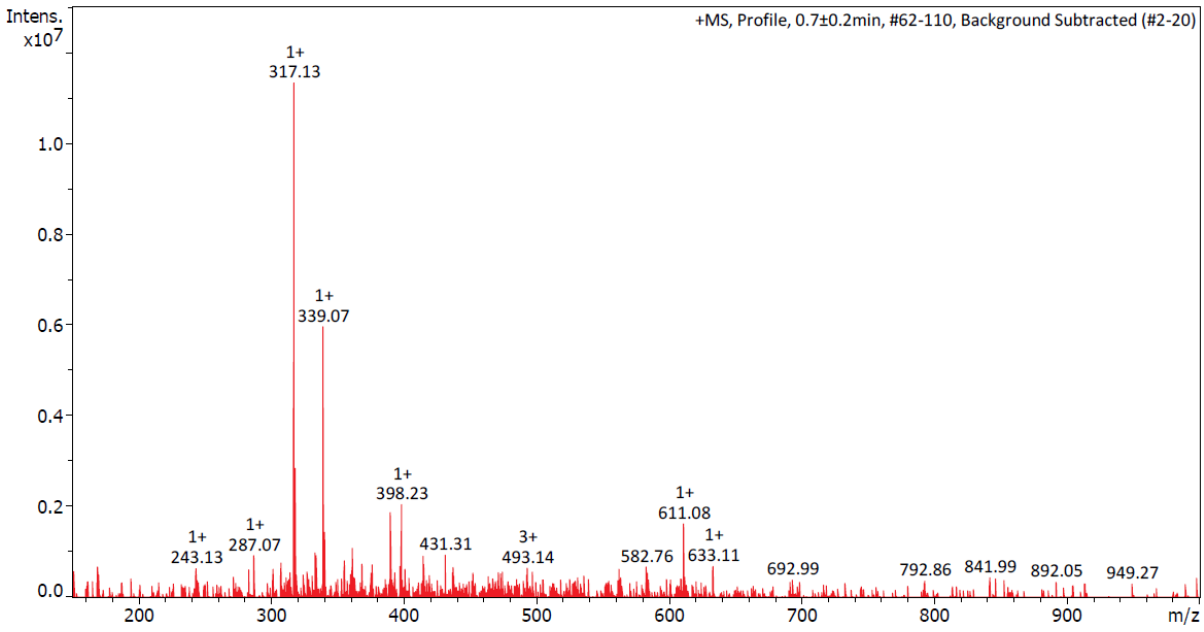

Figure S36. LR-MS (ESI$^+$) spectrum of *N,N'*-(3-aminophenyl)squaramide.

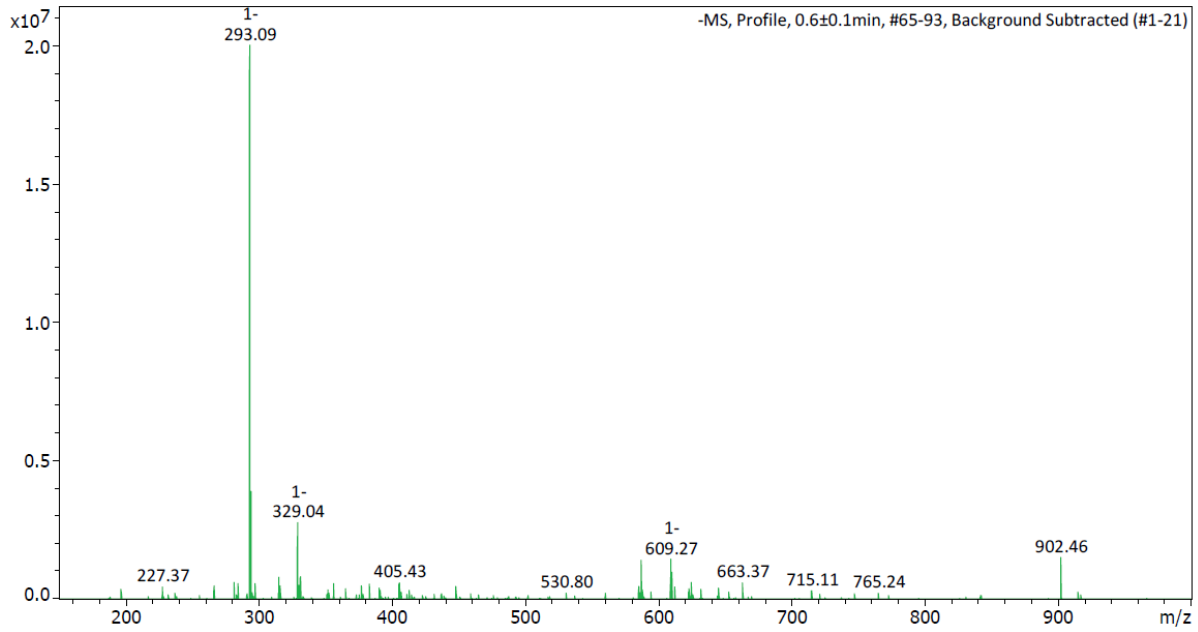

Figure S37. LR-MS (ESI⁻) spectrum of *N,N'*-(3-aminophenyl)squaramide.

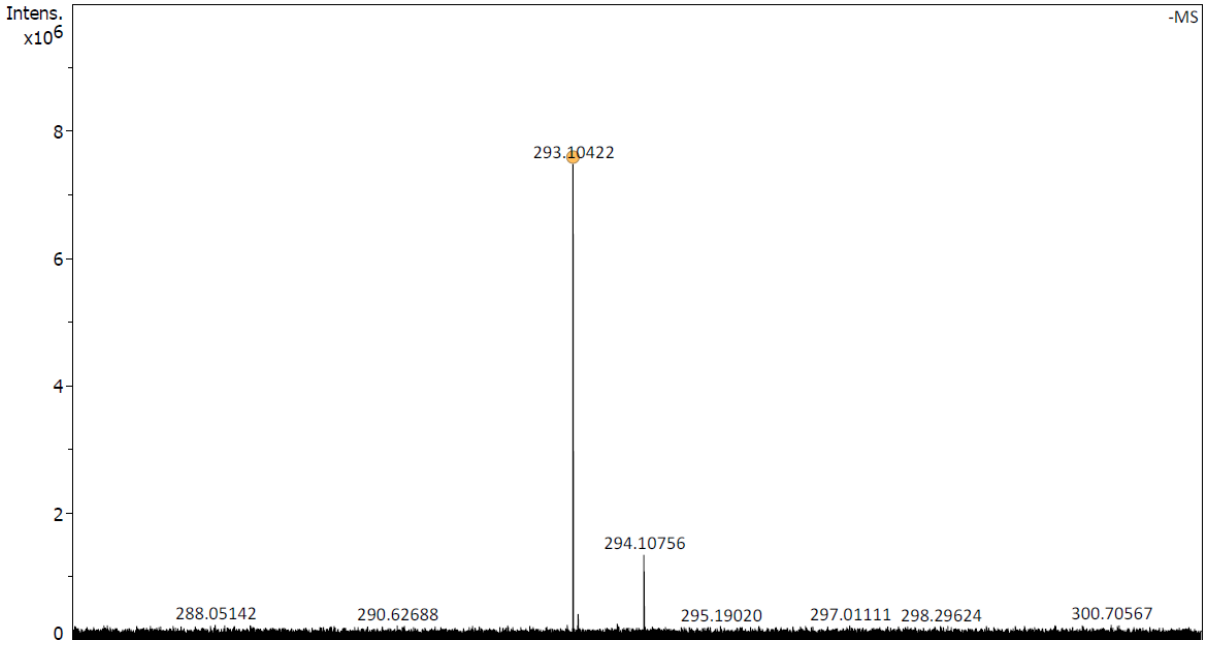

Figure S38. HR-MS (ESI⁻) spectrum of *N,N'*-(3-aminophenyl)squaramide.

N,N'-(4-nitrophenylthiourea)-squaramide (7)

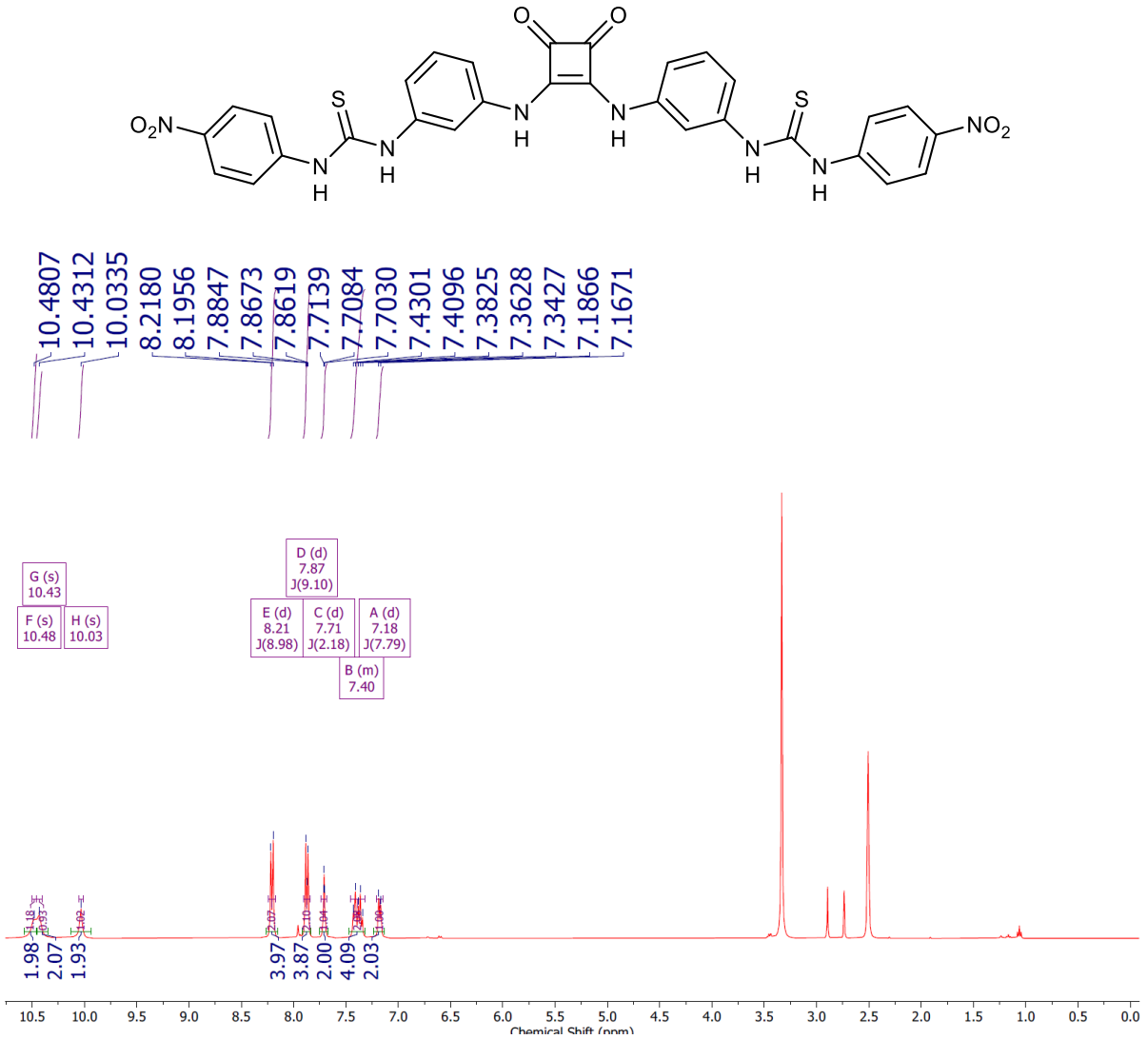

Figure S39. ^{1}H NMR (400 MHz) spectrum of *N,N'*-(4-nitrophenylthiourea)-squaramide in DMSO-d_6 at 298 K. DMF solvent peaks present in the spectrum.

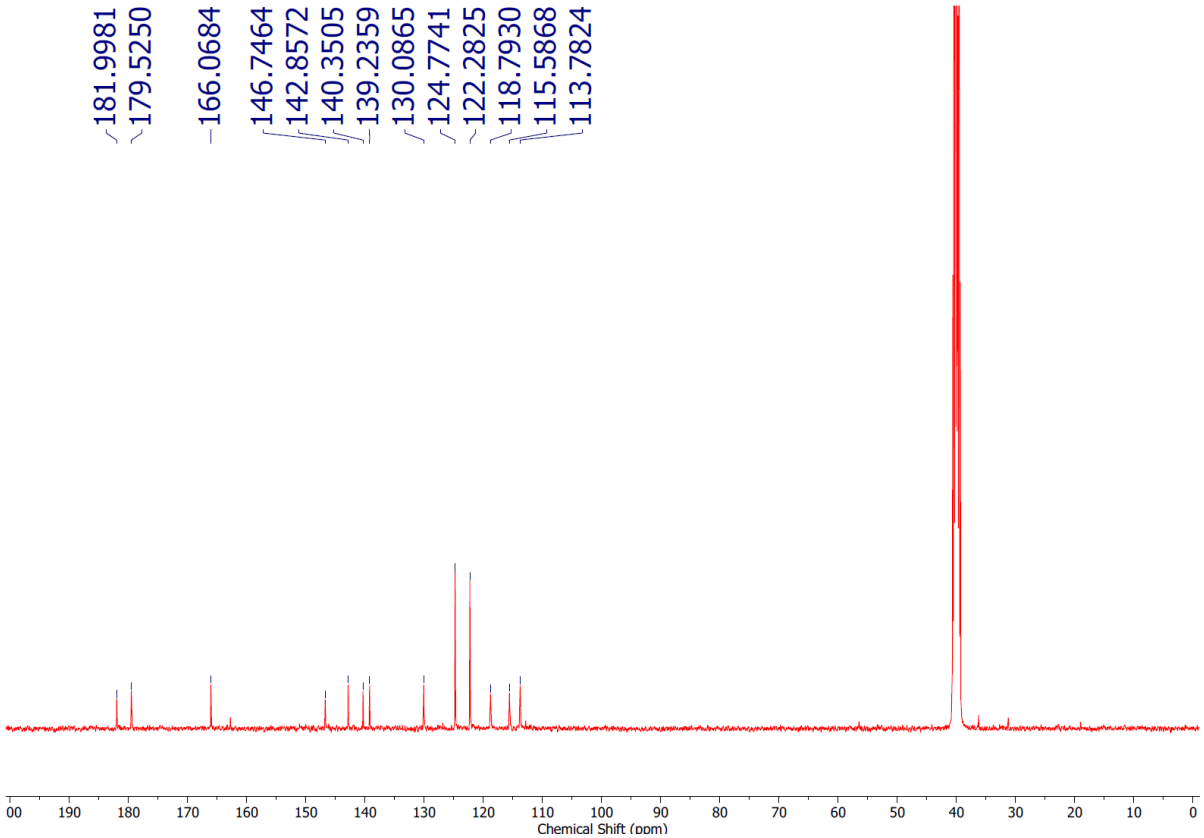

Figure S40. ^{13}C NMR (101 MHz) spectrum of *N,N'*-(4-nitrophenylthiourea)-squaramide in DMSO-d_6 at 298 K. DMF solvent peaks present in the spectrum.

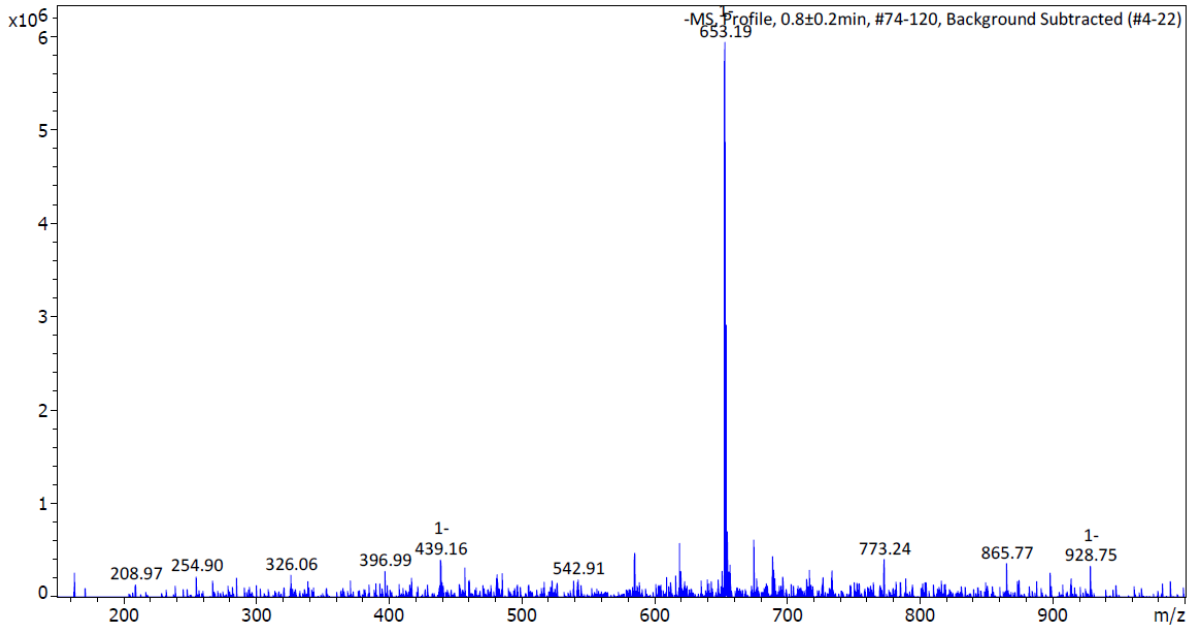

Figure S41. LR-MS (ESI$^-$) spectrum of *N,N'*-(4-nitrophenylthiourea)-squaramide.

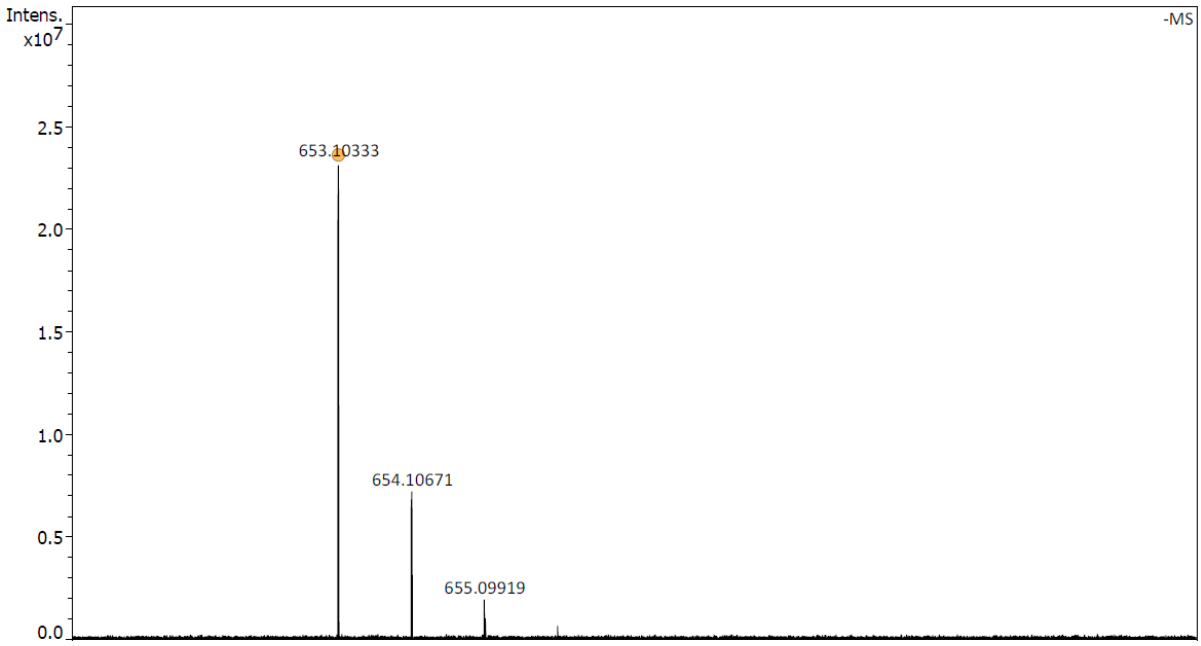

Figure S42. HR-MS (ESI⁻) spectrum of *N,N'*-(4-nitrophenylthiourea)-squaramide.

N,N'-((4-trifluoromethyl)phenyl)squaramide (6)

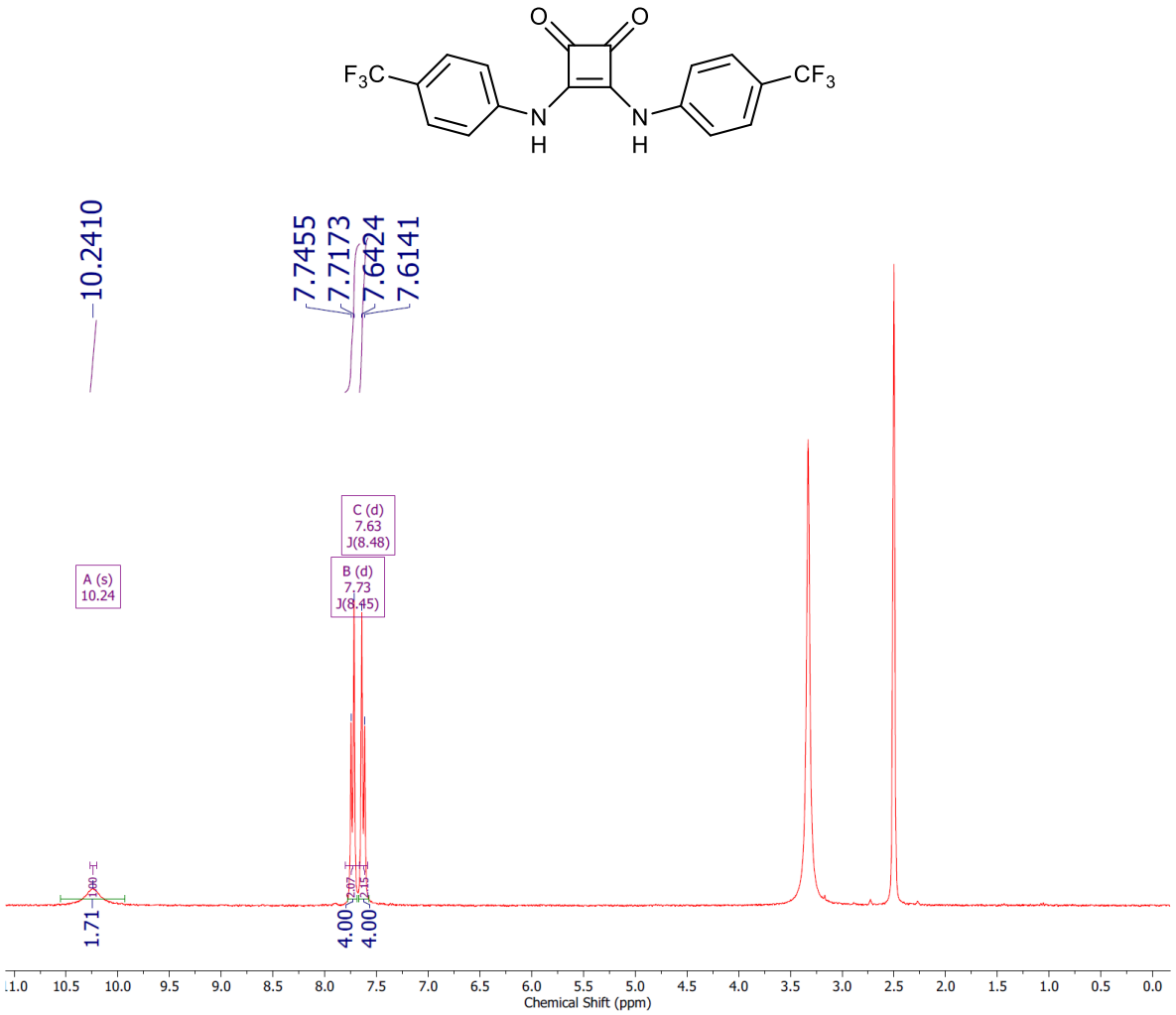

Figure S43. ^{1}H NMR (400 MHz) spectrum of *N,N'*-((4-trifluoromethyl)phenyl)squaramide in DMSO-d_6 at 298 K.

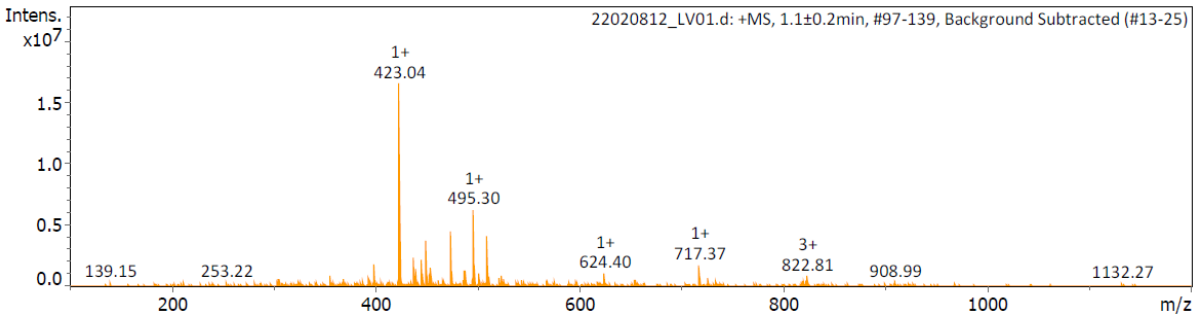

Figure S44. LR-MS (ESI^{+}) spectrum of *N,N'*-((4-trifluoromethyl)phenyl)squaramide.

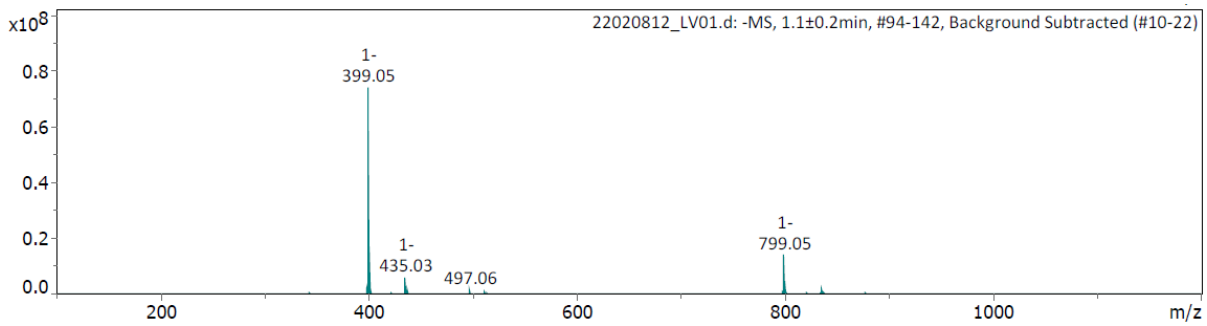

Figure S45. LR-MS (ESI⁻) spectrum of *N,N'*-((4-trifluoromethyl)phenyl)squaramide.

4.2 Evidence of conformational shift

Examining the aromatic regions of the ^{1}H-NMR spectra of compounds **4** and **7** provides evidence for a conformational shift upon dimethylation of the central squaramide.

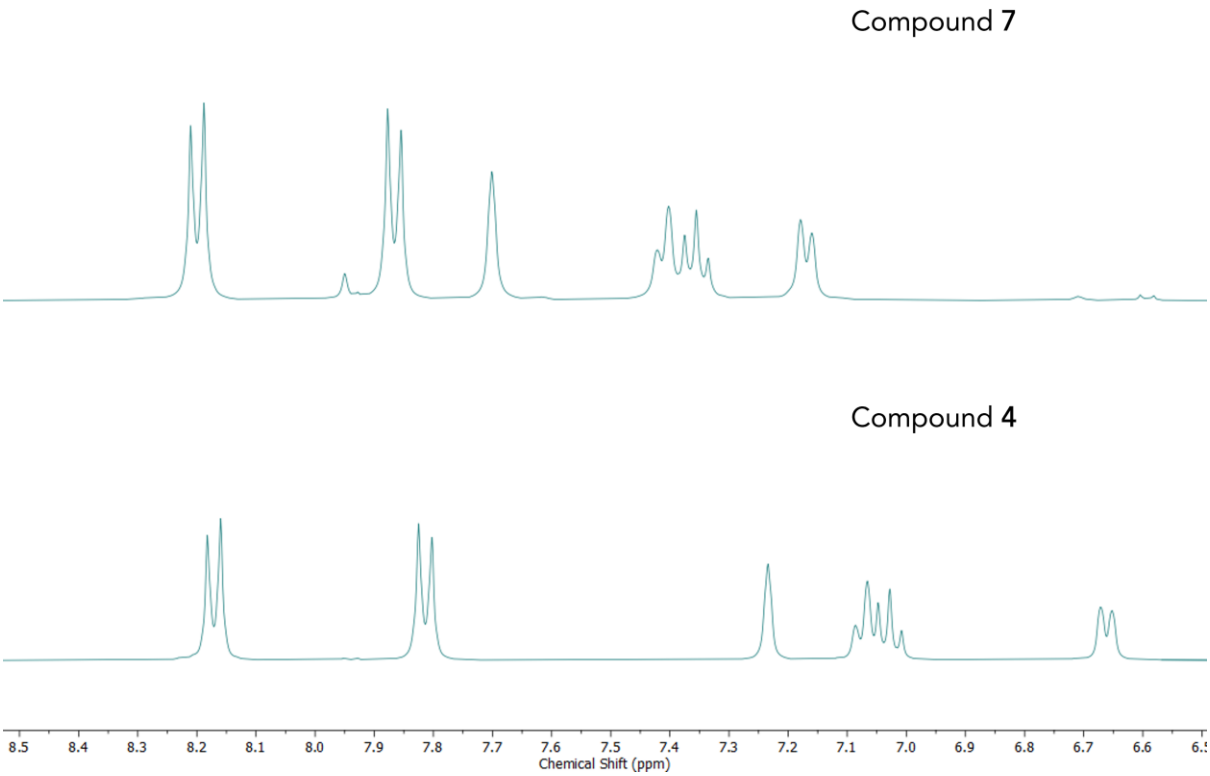

Figure S46. Stack plot showing the aromatic region of the ^{1}H-NMR spectra of compounds 7 (above) and **4** (below).

The two doublet resonances at ~8.22-8.15 ppm and ~7.85-7.78 ppm can be attributed to the distal *para*-nitrophenyl rings, whereas the three remaining resonances located upfield to the doublets can be attributed to the phenyl ring closest to the squaramide. Distinct differences can be identified when comparing the spectrum of the unmethylated (**7**) and dimethylated (**4**) compounds. A large upfield shift is present in the protons associated with

the internal phenyl ring of between $\Delta\delta$ = 0.33−0.51 ppm. This is likely a consequence of the aromatic stacking of the phenyl groups in compound 4 due to the conformational shift to a cis-cis orientation.[2] Such occurrences are commonly observed in π-π stacking interactions, attributed to ring current effects. In this scenario, the strongly shielded region above and below an aromatic ring induces a shielding effect on the opposing ring when adopting a parallel-planar geometry.[3]

5. Experimental Results Tables

5.1 Proton-NMR Titration Experiments

Table S1. Summary of the stability constants (M^{-1}) and covariance of fits for the complexation of receptors 1–5 and Cl^- (as TBA salt) in DMSO-d_6 at 298 K.

Cpd	K_{11} [a] (M^{-1})	K_{12} [a] (M^{-1})	α [b]	Cov_{fit} (1:2)	K_a [a] (M^{-1})	Cov_{fit} (1:1)	$F\,Cov_{fit}$ [c]
1	158	14	0.35	3.6×10^{-5}	47	2.3×10^{-3}	64
2	255	10	0.16	1.1×10^{-3}	55	1.3×10^{-2}	12
3	240	26	0.43	2.6×10^{-4}	78	6.8×10^{-4}	3
4	463	24	0.21	3.3×10^{-4}	92	1.8×10^{-3}	5
5	- [d]	-	-	-	231	2.8×10^{-3}	-

[a] Errors < 10%. [b] The interaction parameter (α) is calculated by multiplying K_{12} by 4 and dividing by K_{11}; a value of α < 1 is indicative of negative cooperativity.[4] [c] The factor of covariance of fit ($F\,Cov_{fit}$) calculated by dividing Cov_{fit} 1:1 by Cov_{fit} 1:2; a value greater than 5 indicates a 1:2 binding model is favoured. [d] Compound **5** could not be fit to a 1:2 model.

Table S2. Summary of the stability constants (M^{-1}) and covariance of fits for the complexation of receptors 1–5 and Cl^- (as TBA salt) in CD_3CN /2% DMSO-d_6 at 298 K.

Cpd	K_{11} [a] (M^{-1})	K_{12} [a] (M^{-1})	α [b]	Cov_{fit} (1:2)	K_a [a] (M^{-1})	Cov_{fit} (1:1)	$F\,Cov_{fit}$ [c]
1	24000	43	0.007	7.1×10^{-5}	1450	9.1×10^{-3}	128
2	40000	28	0.003	1.8×10^{-4}	1300	1.0×10^{-2}	56
3	- [d]	-	-	-	-	-	-
4	104000	47	0.002	8.5×10^{-5}	1500	9.5×10^{-3}	112
5	- [d]	-	-	-	-	-	-

[a] Errors < 20%. [b] The interaction parameter (α) is calculated by multiplying K_{12} by 4 and dividing by K_{11}; a value of α < 1 is indicative of negative cooperativity.[4] [c] Factor of covariance of fit ($F\,Cov_{fit}$) calculated by dividing Cov_{fit} 1:1 by Cov_{fit} 1:2; a value greater than 5 indicates a 1:2 binding model is favoured. [d] Insoluble in solvent mixture.

5.2 Vesicular Anion Transport Assay Experiments

Table S3. EC_{50} values and Hill coefficients (n) from the Cl^-/NO_3^- exchange assay, maximum transport rate at a 0.5 mol% loading of the transporter, and calculated lipophilicity values (*c*log P).

Compound	EC_{50} [a] (mol%)	Hill coefficient (n)	k_{ini} [b] (% s^{-1})	*c* log *P* [c]
1	0.2 ± 0.03	0.8 ± 0.07	1.37 ± 0.07	3.88
2	0.06 ± 0.003	1.2 ± 0.06	2.51 ± 0.9	4.55
3	0.12 ± 0.006	0.9 ± 0.04	0.87 ± 0.04	4.54
4	0.03 ± 0.005	1.3 ± 0.2	1.61 ± 0.07	5.26
5	0.33 ± 0.02	1.4 ± 0.08	0.35 ± 0.01	4.71

[a] EC_{50} calculated at 270 s, shown as receptor:lipid molar percentage. [b] Maximum initial rate calculated at a loading of 0.5 mol% by fitting efflux plots to an exponential decay function. [c] Average *c*log *P* values calculated using VCCLab.[5, 6]

Table S4. Initial rates and electroneutral factor coefficient (E_{nuet}) for compounds 1−5 from the cationophore-coupled ISE assay.

Compound	k_{ini}[a] w/ monensin (% s^{-1})	k_{ini}[a] w/ valinomycin (% s^{-1})	E_{neut}[b]
1	0.74 ± 0.0001	0.15 ± 0.02	4.8
2	1.27 ± 0.04	0.14 ± 0.09	8.9
3	0.83 ± 0.009	0.09 ± 0.01	9.5
4	0.95 ± 0.04	0.19 ± 0.06	4.9
5	0.12 ± 0.009	0.10 ± 0.04	1.9

[a] Maximum initial rate calculated at a loading of 1 mol% by fitting efflux plots to an exponential decay function. [c] Electroneutral factor coefficient calculated by dividing k_{ini} w/ monensin by k_{ini} w/valinomycin.

Table S5. EC_{50} values and Hill coefficients (n) for Compound 1–5 with the NaCl HPTS assay, maximum transport rate at a 0.05 mol% transporter loading.

Compound	EC_{50} [a] (mol%)	Hill coefficient (n)	k_{ini} [b] (10^{-2} % s^{-1})
1	0.0045 ± 0.002	1.3 ± 0.3	4.13 ± 1.0
2	0.0029 ± 0.001	1.3 ± 0.3	5.29 ± 0.8
3	0.0023 ± 0.004	1.2 ± 0.8	5.14 ± 0.4
4	0.0013 ± 0.002	1.1 ± 0.6	6.03 ± 0.7
5	0.0047 ± 0.0005	1.2 ± 0.1	2.74 ± 0.1
6	0.0030 ± 0.0002	0.9 ± 0.04	6.86 ± 0.04

[a] EC_{50} calculated at 200 s, shown as receptor:lipid molar percentage. [b] Maximum initial rate calculated at a loading of 0.05 mol% by fitting efflux plots to an exponential decay function.

6. Proton NMR Titration Anion Binding Studies

6.1 Overview and Procedures

Proton NMR titrations were performed on a Bruker Avance DPX 400 spectrometer. For NMR titrations with chloride, a constant host concentration was maintained (2.0–2.5 mM) using a prepared host solution to dissolve the guest, as tetrabutylammonium (TBA) chloride, to make the guest stock solution. Over the course of the titration, Hamiltonian Microlitre syringes were used to add aliquots of the guest stock solution to the NMR sample of the host solution. Chloride was added as the TBA salt, purchased from Merck, after being dried under a high vacuum (< 1.0 mmHg) for 24 h. Stock solutions of the host were prepared in a relevant solution to the experiment. The host stock solutions (600 µL) were transferred to an air-tight screwcap NMR sample tube (5 mm ID), and the same host stock solution was used to prepare the standard guest titrant solutions containing either 0.1 M or 1 M of TBACl. This ensured a constant concentration of the host for the duration of the titration experiment.

Over the course of the titration, small aliquots (2–200 µL) of the standard guest solution were added to the host solution in the NMR tube. For each titration, 16–20 data points were collected. The number of equiv. of guest present at the end of each titration is labelled in the stacked plots. Before collecting each data point, an aliquot of the standard guest solution was added, and the sample was thoroughly mixed in the NMR tube. The system was allowed to equilibrate for up to 2 min inside the NMR probe before the spectra were collected.

Throughout each titration experiment, all parameters of the NMR spectrometer remained constant.

In all cases, the proton resonances were monitored for changes in chemical shift. When possible, two or more resonances were followed, allowing several data sets to determine the association constant (Ka). Global fitting considers all data sets simultaneously and improves the quality of the non-linear curve fitting. The supramolecular.org web applet was used to fit the titration data with chloride to a 1:1 or 1:2 host:guest binding model.[4] Titrations were performed in two different solvent mixtures (100% DMSO-d_6 and CD_3N-d_3 / 2% DMSO-d_6) to provide a complete picture of the coordination events occurring between this family of molecules and multiple chloride guests.

6.2 Titration Data with TBACl Guest

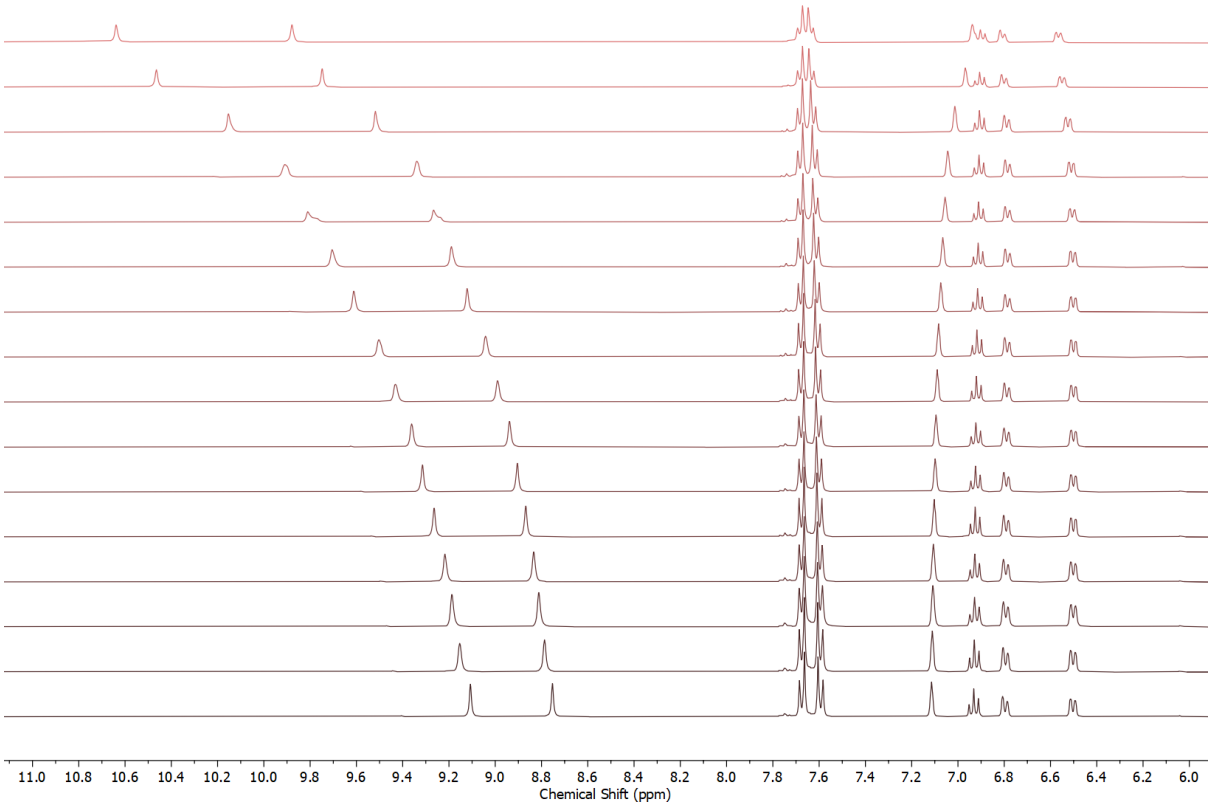

Figure S47. ^{1}H NMR titration spectra as a stack plot for **1** (2.5 mM) + TBACl (0−100 equiv.) in DMSO-d_6 at 298 K.

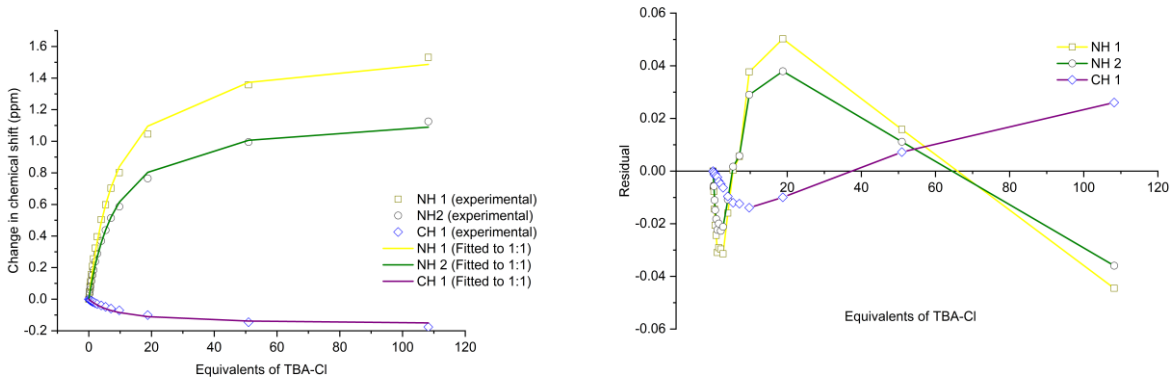

Figure S48. The fitted binding isotherm of 1 + TBACl in DMSO-d6 shows the change in the chemical shift of NH protons fitted to the 1:1 binding model (left). K_a = 47 M^{-1}. Residual plot showing the random error obtained from the binding isotherm fitting (right). Covariance of fit (cov_{fit}) = 2.3 x 10^{-3}. HG values (NH 1 = 1.60, NH 2 = 1.17, CH 1 = -0.16). Link to Bindfit fitting: http://app.supramolecular.org/bindfit/view/351d4b9d-b954-43bf-bc8c-3920466e4cdc.

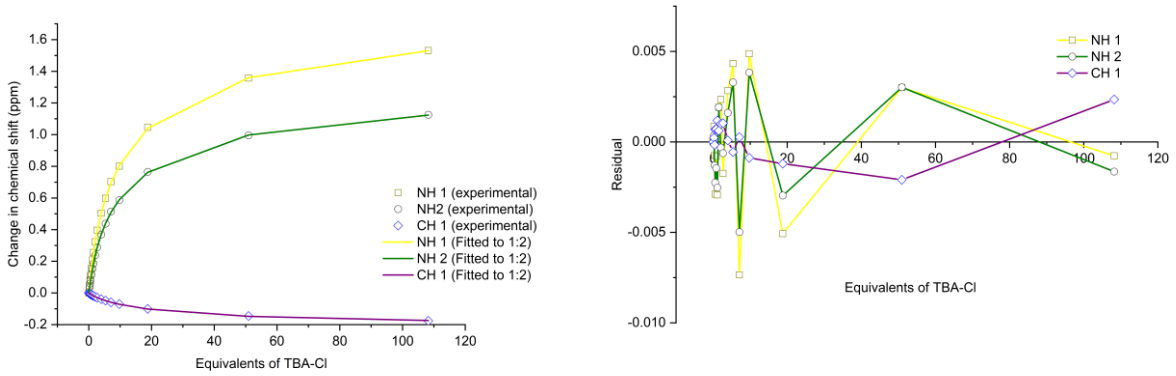

Figure S49. Fitted binding isotherm of **1** + TBACl in DMSO-d_6 showing the change in chemical shift of NH protons fitted to the 1:2 binding model (left). K_{11} = 158 M^{-1}, K_{12} = 14 M^{-1}. Residual plot showing the random error obtained from the binding isotherm fitting (right). Covariance of fit (cov_{fit}) = 3.6 x 10^{-5}. HG values (NH 1 = 0.74, NH 2 = 0.54, CH 1 = -4.9 x 10^{-2}). HG2 values (NH 1 = 1.74, NH 2 = 1.28, CH 1 = -0.21). Link to Bindfit fitting: http://app.supramolecular.org/bindfit/view/3c394bcf-28ab-4b14-94aa-0c623aee361b.

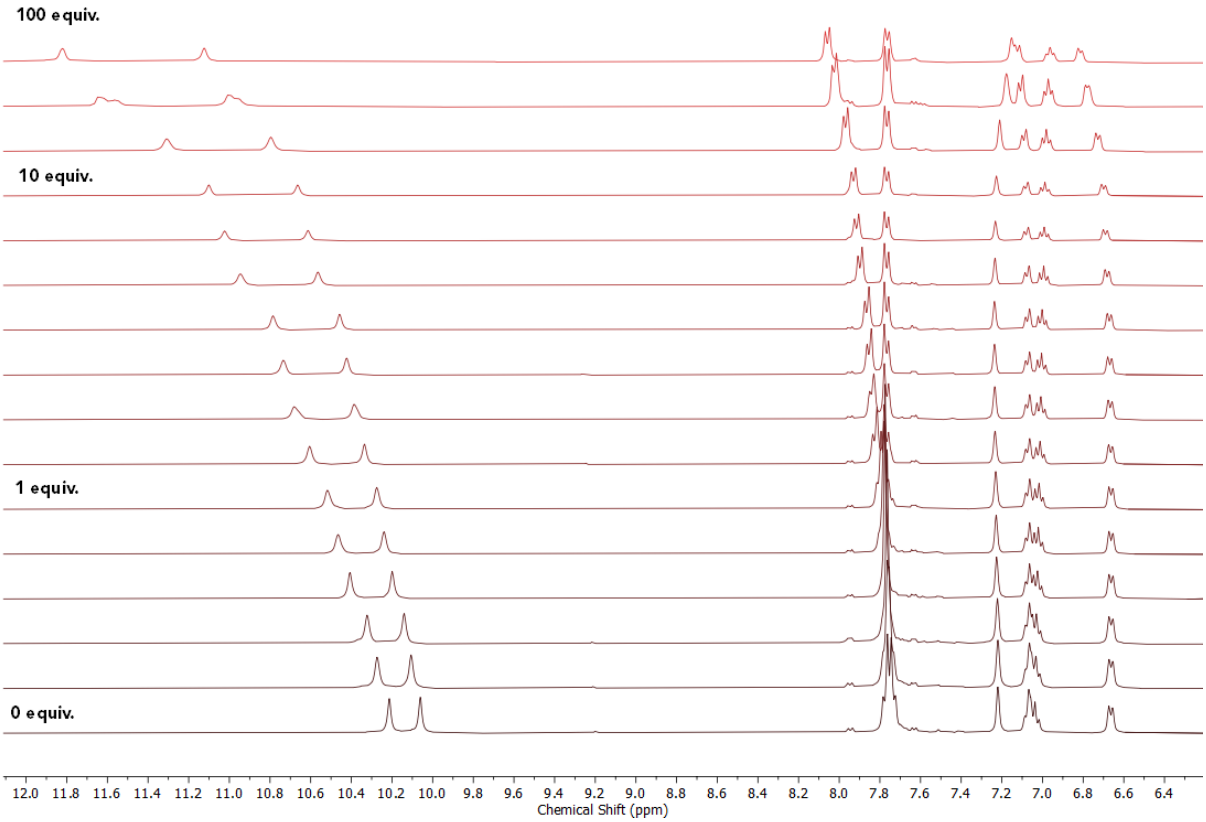

Figure S50. ^{1}H NMR titration spectra as a stack plot for **2** (2.5 mM) + TBACl (0–100 equiv.) in DMSO-d_6 at 298 K.

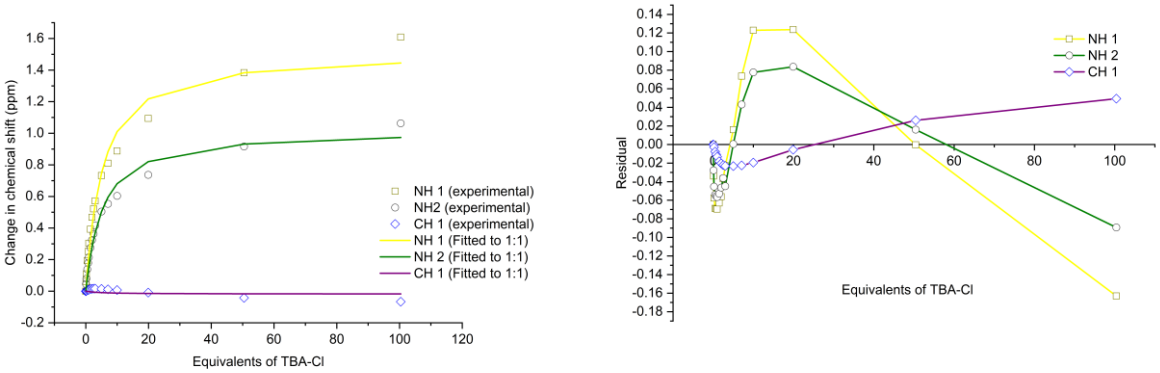

Figure S51. Fitted binding isotherm of **2** + TBACl in DMSO-d_6 showing the change in chemical shift of NH protons fitted to the 1:1 binding model (left). K_a = 55 M^{-1}. Residual plot showing the random error obtained from the binding isotherm fitting (right). Covariance of fit (cov_{fit}) = 1.3 x 10^{-2}. HG values (NH 1 = 1.58, NH 2 = 1.06, CH 1 = -1.9 x 10^{-2}). Link to Bindfit fitting: http://app.supramolecular.org/bindfit/view/3940aafa-3cba-44d7-b24e-087995a4999a.

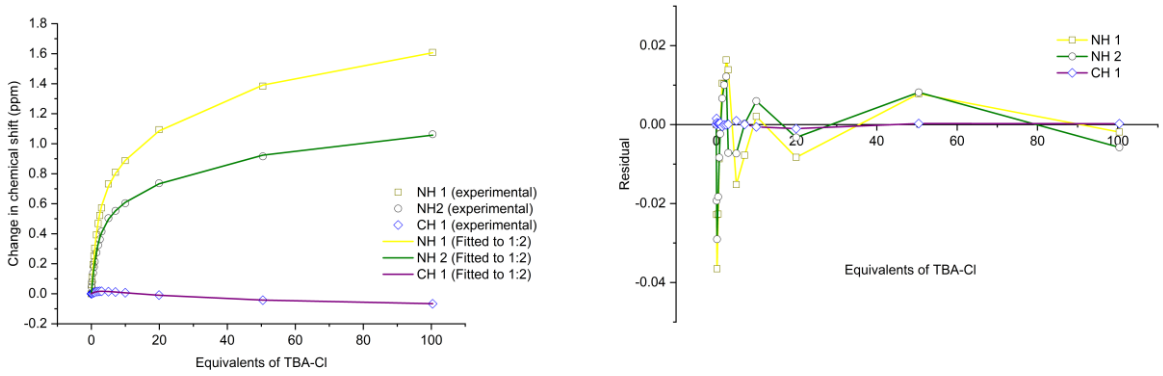

Figure S52. Fitted binding isotherm of **2** + TBACl in DMSO-d_6 showing the change in chemical shift of NH protons fitted to the 1:2 binding model (left). K_{11} = 255 M^{-1}, K_{12} = 10 M^{-1}. Residual plot showing the random error obtained from the binding isotherm fitting (right). Covariance of fit (cov_{fit}) = 1.1 x 10^{-3}. HG values (NH 1 = 0.72, NH 2 = 0.51, CH 1 = -3.5 x 10^{-2}). HG2 values (NH 1 = 1.94, NH 2 = 1.27, CH 1 = -0.10). Link to Bindfit fitting: http://app.supramolecular.org/bindfit/view/ec3e7291-32e8-42ea-866f-97152560aeac.

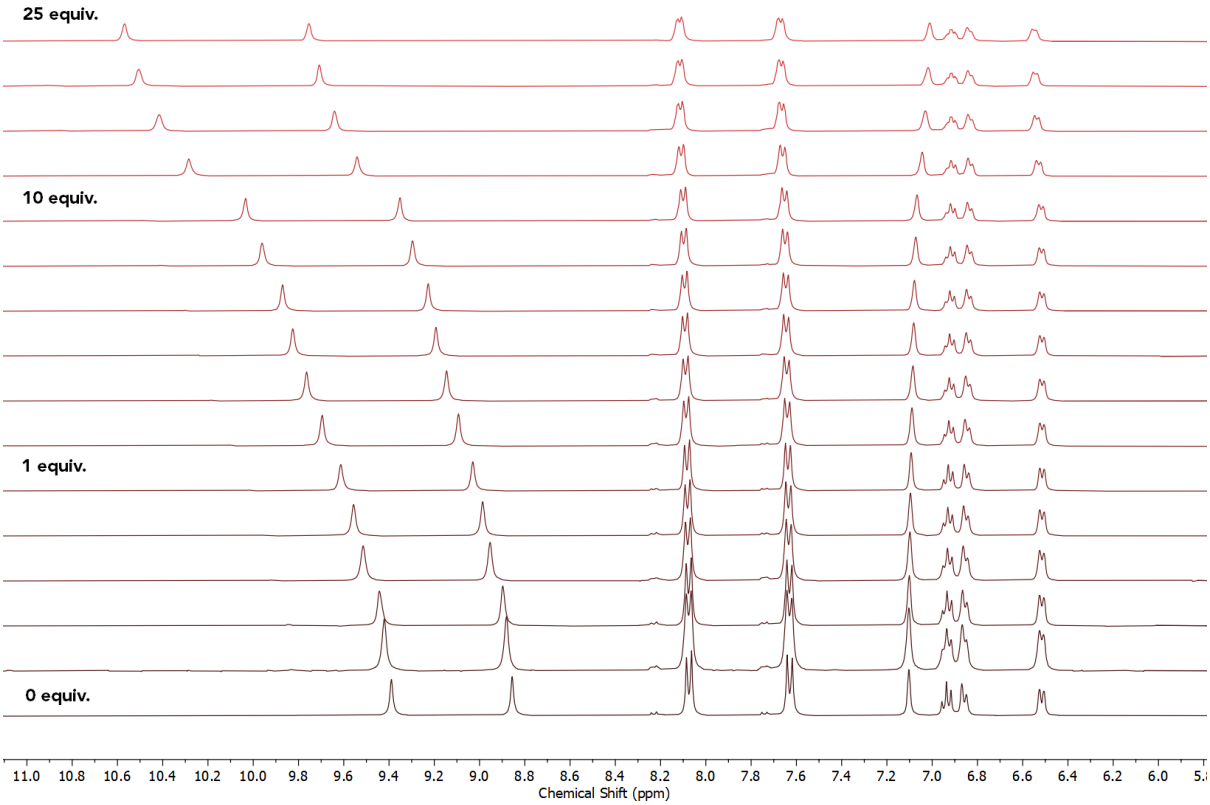

Figure S53. ^{1}H NMR titration spectra as a stack plot for **3** (2.5 mM) + TBACl (0–25 equiv.) in DMSO-d_6 at 298 K.

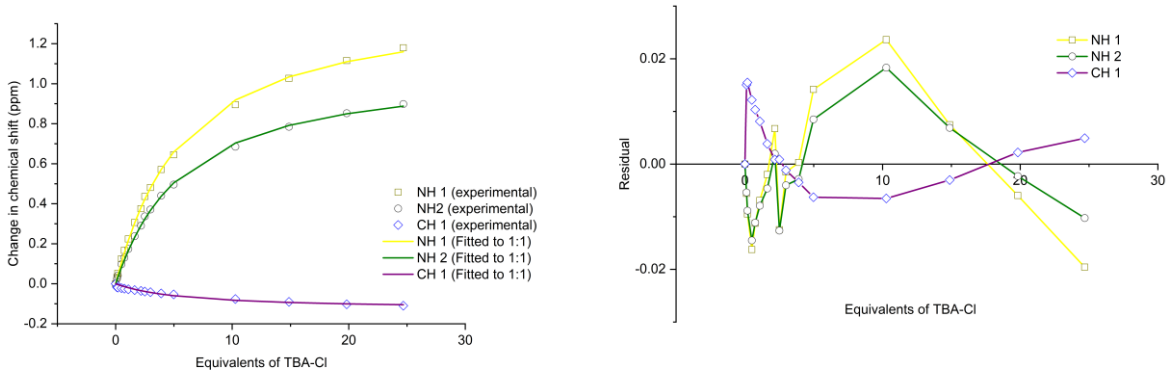

Figure S54. Fitted binding isotherm of **3** + TBACl in DMSO-d_6 showing the change in chemical shift of NH protons fitted to the 1:1 binding model (left). K_a = 78 M^{-1}. Residual plot showing the random error obtained from the binding isotherm fitting (right). Covariance of fit (cov_{fit}) = 6.8 x 10^{-4}. HG values (NH 1 = 1.41, NH 2 = 1.08, CH 1 = -0.13). Link to Bindfit fitting: http://app.supramolecular.org/bindfit/view/9543e43d-5a90-4271-bfe0-ae8516eabfc7.

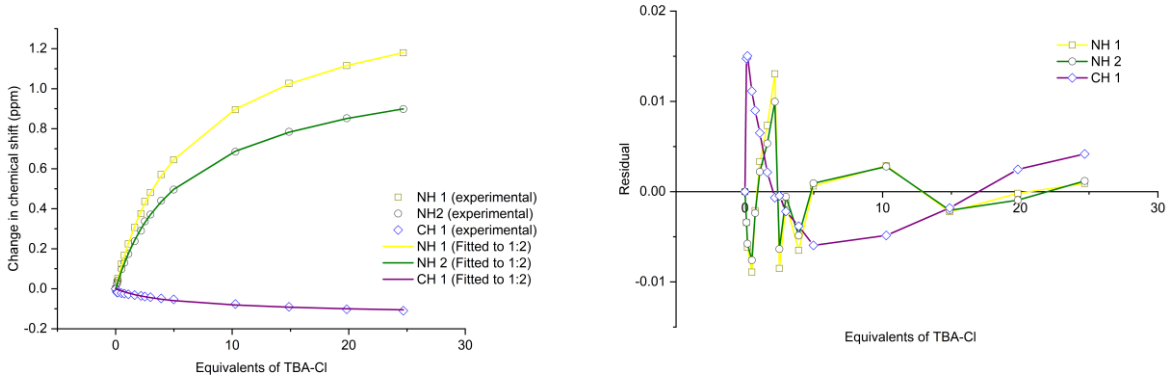

Figure S55. Fitted binding isotherm of **3** + TBACl in DMSO-d_6 showing the change in chemical shift of NH protons fitted to the 1:2 binding model (left). K_{11} = 240 M^{-1}, K_{12} = 26 M^{-1}. Residual plot showing the random error obtained from the binding isotherm fitting (right). Covariance of fit (cov_{fit}) = 2.6 x 10^{-4}. HG values (NH 1 = 0.81, NH 2 = 0.55, CH 1 = -6.2 x 10^{-2}). HG2 values (NH 1 = 1.59, NH 2 = 1.20, CH 1 = -0.14). Link to Bindfit fitting: http://app.supramolecular.org/bindfit/view/2d69dbe3-5334-4ea4-9b51-2d4839b126ab.

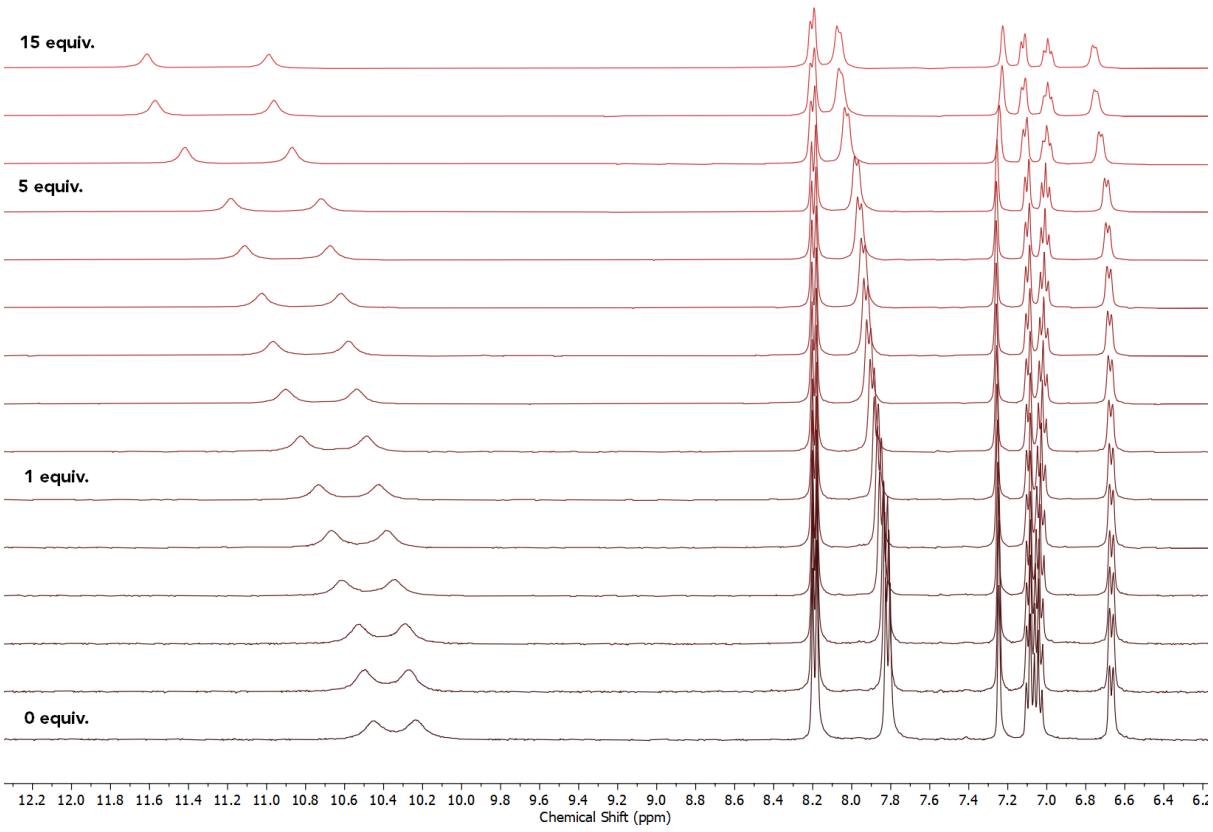

Figure S56. ^{1}H NMR titration spectra as a stack plot for **4** (2.5 mM) + TBACl (0–25 equiv.) in DMSO-d_6 at 298 K.

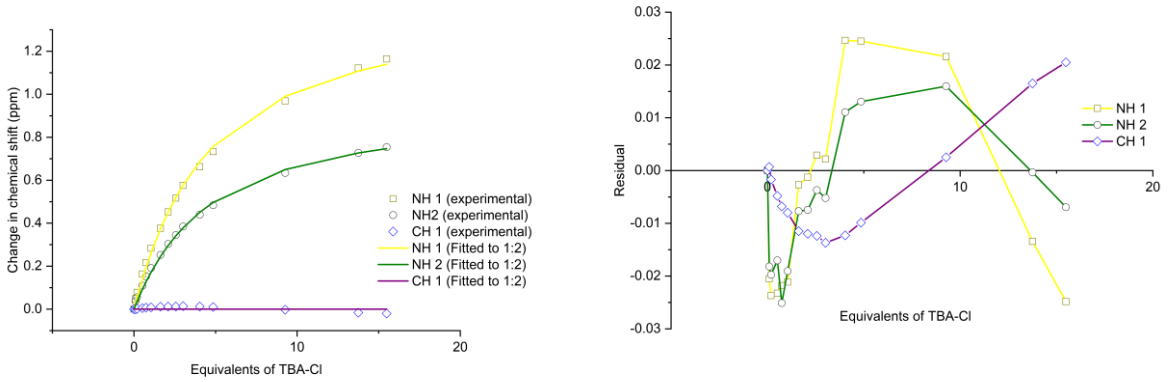

Figure S57. Fitted binding isotherm of **4** + TBACl in DMSO-d_6 showing the change in chemical shift of NH protons fitted to the 1:1 binding model (left). K_a = 93 M^{-1}. Residual plot showing the random error obtained from the binding isotherm fitting (right). Covariance of fit (cov_{fit}) = 1.8 x 10^{-3}. HG values (NH 1 = 1.44, NH 2 = 0.95, CH 1 = 0). Link to Bindfit fitting: http://app.supramolecular.org/bindfit/view/68d61ea4-04fe-4bf3-9b78-db2b71605762.

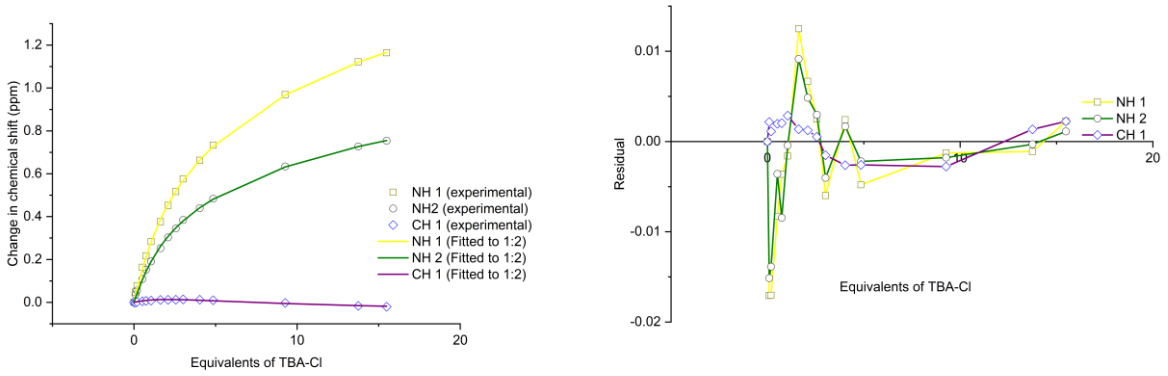

Figure S58. Fitted binding isotherm of **4** + TBACl in DMSO-d_6 showing the change in chemical shift of NH protons fitted to the 1:2 binding model (left). K_{11} = 464 M^{-1}, K_{12} = 24 M^{-1}. Residual plot showing the random error obtained from the binding isotherm fitting (right). Covariance of fit (cov_{fit}) = 3.4 x 10^{-4}. HG values (NH 1 = 0.58, NH 2 = 0.40, CH 1 = 2.8 x 10^{-2}). HG2 values (NH 1 = 1.84, NH 2 = 1.17, CH 1 = -6.8 x 10^{-2}). Link to Bindfit fitting: http://app.supramolecular.org/bindfit/view/5d841f02-4749-4509-affb-9993c1960ecd.

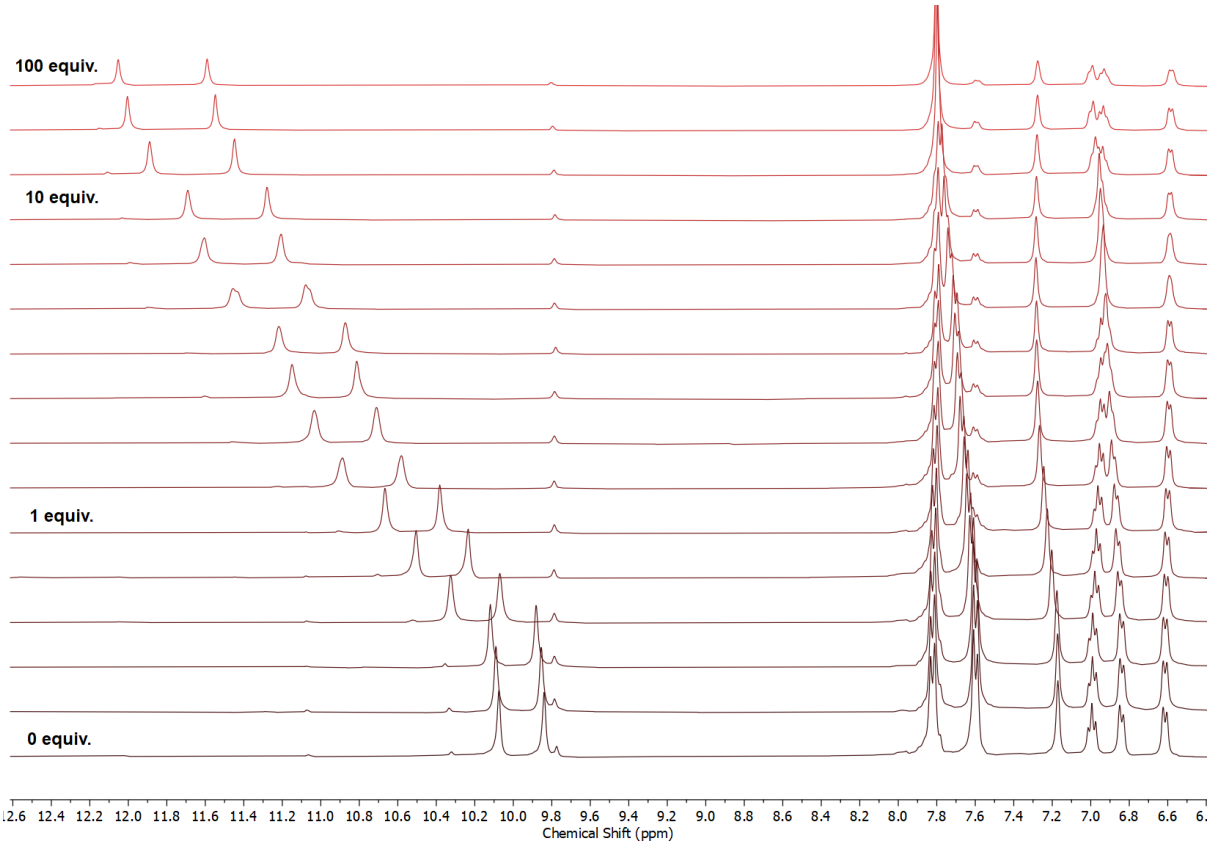

Figure S59. ^{1}H NMR titration spectra as a stack plot for **5** (2.5 mM) + TBACl (0–100 equiv.) in DMSO-d_6 at 298 K.

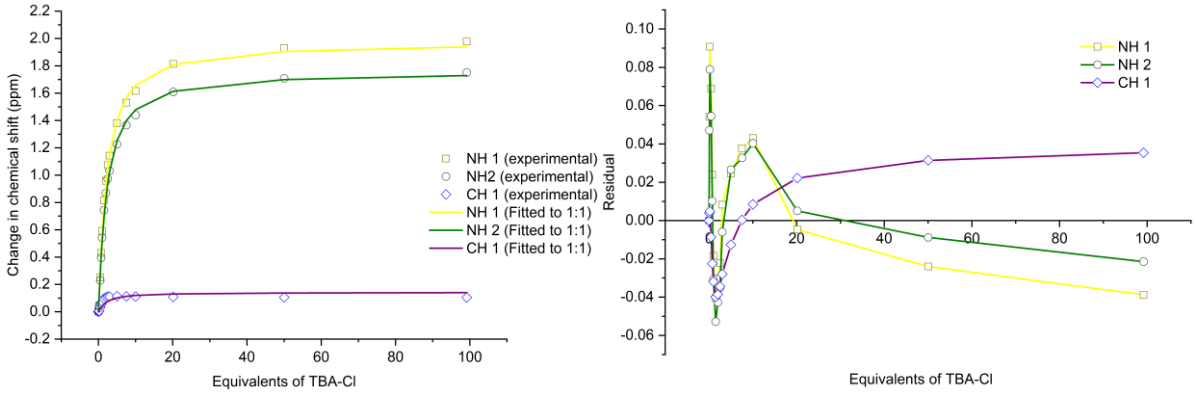

Figure S60. Fitted binding isotherm of **5** + TBACl in DMSO-d_6 showing the change in chemical shift of NH protons fitted to the 1:1 binding model (left). K_a = 230 M^{-1}. Residual plot showing the random error obtained from the binding isotherm fitting (right). Covariance of fit (cov_{fit}) = 2.8 x 10^{-3}. HG values (NH 1 = 1.97, NH 2 = 1.76, CH 1 = 0.14). Link to Bindfit fitting: http://app.supramolecular.org/bindfit/view/11c89b77-404c-40ee-a289-9f90d90d331a.

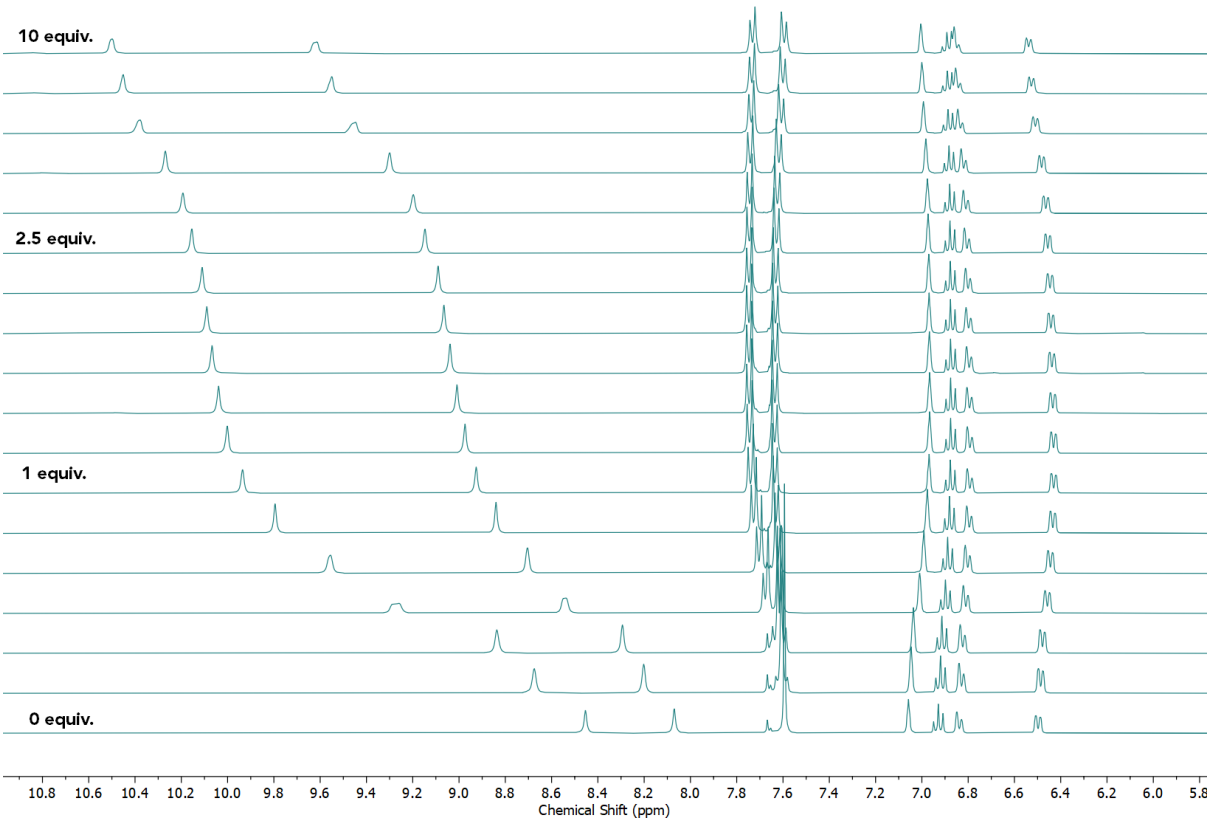

Figure S61. ^{1}H NMR titration spectra as a stack plot for **1** (2 mM) + TBACl (0–10 equiv.) in CD_3N-d_3 / 2% DMSO-d_6 at 298 K.

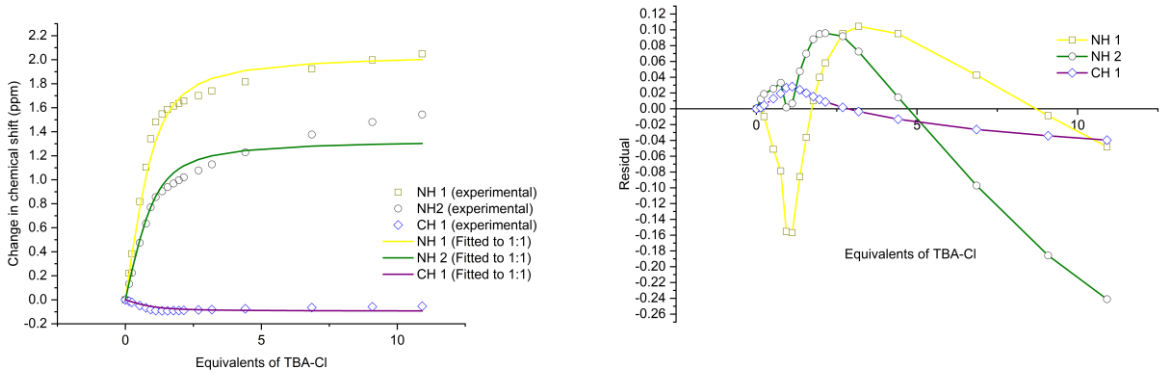

Figure S62. Fitted binding isotherm of **1** + TBACl in CD_3N-d_3 / 2% DMSO-d_6 showing the change in chemical shift of NH protons fitted to the 1:1 binding model (left). K_a = 1450 M^{-1}. Residual plot showing the random error obtained from the binding isotherm fitting (right). Covariance of fit (cov_{fit}) = 9.10 x 10^{-3}. HG values (NH 1 = 2.05, NH 2 = 1.34, CH 1 = -0.09). Link to Bindfit fitting: http://app.supramolecular.org/bindfit/view/4fd53520-5705-4ec4-8b56-6e1393c29887.

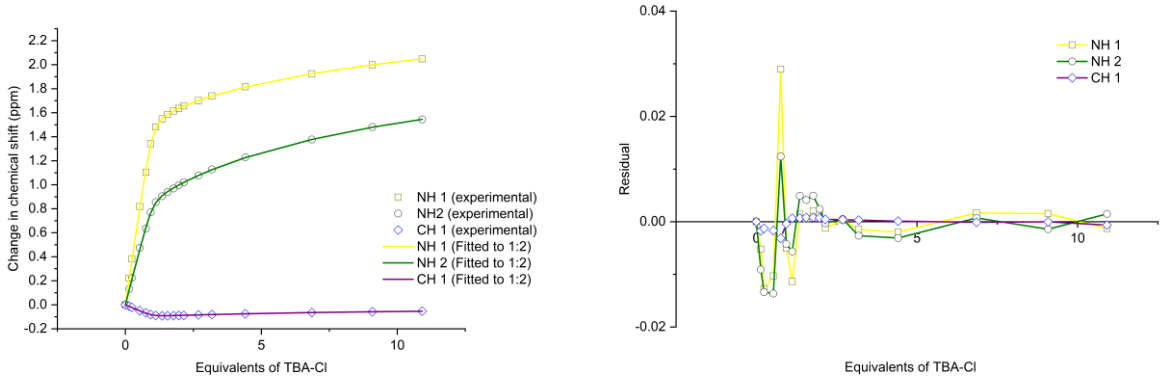

Figure S63. Fitted binding isotherm of **1** + TBACl CD_3N-d_3 / 2% DMSO-d_6 showing the change in chemical shift of NH protons fitted to the 1:2 binding model (left). K_{11} = 24000 M^{-1}, K_{12} = 43 M^{-1}. Residual plot showing the random error obtained from the binding isotherm fitting (right). Covariance of fit (cov_{fit}) = 7.10 x 10^{-5}. HG values (NH 1 = 1.58, NH 2 = 0.90, CH 1 = -0.10). HG2 values (NH 1 = 2.48, NH 2 = 2.14, CH 1 = -1.2 x 10^{-2}). Link to Bindfit fitting: http://app.supramolecular.org/bindfit/view/9ca9070c-145a-4eea-ac16-b72126d41618.

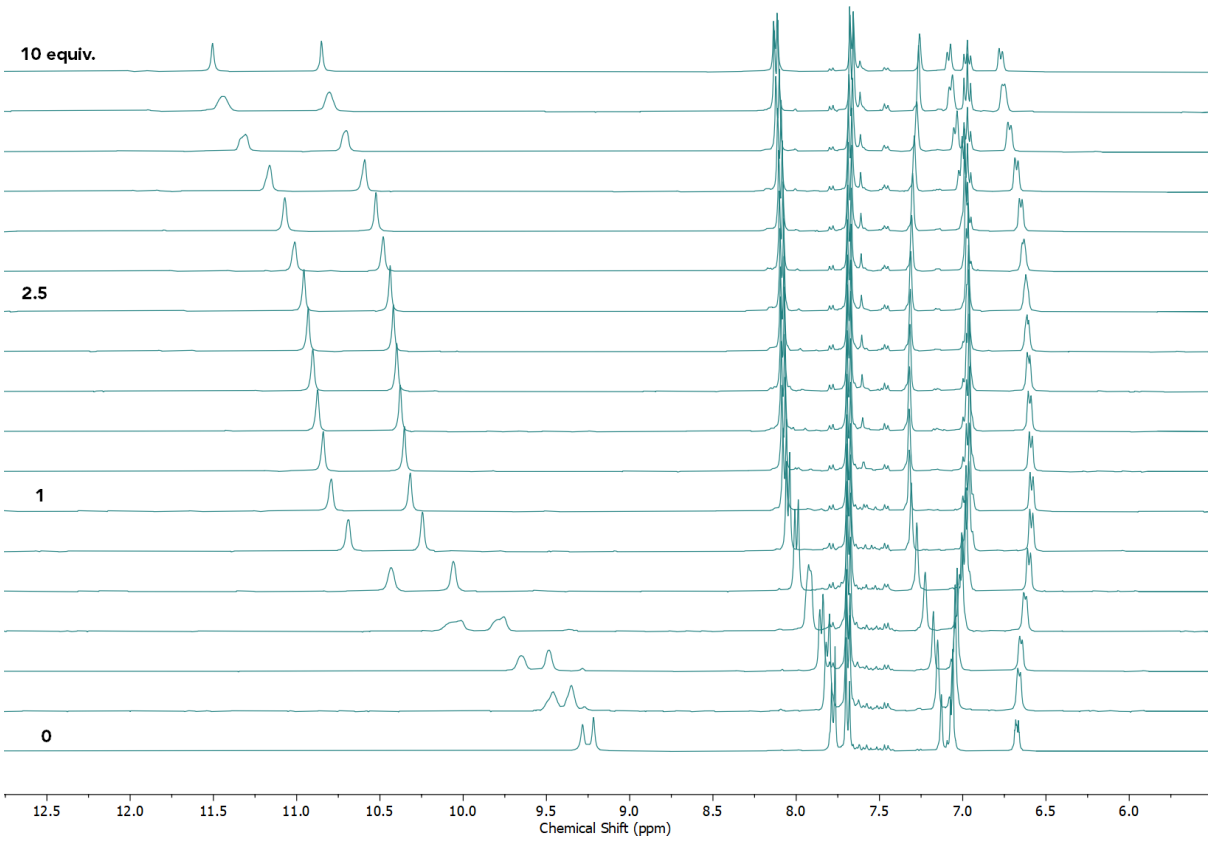

Figure S64. ^{1}H NMR titration spectra as a stack plot for **2** (2 mM) + TBACl (0–10 equiv.) in CD_3N-d_3 / 2% DMSO-d_6 at 298 K.

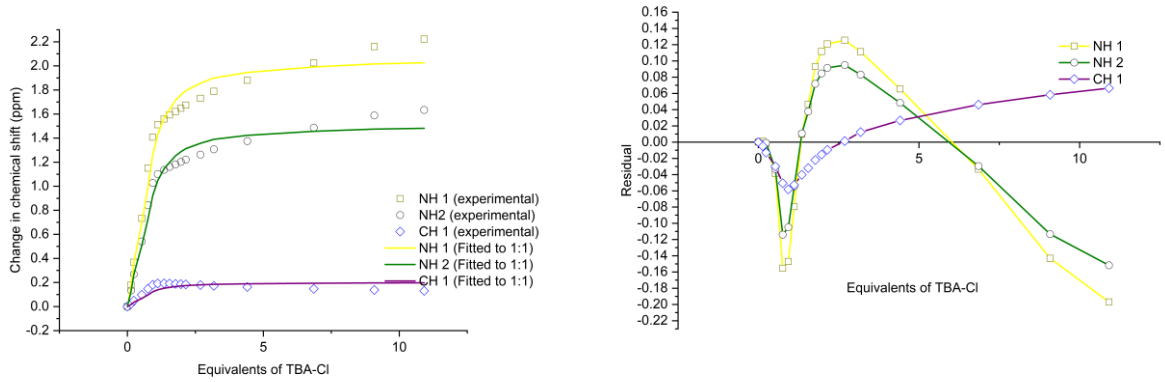

Figure S65. Fitted binding isotherm of **2** + TBACl CD_3N-d_3 / 2% DMSO-d_6 showing the change in chemical shift of NH protons fitted to the 1:1 binding model (left). K_a = 1300 M^{-1}. Residual plot showing the random error obtained from the binding isotherm fitting (right). Covariance of fit (cov_{fit}) = 1.0 x 10^{-2}. HG values (NH 1 = 2.07, NH 2 = 1.51, CH 1 = 0.20). Link to Bindfit fitting: http://app.supramolecular.org/bindfit/view/96520962-3a68-4f7b-a1e6-989c81041969.

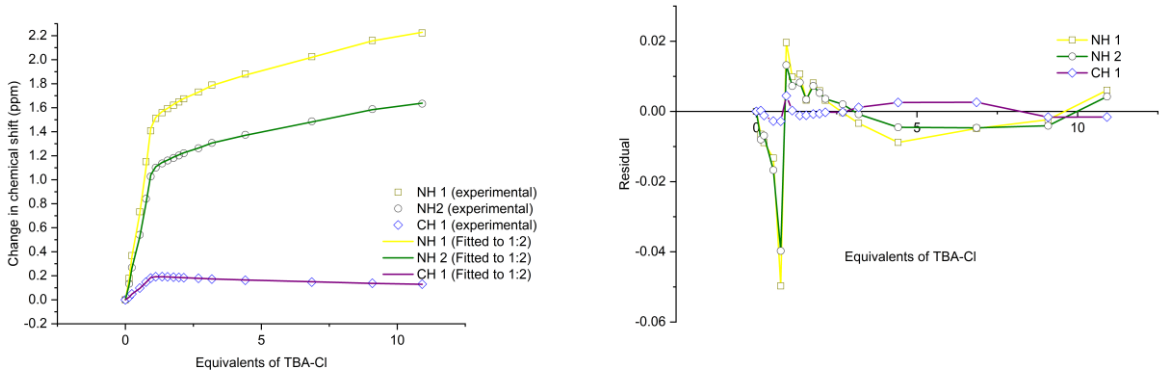

Figure S66. Fitted binding isotherm of **2** + TBACl CD_3N-d_3 / 2% DMSO-d_6 showing the change in chemical shift of NH protons fitted to the 1:2 binding model (left). K_{11} = 40000 M^{-1}, K_{12} = 28 M^{-1}.. Residual plot showing the random error obtained from the binding isotherm fitting (right). Covariance of fit (cov_{fit}) = 1.8 x 10^{-4}. HG values (NH 1 = 1.52, NH 2 = 1.11, CH 1 = 0.20). HG2 values (NH 1 = 2.96, NH 2 = 2.19, CH 1 = 5.3 x 10^{-2}). Link to Bindfit fitting: http://app.supramolecular.org/bindfit/view/233df8c4-76f7-418c-a864-80c7e1739773.

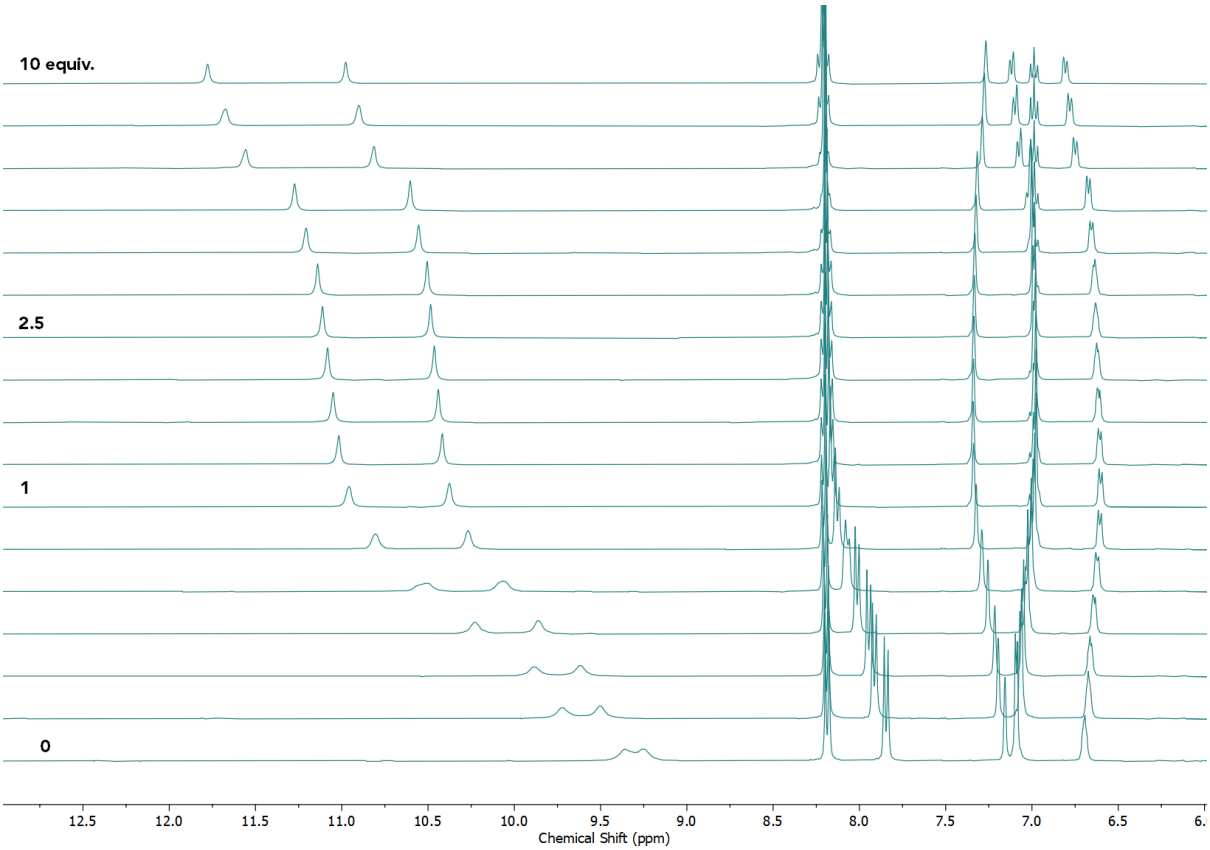

Figure S67. ^{1}H NMR titration spectra as a stack plot for **4** (2 mM) + TBACl (0–10 equiv.) in CD_3N-d_3 / 2% DMSO-d_6 at 298 K.

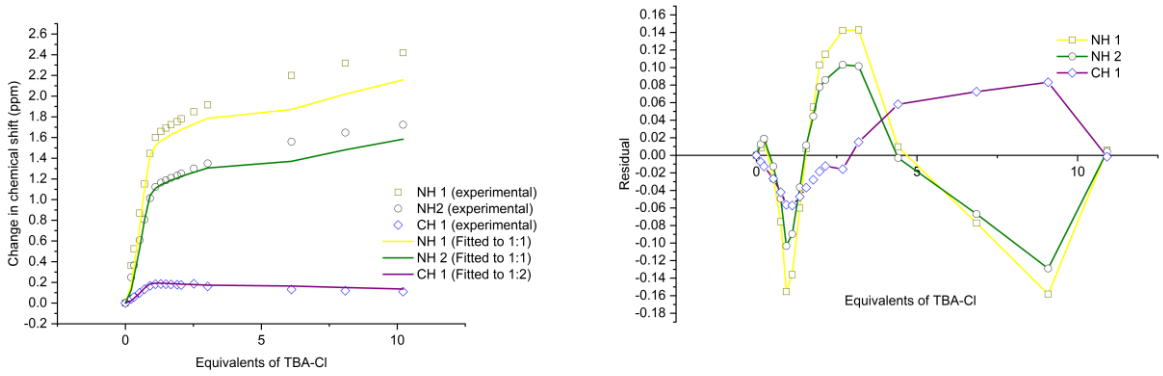

Figure S68. Fitted binding isotherm of **4** + TBACl CD_3N-d_3 / 2% DMSO-d_6 showing the change in chemical shift of NH protons fitted to the 1:1 binding model (left). K_a = 1500 M^{-1}. Residual plot showing the random error obtained from the binding isotherm fitting (right). Covariance of fit (cov_{fit}) = 9.5 x 10^{-3}. HG values (NH 1 = 2.33, NH 2 = 1.64, CH 1 = 0.20). Link to Bindfit fitting: http://app.supramolecular.org/bindfit/view/ed46e9d4-4eff-42e6-8fdc-1e81d3ef7bef.

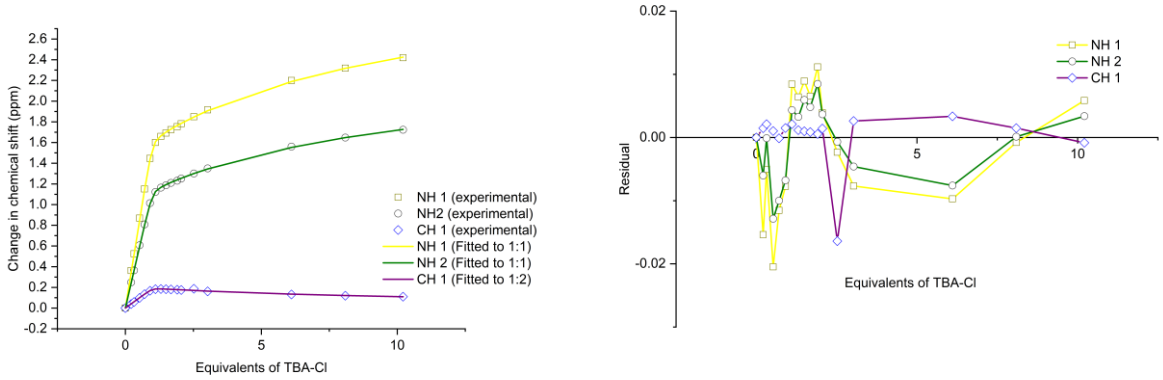

Figure S69. Fitted binding isotherm of **4** + TBACl CD_3N-d_3 / 2% DMSO-d_6 showing the change in chemical shift of NH protons fitted to the 1:2 binding model (left). K_{11} = 104000 M^{-1}, K_{12} = 47 M^{-1}. Residual plot showing the random error obtained from the binding isotherm fitting (right). Covariance of fit (cov_{fit}) = 8.4 x 10^{-5}. HG values (NH 1 = 1.64, NH 2 = 1.15, CH 1 = 0.19). HG2 values (NH 1 = 3.25, NH 2 = 2.34, CH 1 = 2.3 x 10^{-2}). Link to Bindfit fitting: http://app.supramolecular.org/bindfit/view/eea6eb5d-d95c-48e7-8627-9e4c202b1cb9.

7. Molecular Modelling

A PM6 semi-empirical model was calculated for compound **4** in the free ground state and in the presence of Cl^- using Spartan to elucidate the equilibrium geometry of the binding modes for each receptor.

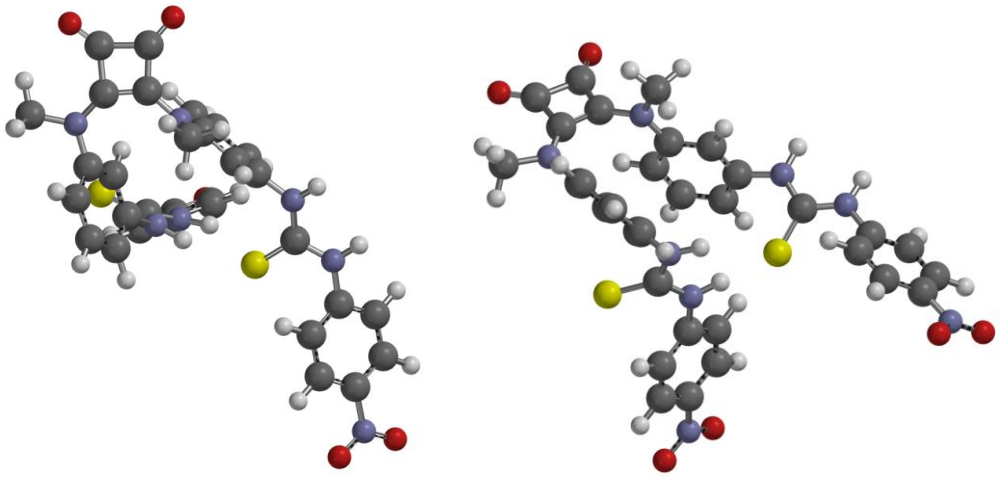

Figure S70. Ground-state equilibrium geometry calculated for compound **4** as a free receptor. An intramolecular hydrogen bond is present between the thiourea groups.

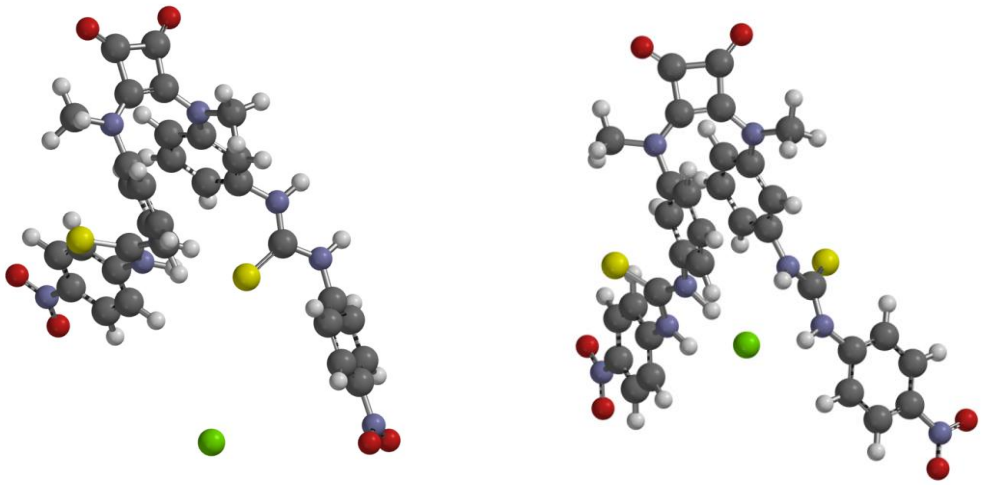

Figure S71. Left: Introduction of a chloride anion to the ground-state equilibrium geometry of free receptor **4**. Right: Ground-state equilibrium geometry calculated for compound **4** in the presence of Cl^-.

The initial hypothesis for the ground state orientation was that the π-π stacking of the aromatic rings closest to the demethylated squaramide would be the strongest interaction,

leading to a preorganised binding site. The ground state calculations show that the dimethylation of the squaramide and π-π stacking of the adjacent aromatic rings is not enough to inhibit the interaction between the two thiourea groups, which kink out of plane to facilitate an intramolecular hydrogen bond. This interaction has been seen in other dual hydrogen bond donor motifs and leads to diminished anion binding affinity, as the intramolecular bond must first be broken before an anionic guest can enter the binding cavity.

The introduction of Cl^- results in a conformational rearrangement to the orientated binding mode, as expected. The cis-cis conformation and π-π stacking of the aromatic rings are present in the Cl^- binding mode.

8. Cl^-/NO_3^- Exchange Assay – Hill Analysis

8.1 General Vesicle Preparation

Unilamellar vesicles were prepared following a procedure outlined previously by the Gale group.[7] A chloroform solution of POPC (37.5 mM, 4 mL) was transferred to a pre-weighed round-bottom flask, and the solvent was removed using a rotary evaporator. The pressure was lowered slowly to ensure the formation of a smooth lipid film. Subsequently, the film was dried in vacuo for 4–24 h, and the mass of lipid was recorded. The lipids were rehydrated with 4 mL of the respective internal solution (this number should correspond to the volume of POPC solution used initially) and vortexed until all lipids were removed from the sides of the flask and were suspended in solution. The lipids were subjected to 9 freeze-thaw cycles by freezing using a dry ice/acetone bath and thawing in lukewarm water. Following this, the vesicles were left to rest at room temperature for 30 min. The lipids were extruded through a 200 nm polycarbonate membrane 25 times to form monodisperse vesicles. Only 1 mL of solution was extruded at a time before being collected.

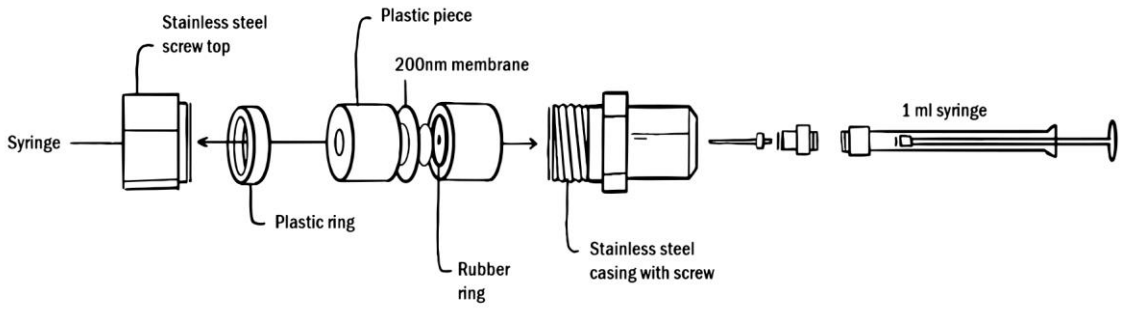

Figure S72. Schematic diagram of the extrusion kit with labelled components.

Finally, any residual unencapsulated salt from the internal solution was either removed via dialysis for 12 h in the desired external solution or through size-exclusion using a B19 column packed with hydrated G-25 Sephadex®, which had been pre-saturated with the respective external solution. The lipid suspensions were diluted with the external solution to afford a stock solution (10 mL) of a known concentration.

7.2 Electrode Calibration and Conversion of Raw Data

An Accumet chloride ion-selective electrode (ISE) was used for the Cl^-/NO_3^- exchange assay and the cationophore coupled assay. Before each set of experiments began, electrode calibration was required to correct any drift between recorded datasets. The electrode was submerged in a sequence of NaCl solutions of increasing concentration (M), and the reading from the electrode was recorded after stabilising after 5−15 min. The electrode potential reading, *y*, was plotted against NaCl concentration (M), *x*, and fitted to a simplified Nernst equation using *OriginPro.* The equation is given as follows:

$$y = (P_1 log_{10} x) + P_2$$

Equation S1. Calibration of electrode potential data using a simplified Nernst equation.

Where P_1 and P_2 are the calibration parameters. The chloride ion concentration at any given time during the experiments can be calculated by substituting P_1, P_2 and *y*, the electrode potential reading, into the equation and solving for *x*, the chloride ion concentration. By subtracting the chloride concentration at $t = 0$ from the concentration at a given time during the experiment, the total chloride concentration released from the vesicles at that given time can be calculated. Conversion to percentage chloride efflux was achieved by normalising the chloride concentration at time (*t*) using the 100% chloride efflux value recorded at the end of the experiment ($t = 420$ s) when the vesicles were lysed with a water dispersion of Triton X-100 (10% v/v).

7.3 Dose-Response Hill Analysis Assay Conditions

Vesicles were prepared using an internal solution of NaCl (487 mM) and buffered to pH 7.2 using a sodium phosphate salt buffer of NaH_2PO_4 (1.2 mM) and Na_2HPO_4 (4 mM). An external solution containing $NaNO_3$ (487 mM) was prepared separately with the same sodium phosphate salt buffer and adjusted to pH 7.2 using an aqueous solution of dilute NaOH. Following the freeze-thaw cycles and extrusion, the NaCl lipids were dialysed in the $NaNO_3$ external solution (~ 1600 mL) for 12h. The lipid stock solution (10 mL) was diluted with the

external solution to give both a concentration and volume suitable for ISE experiments (1 mM, 5 mL).

Each receptor was added as a DMSO solution (10 μL) at t = 0 s, and the change in chloride concentration was recorded using an Accumet chloride ISE. At t = 300 s, a detergent solution (Triton X-100 (10% *v/v* in H_2O), 50 μL) was injected to lyse the vesicles, and a final chloride concentration reading was recorded at t = 420 s to provide a 100% chloride efflux reading for use in calibration.

Dose-response experiments were performed at six transporter concentrations, and a blank DMSO run, and percentage efflux at t = 270 s was recorded for each concentration tested. The chloride efflux (%) at t = 270 s was plotted against receptor concentration (mol%, with respect to lipid concentration). The recorded data was fit to the Hill Equation, using *Origin 2021b (Academic)*, given as:

$$y = V_{max}\frac{x^n}{k^n + x^n}$$

Equation S2. The Hill equation.

Where y represents the percentage of chloride efflux at t = 270 s, x is the transporter concentration (mol%, with respect to lipids concentration), and V_{max}, k and n are the parameters to be fitted. V_{max} represents the maximum chloride efflux (typically fixed to 100%), and n can be interpreted as the Hill coefficient. A derived equation was used to calculate the EC_{50} value, the transporter concentration required to facilitate 50% chloride efflux, given as:

$$\mathrm{EC}_{50} = k\left(\frac{50}{y_1 - y_0 - 50}\right)^{\frac{1}{n}}$$

Equation S3. The adapted EC_{50} equation.

Where k and n are the derived parameters from the Hill equation, y_0 is the percentage chloride efflux at t = 0 s, and y_1 is the percentage chloride efflux at t = 300 s.

7.4 Maximum Rate Calculations

The maximum rate of chloride efflux was calculated for receptors **1**, **2**, **4**–**6**, and inclusion complexes HP-β-CD·(**1**, **2**, **4**, **6**) at 2 mol% by fitting the efflux plot at the given concentration to **Equation S4**, in *OriginPro* given as:

$$y = A_1 e^{\left(\frac{-x}{t_1}\right)} + A_2 e^{\left(\frac{-x}{t_2}\right)} + y_0$$

Equation S4. A non-linear exponential decay function.

where y represents the percentage of chloride efflux (%), x is the receptor concentration (mol%), y_0 is the percentage chloride efflux at t = 0 s, and A_1, A_2, t_1, and t_2 are the derived parameters. The maximum rate was obtained by calculating the first derivative at x = 0, which is given as:

$$K_{initial} = \frac{-A_1}{t_1} - \frac{A_2}{t_2}$$

Equation S5. Derivative of the decay function used to determine the maximum rate given in % s^{-1}.

The maximum rate of chloride efflux was calculated for receptor **3** at 2 mol% by fitting the efflux plot at the given concentration to a non-linear Boltzmann curve function in *Origin 2021b (Academic)*, given as:

$$y = A_2 + \frac{(A_1 - A_2)}{(1 + e^{(\frac{x - x_0}{dx})})}$$

Equation S6. The Boltzmann function was used to fit the efflux plots for compound **3**.

where y represents the percentage of chloride efflux (%), x is the receptor concentration (mol%), and A_1, A_2, x_0, and dx are the derived parameters. The maximum rate was obtained by calculating the first derivative at x = 0, which is given as:

$$K_{max} = \frac{A_2 - A_1}{4dx}$$

Equation S7. Derivative of the Boltzmann function used to determine the maximum rate given in %s^{-1}.

7.5 Cl^-/NO_3^- Exchange Assay – Efflux and Hill Plots

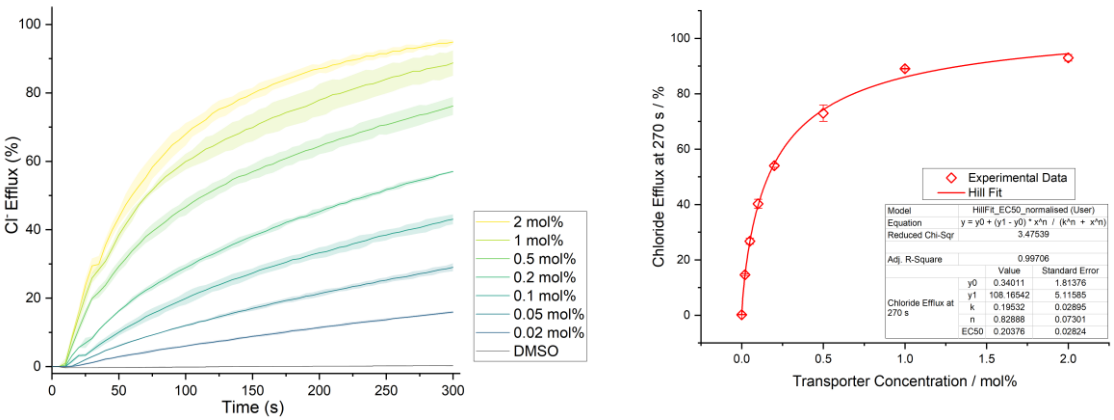

Figure S73. Hill analysis of Cl^-/NO_3^- exchange facilitated by **1**. Each data point is the average of two repeats with error bars to show standard deviation. A run of pure DMSO was used as a control.

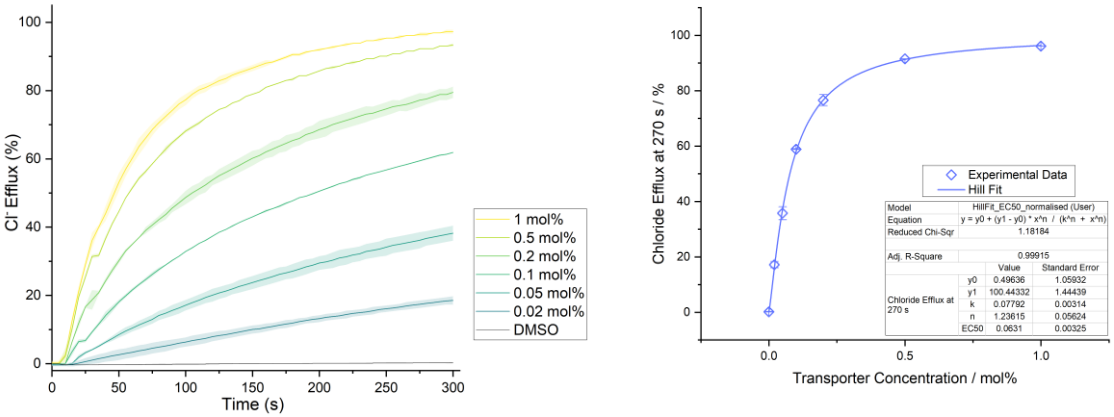

Figure S74. Hill analysis of Cl^-/NO_3^- exchange facilitated by **2**. Each data point is the average of two repeats with error bars to show standard deviation. A run of pure DMSO was used as a control.

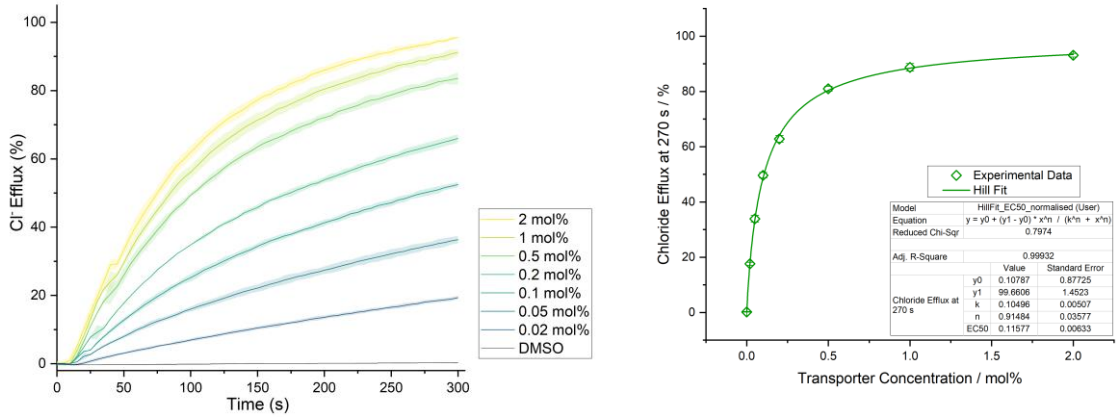

Figure S75. Hill analysis of Cl^-/NO_3^- exchange facilitated by **3**. Each data point is the average of two repeats with error bars to show standard deviation. A run of pure DMSO was used as a control.

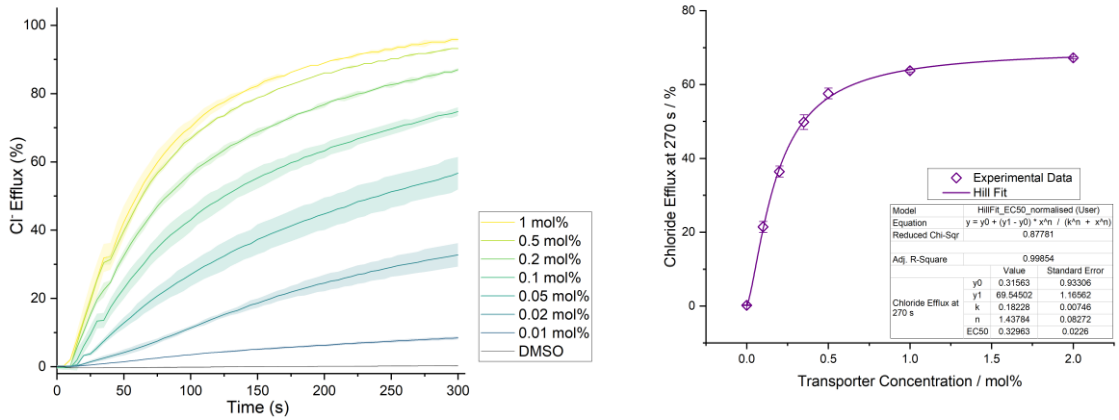

Figure S76. Hill analysis of Cl^-/NO_3^- exchange facilitated by **4**. Each data point is the average of two repeats with error bars to show standard deviation. A run of pure DMSO was used as a control.

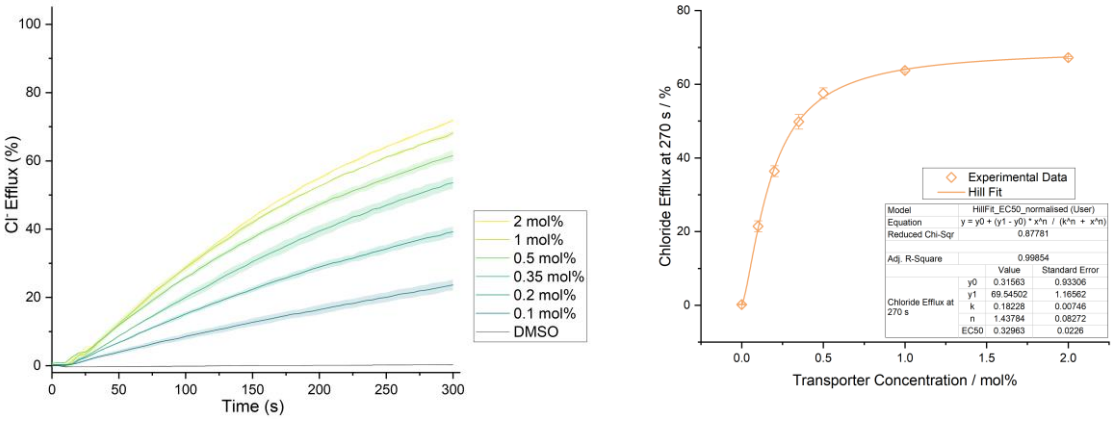

Figure S77. Hill analysis of Cl^-/NO_3^- exchange facilitated by **5**. Each data point is the average of two repeats with error bars to show standard deviation. A run of pure DMSO was used as a control.

8. ISE Cationophore Coupled Assay

Vesicles were prepared following the procedure described above with an internal solution of KCl (300 mM), with a sodium phosphate salt buffer consisting of NaH2PO4 (1.2 mM) and Na2HPO4 (4mM) and adjusted to pH 7.2. Two external solutions were prepared and buffered to pH 7.2 with sodium phosphate salts (5 mM); one containing KNO3 (333 mM) and the other a solution of KGlu (300 mM). Following extrusion, the vesicles were passed through a G-25 Sephadex® size-exclusion column, which had been pre-rinsed with the KGlu external solution. The same solution was used as the eluent, and once the vesicles were collected, the volume was diluted to 10 mL using the KGlu external solution.

Each experiment was prepared by adding 0.5 mL of the vesicle solution to 4. 5 mL of either KNO3 or KGlu solution. The transporter was added as a DMSO solution (10 μL) to initiate transport at t = 0 s. The transporter concentration was chosen to match the EC50 value determined in the Cl−/NO3− exchange ISE assay. Efflux data was collected until t = 300 s using an Accumet chloride ISE before detergent (Triton X-100 (10% v/v in H2O), 50 μL) was added to lyse the vesicles and release any remaining internal chloride solution. A final reading of the 100% chloride efflux value was recorded at t = 420 s for calibration purposes.

Cationophore-coupled experiments were conducted by preparing an experimental vesicle solution (0.5 mL) suspended in the KGluc external solution (4.5 mL). A DMSO solution of either valinomycin or monensin (10 μL) was added at t = −30 s to give a cationophore concentration of 0.1 mol% with respect to lipid concentration. The transporter was added as

a DMSO solution (10 μL) at t = 0 s to initiate the experiments, and efflux was recorded as described in the paragraph above. Each experiment was completed in duplicate for accuracy and data redundancy.

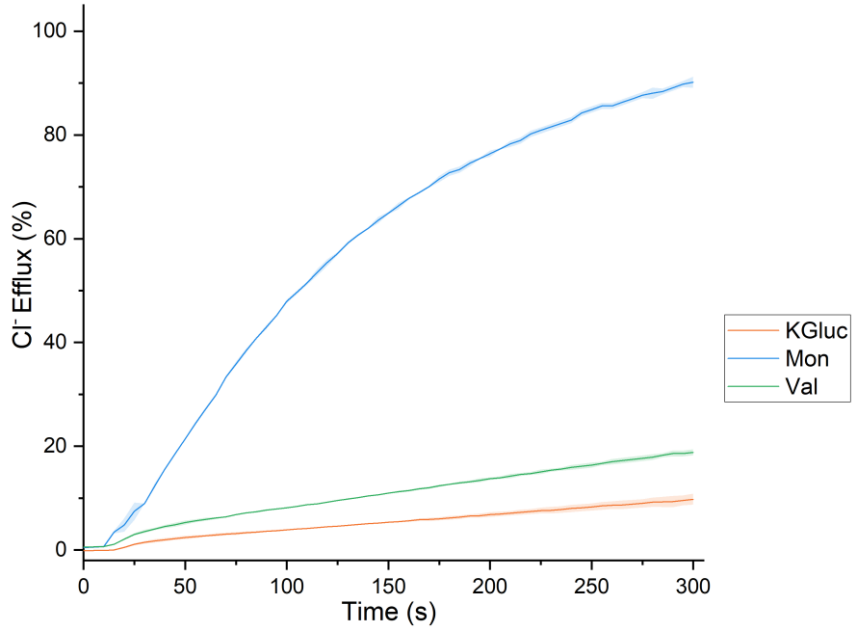

Figure S78. Chloride efflux facilitated by **1** (1 mol%) in POPC vesicles loaded with 300 mM KCl and suspended in an isotonic external solution containing KGlu. Experiments were performed in the presence of solely the anionophore (orange) and the presence of 0.1 mol% monensin (blue) and 0.1 mol% valinomycin (green). Each data point is the average of two repeats, with the error bars (shaded areas) showing the standard deviation.

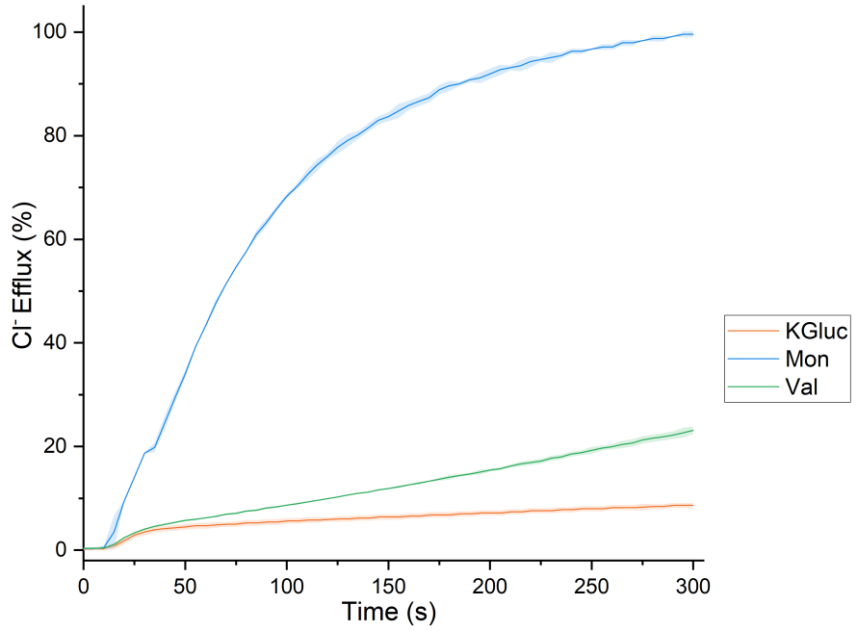

Figure S79. Chloride efflux facilitated by **2** (1 mol%) in POPC vesicles loaded with 300 mM KCl and suspended in an isotonic external solution containing KGlu. Experiments were performed in the presence of solely the anionophore (orange) and the presence of 0.1 mol% monensin (blue) and 0.1 mol% valinomycin (green). Each data point is the average of two repeats, with the error bars (shaded areas) showing the standard deviation.

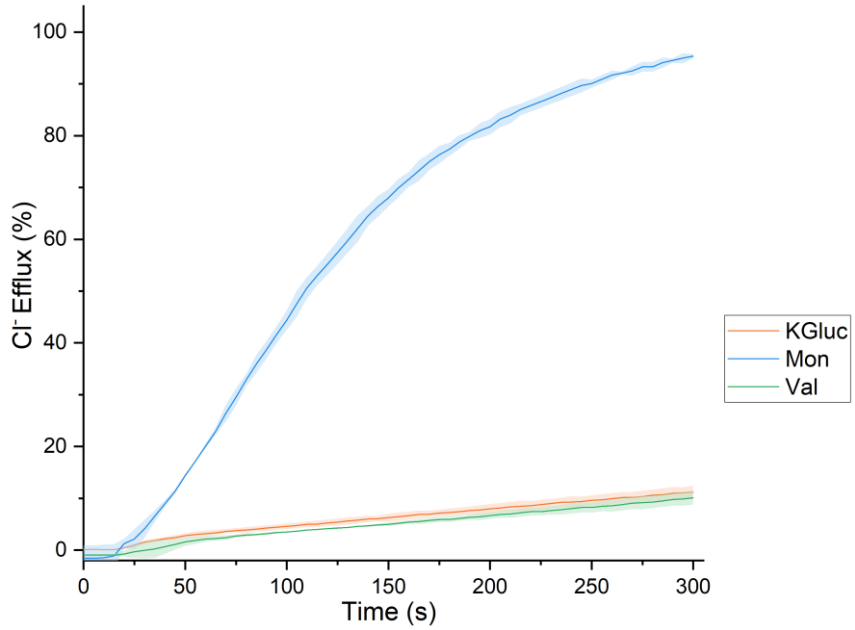

Figure S80. Chloride efflux facilitated by **3** (1 mol%) in POPC vesicles loaded with 300 mM KCl and suspended in an isotonic external solution containing KGlu. Experiments were performed in the presence of solely the anionophore (orange) and the presence of 0.1 mol% monensin (blue) and 0.1 mol% valinomycin (green). Each data point is the average of two repeats, with the error bars (shaded areas) showing the standard deviation.

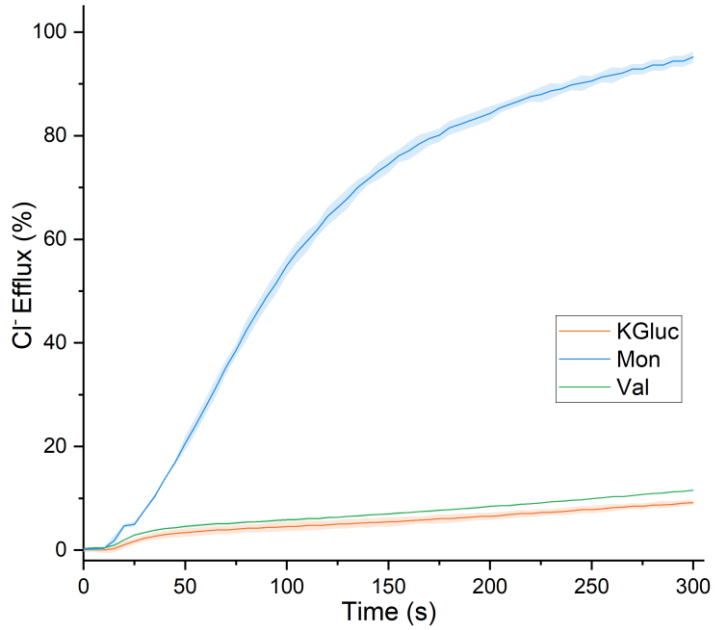

Figure S81. Chloride efflux facilitated by **4** (1 mol%) in POPC vesicles loaded with 300 mM KCl and suspended in an isotonic external solution containing KGlu. Experiments were performed in the presence of solely the anionophore (orange) and the presence of 0.1 mol% monensin (blue) and 0.1 mol% valinomycin (green). Each data point is the average of two repeats, with the error bars (shaded areas) showing the standard deviation.

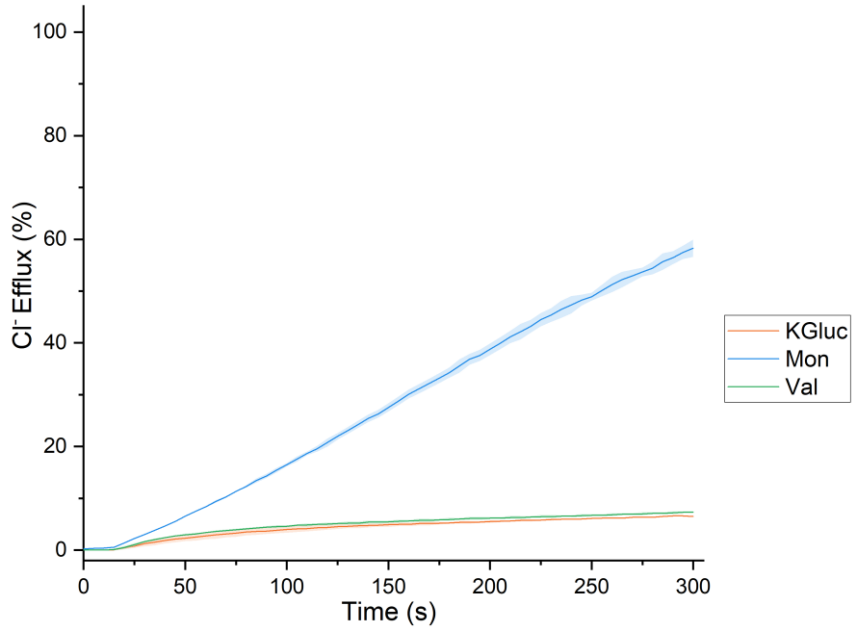

Figure S82. Chloride efflux facilitated by **5** (1 mol%) in POPC vesicles loaded with 300 mM KCl and suspended in an isotonic external solution containing KGlu. Experiments were performed in the presence of solely the anionophore (orange) and the presence of 0.1 mol% monensin (blue) and 0.1 mol% valinomycin (green). Each data point is the average of two repeats, with the error bars (shaded areas) showing the standard deviation.

9. HPTS Assay Hill Analyses

An external solution of NaCl (100 mM) was prepared with HEPES buffer (10 mM) and adjusted to pH 7.0. An internal solution was prepared using the same external solution but with the addition of pH-sensitive fluorescent dye HPTS (1 mM). Lipids were prepared following the procedure outlined above. After extrusion, the vesicles were passed through a G-25 Sephadex® column pre-rinsed with the external NaCl solution. The vesicles were collected and diluted with the external solution to a 10 mL volume with a known concentration.[8]

For a given experiment, the prepared vesicles were diluted to a concentration of 0.1 mM in a 2.5 mL plastic cuvette. In these experiments, a pH gradient is required to drive transport through the vesicle membrane before the transporter is added. An aliquot of aqueous NaOH solution (25 μL, 0.5 M) was added at approximately $t = -30$ s to increase the pH of the external solution by approx. one pH unit to pH 8.0. Transport was initiated with the addition of the transporter as a DMSO solution (5 μL) and ended with the addition of detergent (Triton X-100 (10% v/v in water), 25 μL) was added at t = 210 s to lyse the vesicles, and a final fluorescence intensity reading was recorded at t = 300 s to signify 100% proton efflux.

The changes in the fluorescent activity of intravesicular HPTS were used to detect pH changes during the experiments and represent proton efflux. The acidic and basic forms of the HPTS probe were excited at λ_{ex} = 403 nm and λ_{ex} = 460 nm, respectively, and the fluorescence emission of both forms recorded at λ_{em} = 510 nm. The intensity ratio of the basic form to the acidic form was determined, and the fractional fluorescence intensity (I_F) was calculated using the equation:

$$I_F = \frac{R_t - R_0}{R_d - R_0}$$

Equation S8. Used for the conversion of raw HPTS data into fractional fluorescence intensity.

Where R_t is the ratiometric fluorescence value at a given time (t), R_0 is the ratiometric fluorescence value at t = 0 s, and R_d is the fluorescence ratiometric value recorded at t = 360 s following the addition of detergent.

Dose-response experiments were performed at six transporter concentrations plus a blank DMSO control run. The fractional fluorescence intensity (I_F) was plotted as a function of transporter concentration (mol%, with respect to lipid concentration). The I_F value at t = 200 s for each tested transporter concentration was fit to an adapted Hill Equation, using *Origin 2021b (Academic)*, given as:

$$y = y_0 + (y_{max} - y_0)\frac{x^n}{k^n + x^n}$$

Equation S9. The modified Hill equation was employed in the **HPTS** assay.

Where y_0 is the I_F value at t = 200 s for the DMSO blank run, y_{max} is the maximum I_F value, n is the Hill coefficient, and k is a derived parameter. EC_{50} values were calculated by applying Equation 3 used for the ISE dose-response studies.

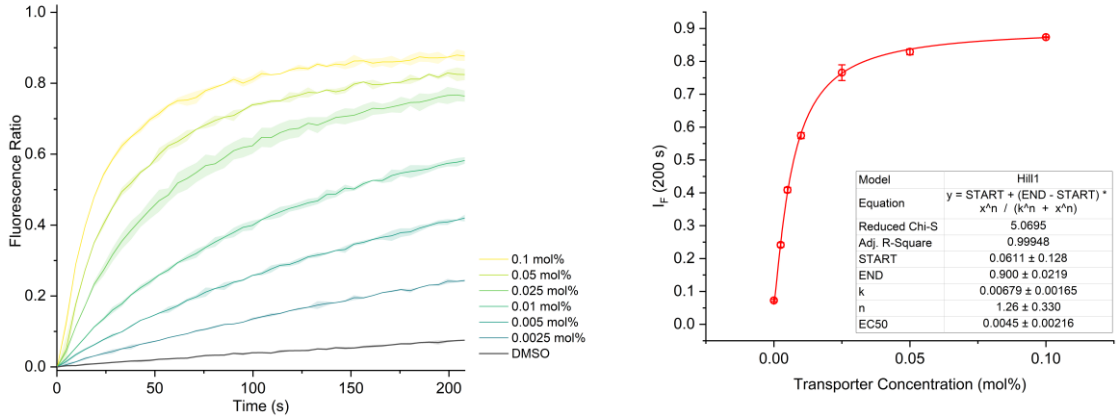

Figure S83. Efflux plot and Hill analysis of H^+/Cl^- symport (or Cl^-/OH^- antiport) facilitated by **1** in the NaCl HPTS assay. Each data point is the average of two repeats, with the error bars showing the standard deviation. A run of pure DMSO was used as a control.

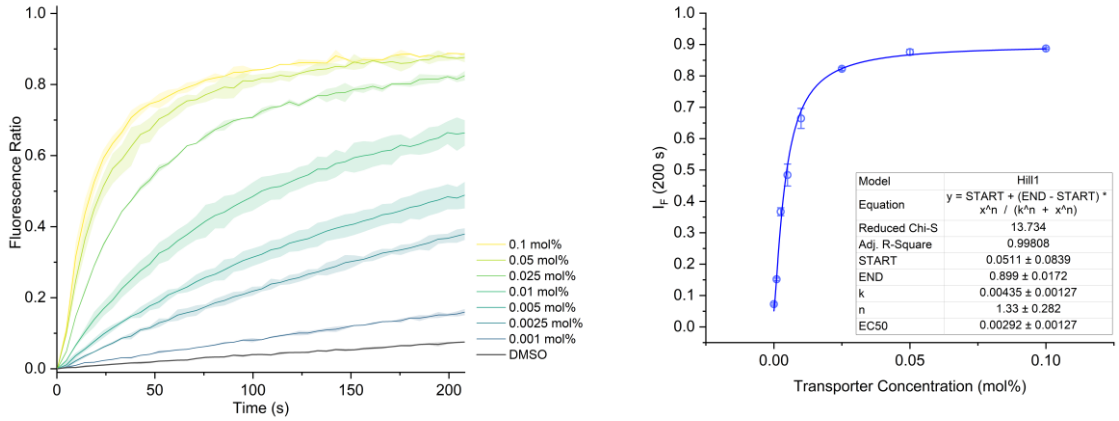

Figure S84. Efflux plot and Hill analysis of H^+/Cl^- symport (or Cl^-/OH^- antiport) facilitated by **2** in the NaCl HPTS assay. Each data point is the average of two repeats, with the error bars showing the standard deviation. A run of pure DMSO was used as a control.

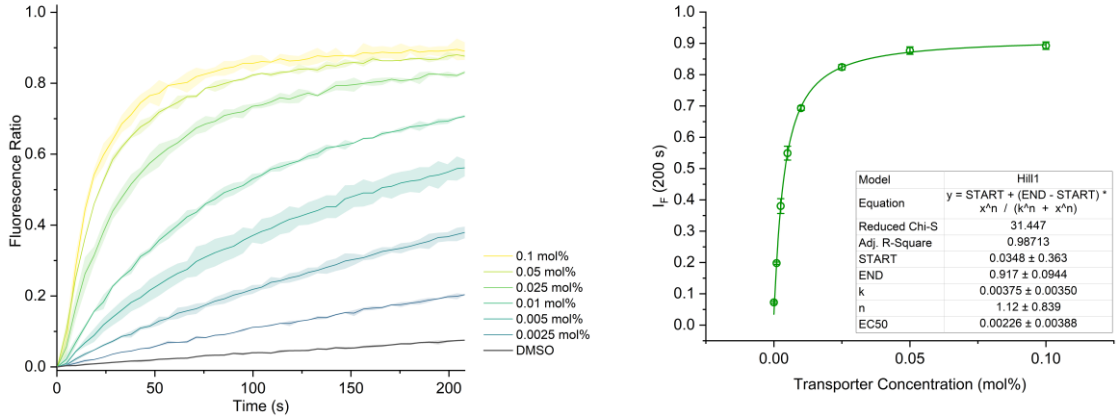

Figure S85. Efflux plot and Hill analysis of H^+/Cl^- symport (or Cl^-/OH^- antiport) facilitated by **3** in the NaCl HPTS assay. Each data point is the average of two repeats, with the error bars showing the standard deviation. A run of pure DMSO was used as a control.

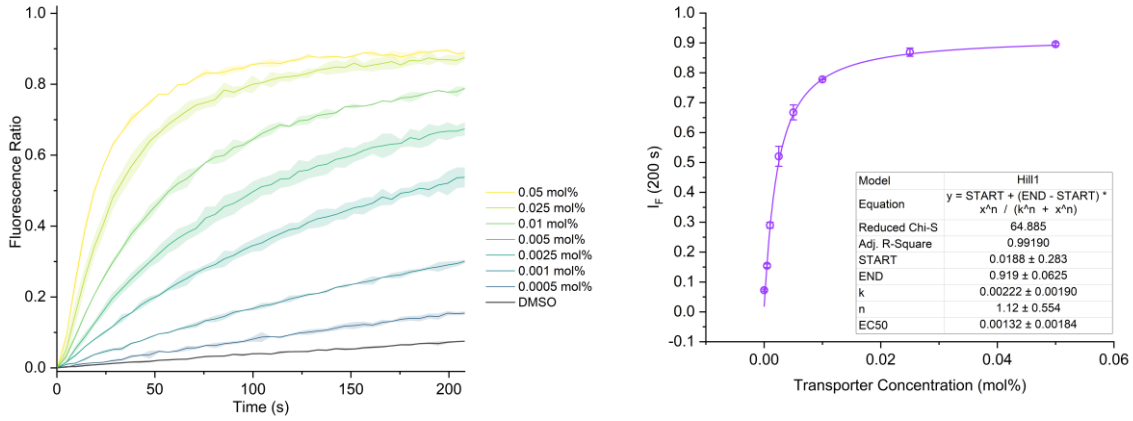

Figure S86. Efflux plot and Hill analysis of H^+/Cl^- symport (or Cl^-/OH^- antiport) facilitated by **4** in the NaCl HPTS assay. Each data point is the average of two repeats, with the error bars showing the standard deviation. A run of pure DMSO was used as a control.

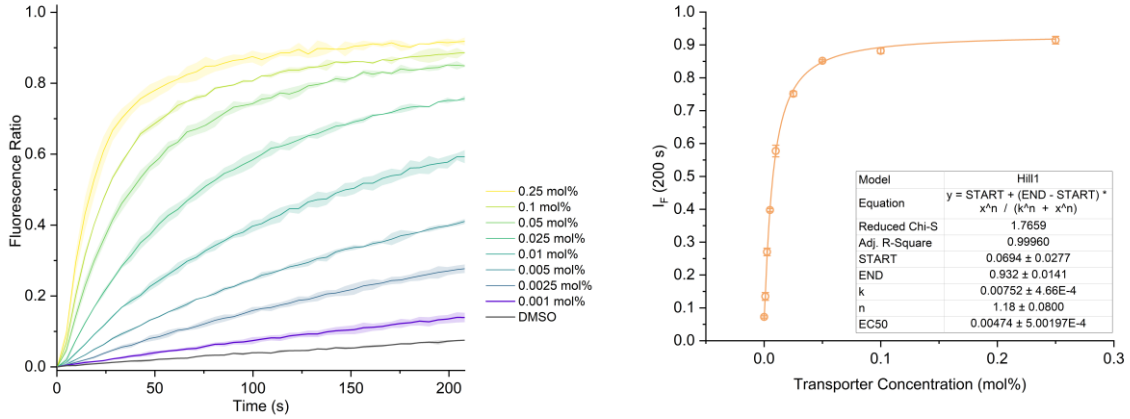

Figure S87. Efflux plot and Hill analysis of H^+/Cl^- symport (or Cl^-/OH^- antiport) facilitated by **5** in the NaCl HPTS assay. Each data point is the average of two repeats, with the error bars showing the standard deviation. A run of pure DMSO was used as a control.

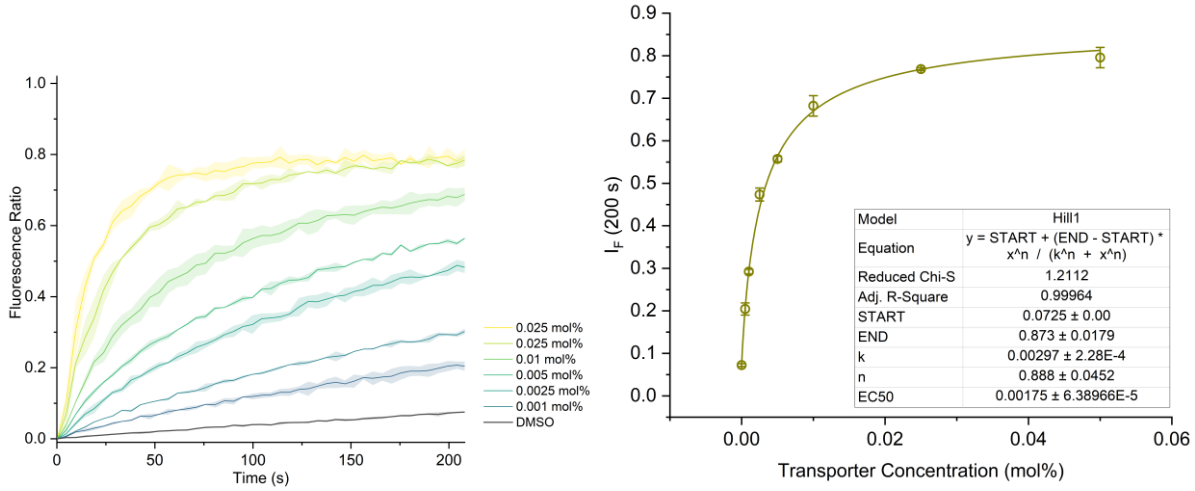

Figure S88. Efflux plot and Hill analysis of H^+/Cl^- symport (or Cl^-/OH^- antiport) facilitated by **6** in the NaCl HPTS assay. Each data point is the average of two repeats, with the error bars showing the standard deviation. A run of pure DMSO was used as a control.

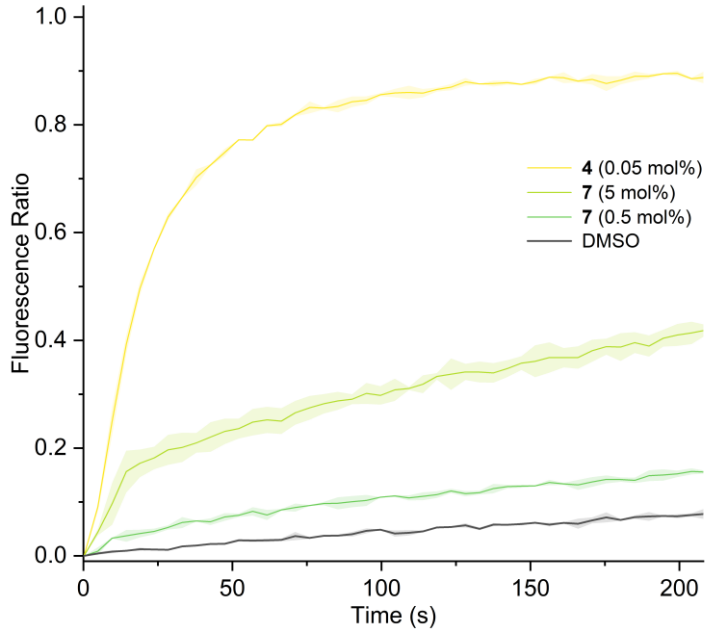

Figure S89. Efflux plot of H^+/Cl^- symport (or Cl^-/OH^- antiport) facilitated by **4** in the NaCl HPTS assay at 0.05 mol% (yellow), **7** at 5 mol% (light green) and 0.5 mol% (dark green). Each data point is the average of two repeats, with the error bars showing the standard deviation. A run of pure DMSO was used as a control.

10. HPTS Assay BSA Mechanistic Studies

An external solution of KCl (100 mM) was prepared and adjusted to pH 7.0 using HEPES buffer (10 mM). An internal solution was prepared using the same external solution with the addition of the pH-sensitive fluorescent dye HPTS (1 mM). Lipids were prepared following the procedure outlined above. After extrusion, they were passed through a G-25 Sephadex® column pre-rinsed with the external KCl solution. The vesicles were collected and diluted with the external solution to a 10 mL volume with a known concentration.

Untreated vesicle experiments were conducted by diluting the vesicle suspension with an additional external solution to afford a 0.1 mM concentration in 2.5 mL. An aliquot of the aqueous NaOH solution (25 μL, 0.5 M) was added at approximately t = −30 s before the experiment was initiated with the addition of the transporter DMSO solution (5 μL). The concentration of the transporter was determined by the EC50 calculated using the HPTS NaCl assay. Detergent (Triton X-100 (10% v/v in water), 25 μL) was added at t = 210 s to lyse the vesicles, and a final reading was recorded at t = 300 s to signify 100% proton efflux.

Fatty acid-free vesicles were produced by stirring a portion of the vesicle-suspended solution for 30 min in the presence of 1 mol% bovine serum albumin (BSA), which sequestered the

membrane-embedded fatty acids. The experimental procedure continued with the description outlined above for the untreated vesicles. Finally, a known quantity of fatty acids was added to the BSA-treated vesicles as an oleic acid solution (10 mol%) 5 min prior to the remaining set of experiments. A DMSO blank run was also performed, and experiments were repeated in duplicate.

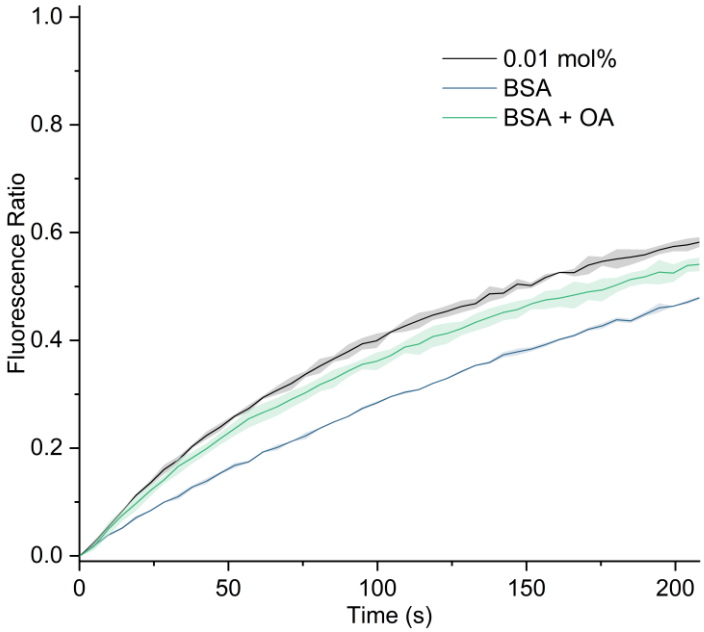

Figure S90. HPTS KCl base pulse assay for **1** (0.01 mol%) in untreated vesicles (black), in vesicles treated with BSA (blue), and in BSA-treated vesicles after the addition of OA (green). Each data point is the average of two repeats, with the error bars showing the standard deviation.

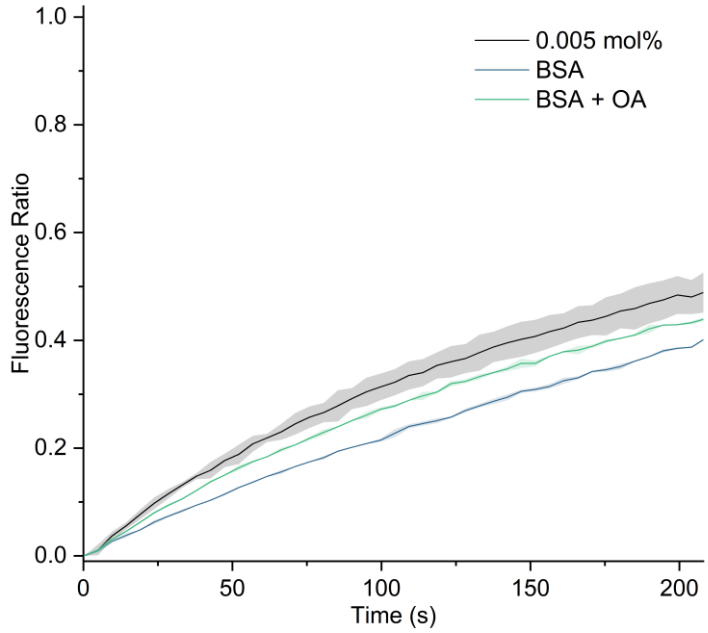

Figure S91. HPTS KCl base pulse assay for **2** (0.005 mol%) in untreated vesicles (black), in vesicles treated with BSA (blue), and in BSA-treated vesicles after the addition of OA (green). Each data point is the average of two repeats, with the error bars showing the standard deviation.

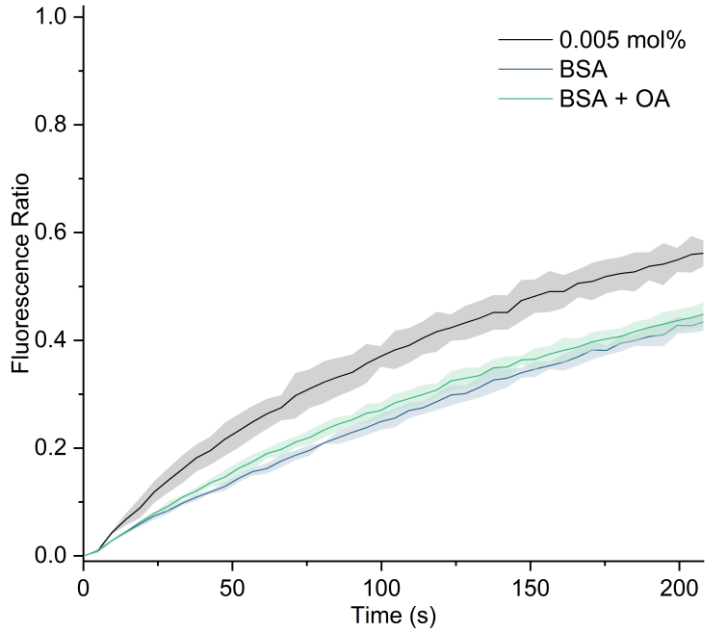

Figure S92. HPTS KCl base pulse assay for **3** (0.005 mol%) in untreated vesicles (black), in vesicles treated with BSA (blue), and in BSA-treated vesicles after the addition of OA (green). Each data point is the average of two repeats, with the error bars showing the standard deviation.

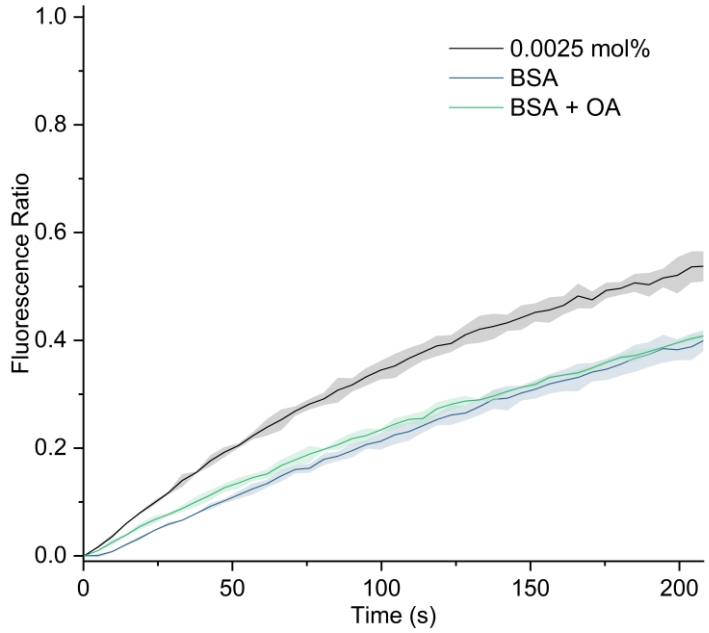

Figure S93. HPTS KCl base pulse assay for **4** (0.0025 mol%) in untreated vesicles (black), in vesicles treated with BSA (blue), and in BSA-treated vesicles after the addition of OA (green). Each data point is the average of two repeats, with the error bars showing the standard deviation.

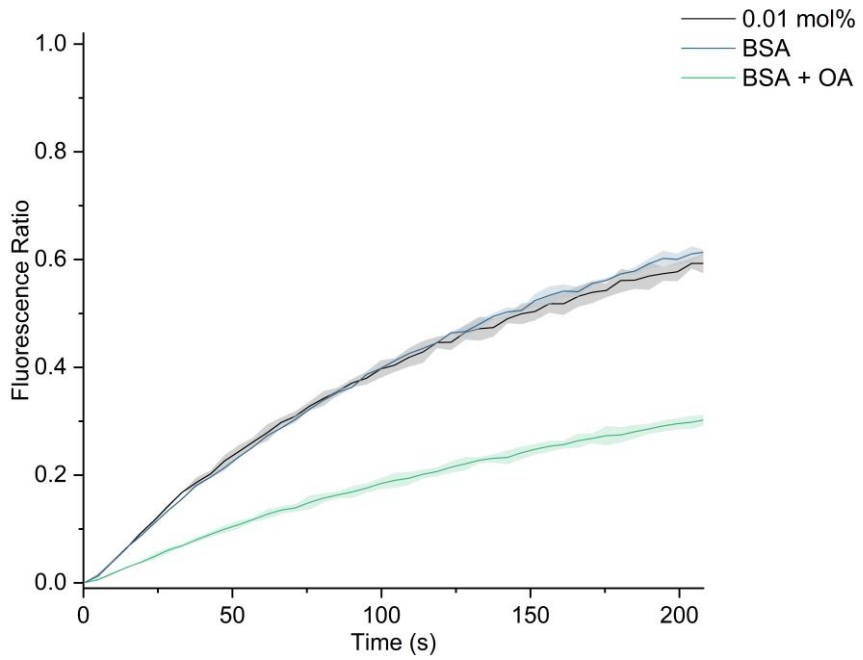

Figure S94. HPTS KCl base pulse assay for **5** (0.01 mol%) in untreated vesicles (black), in vesicles treated with BSA (blue), and in BSA-treated vesicles after the addition of OA (green). Each data point is the average of two repeats, with the error bars showing the standard deviation.

11. HPTS Anion Selectivity Assay

Vesicles were prepared via the method described above with an internal solution of NaCl (100 mM) and HPTS (1 mM), buffered with HEPES (10 mM) and adjusted to pH 7.0. Six separate external solutions were made in an isotonic HEPES buffer containing NaCl, NaBr, NaI, $NaNO_3$ or $NaClO_4$, respectively (All at a concentration of 100 mM).[9] After extrusion, vesicles were eluted through a G-25 Sephadex® size-exclusion column pre-rinsed with the NaCl external solution, which was also used as the eluent. To a 4.5 mL plastic cuvette, and during each experiment, a vesicle suspension was made by diluting it with the chosen external solution (0.1 mM, 2.5 mL). Anion exchange was initiated by adding the transporters as a DMSO solution (5 μL) at a concentration higher than the EC_{50} value determined in the NaCl HPTS assay. Note that NaI contained elemental iodine impurities, which may act as a transporter for I^-. To account for this, rather than waiting approx. 30 s for system equilibration; if the fluorescence ratios became too different, the transporter was added immediately.

Conversion from I_F to ΔpH was performed using the equation:

$$y = \log\frac{ax - b}{c - x}$$

$$\text{where } x = \frac{I_{460}}{I_{403}}, \qquad y = \text{pH}$$

Equation S10. Conversion from intensity ratios into pH.

A DMSO control run was also performed, and experiments were repeated in duplicate for accuracy and data redundancy.

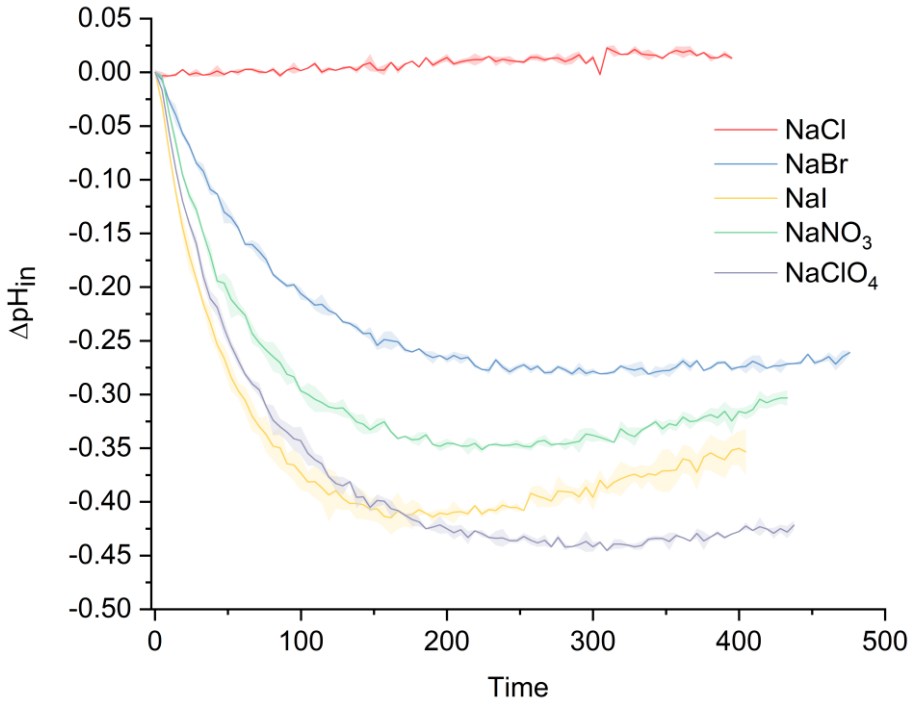

Figure S95. The pH gradient assay for **3** (0.01 mol%, added at t = 0 s). Initial conditions: In: NaCl (100 mM), HPTS (1 mM), HEPES (10 mM), pH 7.0; Out: NaX (100 mM), HEPES (10 mM), pH 7.0. [POPC] = 0.1 mM, [DMSO] = 5 μL. Errors bars (shaded area) represent standard deviations from two runs.

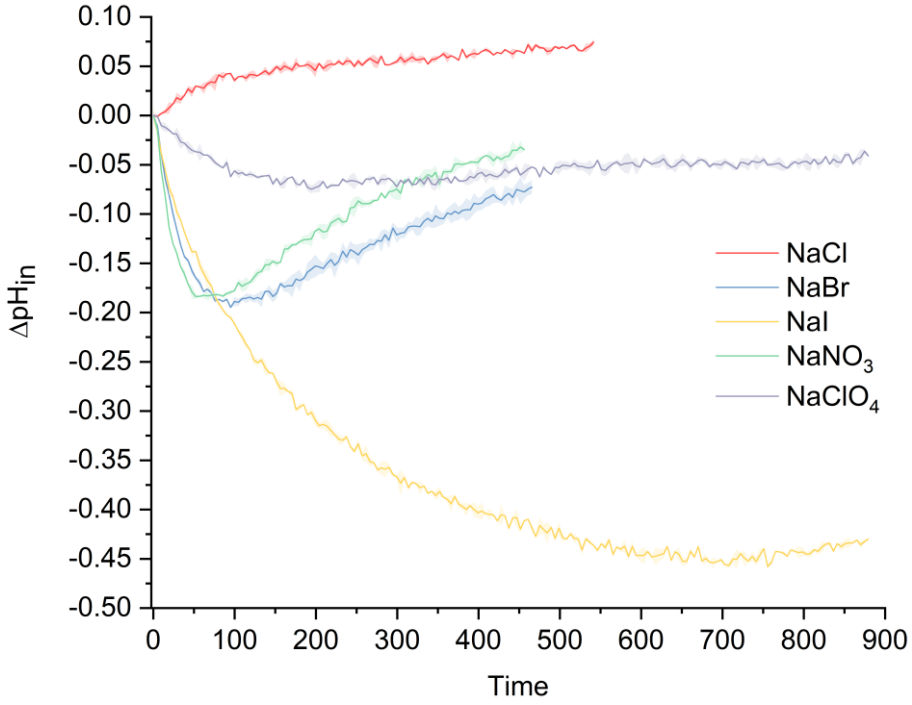

Figure S96. The pH gradient assay for **4** (0.01 mol%, added at *t* = 0 s). Initial conditions: In: NaCl (100 mM), HPTS (1 mM), HEPES (10 mM), pH 7.0; Out: NaX (100 mM), HEPES (10 mM), pH 7.0. [POPC] = 0.1 mM, [DMSO] = 5 μL. Errors bars (shaded area) represent standard deviations from two runs.

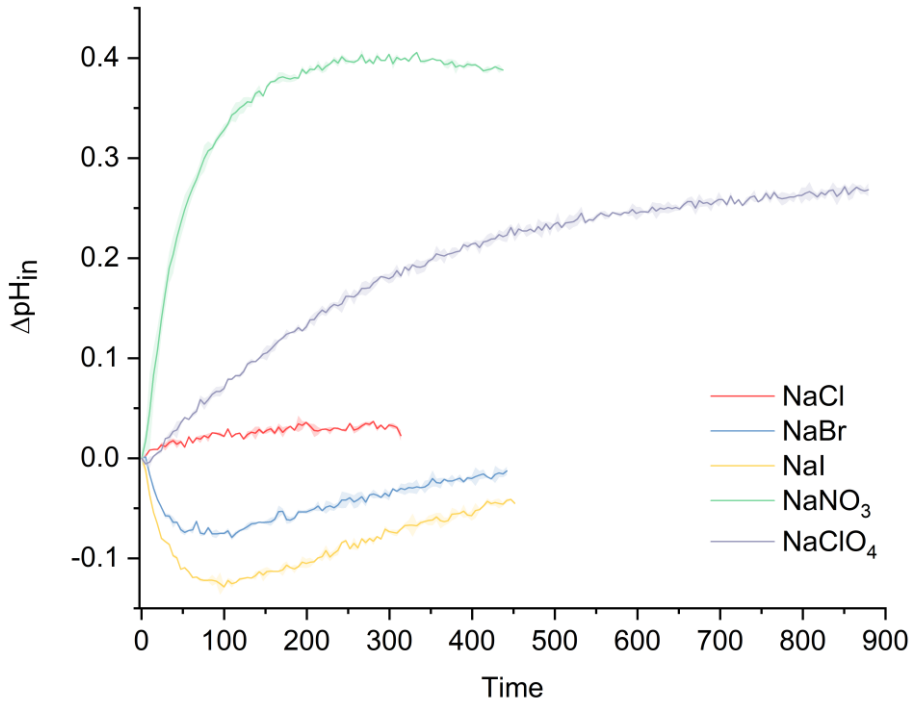

Figure S97. The pH gradient assay for **5** (0.025 mol%, added at *t* = 0 s). Initial conditions: In: NaCl (100 mM), HPTS (1 mM), HEPES (10 mM), pH 7.0; Out: NaX (100 mM), HEPES (10 mM), pH 7.0. [POPC] = 0.1 mM, [DMSO] = 5 μL. Errors bars (shaded area) represent standard deviations from two runs.

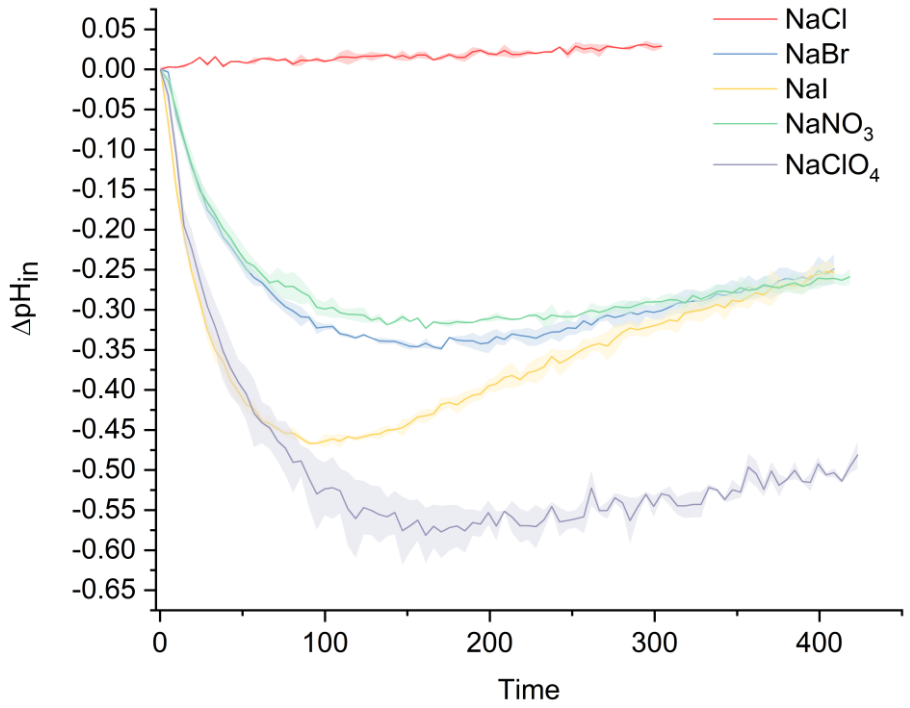

Figure S98. The pH gradient assay for **6** (0.01mol%, added at *t* = 0 s). Initial conditions: In: NaCl (100 mM), HPTS (1 mM), HEPES (10 mM), pH 7.0; Out: NaX (100 mM), HEPES (10 mM), pH 7.0. [POPC] = 0.1 mM, [DMSO] = 5 μL. Errors bars (shaded area) represent standard deviations from two runs.

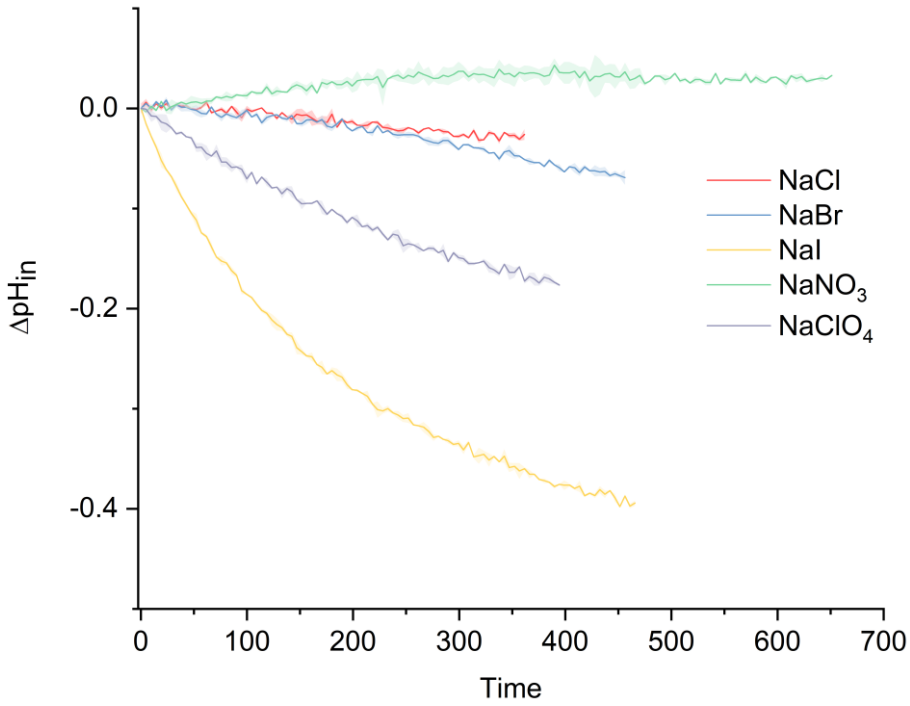

Figure S99. The pH gradient assay for the DMSO control. Initial conditions: In: NaCl (100 mM), HPTS (1 mM), HEPES (10 mM), pH 7.0; Out: NaX (100 mM), HEPES (10 mM), pH 7.0. [POPC] = 0.1 mM, [DMSO] = 5 µL. Errors bars (shaded area) represent standard deviations from two runs.

12. HPTS Carrier Mechanism Assay: DPPC Vesicles

Whether an anionophore transports cargo via channel formation or a carrier mechanism can be determined by repeating the HPTS NaCl assay using vesicles made of 1,2-dipalmitoyl-*sn*-glycero-3-phosphocholine (DPPC). DPPC has a phase transition temperature of 41 °C, whereas the phase transition temperature of POPC is -2 °C. Below this temperature, the arrangement of phospholipids in the vesicles is more ordered, and the fatty acid tails are more rigid (gel phase). Above this temperature, the lipid bilayer enters a less ordered phase (fluid), characterised by greater permeability. Transport experiments are conducted at 25 °C and 45 °C. Channels are not affected by the greater rigidity of the lipid bilayer at lower temperatures, whereas the function of a mobile carrier should be diminished. A significant difference in transport activity at the two temperatures indicates that the compound operates via a carrier mechanism.

A weight amount of DPPC (60 mg) was dissolved in 2 mL of chloroform (39 mM and transferred to a pre-weighed round-bottom flask. The solvent was removed using a rotary evaporator. The pressure was lowered slowly to ensure the formation of a smooth lipid film. Subsequently, the film was dried in vacuo for 4–24 h, and the mass of lipid was recorded.

The lipids were rehydrated with 2 mL of internal solution (NaCl: 100mM, HEPES: 10 mM, HPTS: 1 mM), sonicated for 5 min and then heated to 50 °C with stirring for 30 min until all lipids were removed from the sides of the flask and were suspended in solution. The lipids were subjected to 9 freeze-thaw cycles by freezing using a liquid nitrogen bath and thawing in 50 °C water to bring the vesicles back above the lipid phase transition temperature. Following this, the vesicles were left to rest at room temperature for 30 min. The lipids were extruded through a 200 nm polycarbonate membrane 25 times to form monodisperse vesicles. This was also conducted at 50 °C by wrapping the extrusion frame with tinfoil onto a hotplate. Only 1 mL of solution was extruded at a time before being collected. Finally, any residual unencapsulated salt from the internal solution was removed through size-exclusion using a B19 column packed with hydrated G-25 Sephadex®, pre-saturated with the respective external solution. The lipid suspensions were diluted with the external solution to afford a stock solution (10 mL) of a known concentration.

For a given experiment, the prepared vesicles were diluted to a concentration of 0.1 mM in a 2.5 mL plastic cuvette. An aliquot of aqueous NaOH solution (25 μL, 0.5 M) was added at approximately $t = -30$ s to increase the pH of the external solution by approx. one pH unit to pH 8.0. Transport was initiated with the addition of the transporter as a DMSO solution (5 μL) and ended with the addition of detergent (Triton X-100 (10% v/v in water), 25 μL) was added at $t = 210$ s to lyse the vesicles, and a final fluorescence intensity reading was recorded at $t = 300$ s to signify 100% proton efflux. The changes in the fluorescent activity of intravesicular HPTS were tracked and converted to fractional fluorescence intensity using **equations S8** and **S9**. The experiments were conducted at 25 °C and then repeated at 45 °C.

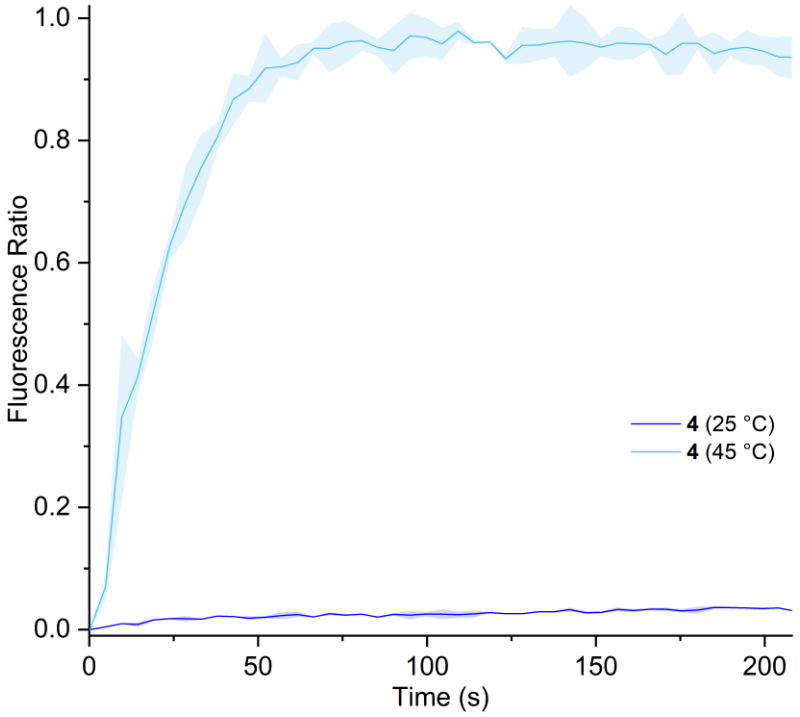

Figure S100. Efflux plot for the temperature-dependent DPPC vesicle assay for compound **4** (0.05 mol%). Experiments were conducted at 25 °C (purple) and 45 °C (blue). Each data point is the average of two repeats, with the error bars showing the standard deviation.

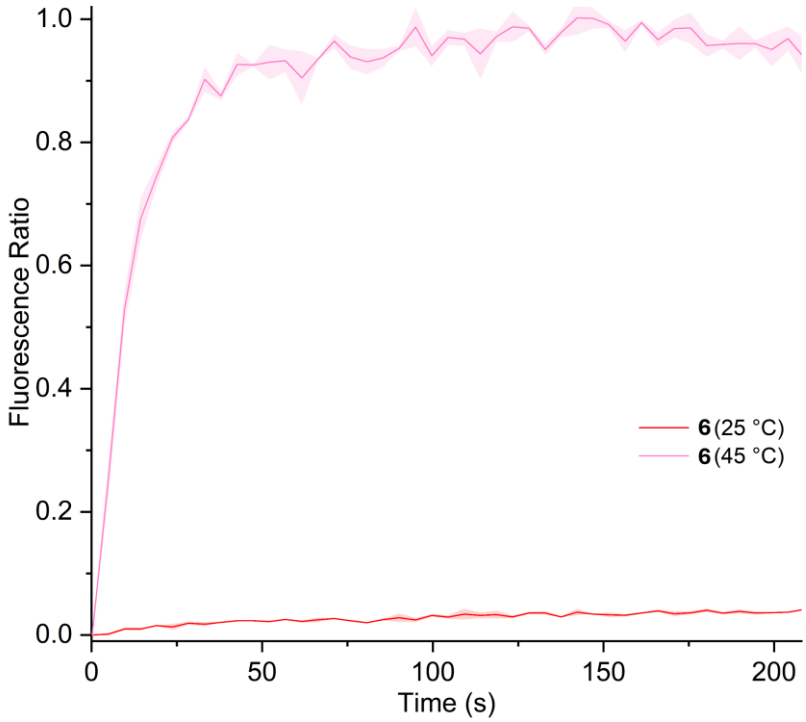

Figure S101. Efflux plot for the temperature-dependent DPPC vesicle assay for compound **6** (0.05 mol%). Experiments were conducted at 25 °C (red) and 45 °C (pink). Each data point is the average of two repeats, with the error bars showing the standard deviation.

A significant change in transport activity is seen for both compounds above and below the lipid phase transition temperature of DPPC. This indicates that Cl^- transport is facilitated by a carrier mechanism.

13. MTS Cell Viability Assay

Human MDA-MB-231 breast cancer cells and A549 pulmonary epithelial cells (ATCC) were cultured in Dulbecco's Modified Eagle Medium containing 1% (v/v) penicillin/streptomycin (Merck, Darmstadt, Germany) and 10% (v/v) foetal bovine serum (Thermo Fisher Scientific, Waltham, MA, USA). Cells were cultured at 37 °C in a humidified atmosphere of 5% CO_2 and harvested at 80–90% confluency using trypsin/EDTA after washing with Dulbecco's phosphate-buffered saline (dPBS, Merck). Test compounds were administered to cells using a DMSO vehicle (to a final concentration containing 1% DMSO v/v) and were compared against cells treated with DMSO alone (vehicle-only control).

The effects of compounds **1**–**7** on cell viability were examined using an MTS assay. MDA-MB-231 cells were seeded in triplicate in 96-well plates (density of 3.5 x 10^3 cells per well) in complete media and incubated for 24 h. Separately, various concentrations of the compounds to be tested were prepared in complete media (5 µL of compound in DMSO to 995 µL of media, 200–10 µM). After removing the well media, the cells were treated with DMSO:media solutions and incubated for an additional 72 h. Subsequently, the DMSO:media solutions were replaced with untreated media and incubated with CellTiter MTS 96 Aqueous MTS Reagent Powder (Promega) and phenazine ethosulfate (Sigma Aldrich) under dark conditions for approx. 3 h. Cell viability was measured by monitoring the conversion of MTS to formazan via dehydrogenase enzymes in metabolically active cells. The absorbance at 490 nm (the absorbance wavelength of formazan) for each well was measured using a Tecan Infinite M1000 Pro plate reader (CellTiter 96 Aqueous Non-Radioactive Cell Proliferation Assay, Promega). The procedure was repeated three times to give a total of nine readings for each concentration. Compound **3** was excluded from testing due to poor solubility issues in the DMSO:media solutions. Likewise, compound **5** was not tested at 200 µM. Compound **6** acted as a positive control, as its cytotoxic properties have previously been reported.[10] Compound **7** served as a negative control. The assay was repeated under the same conditions to examine the cell viability of A549 cells.

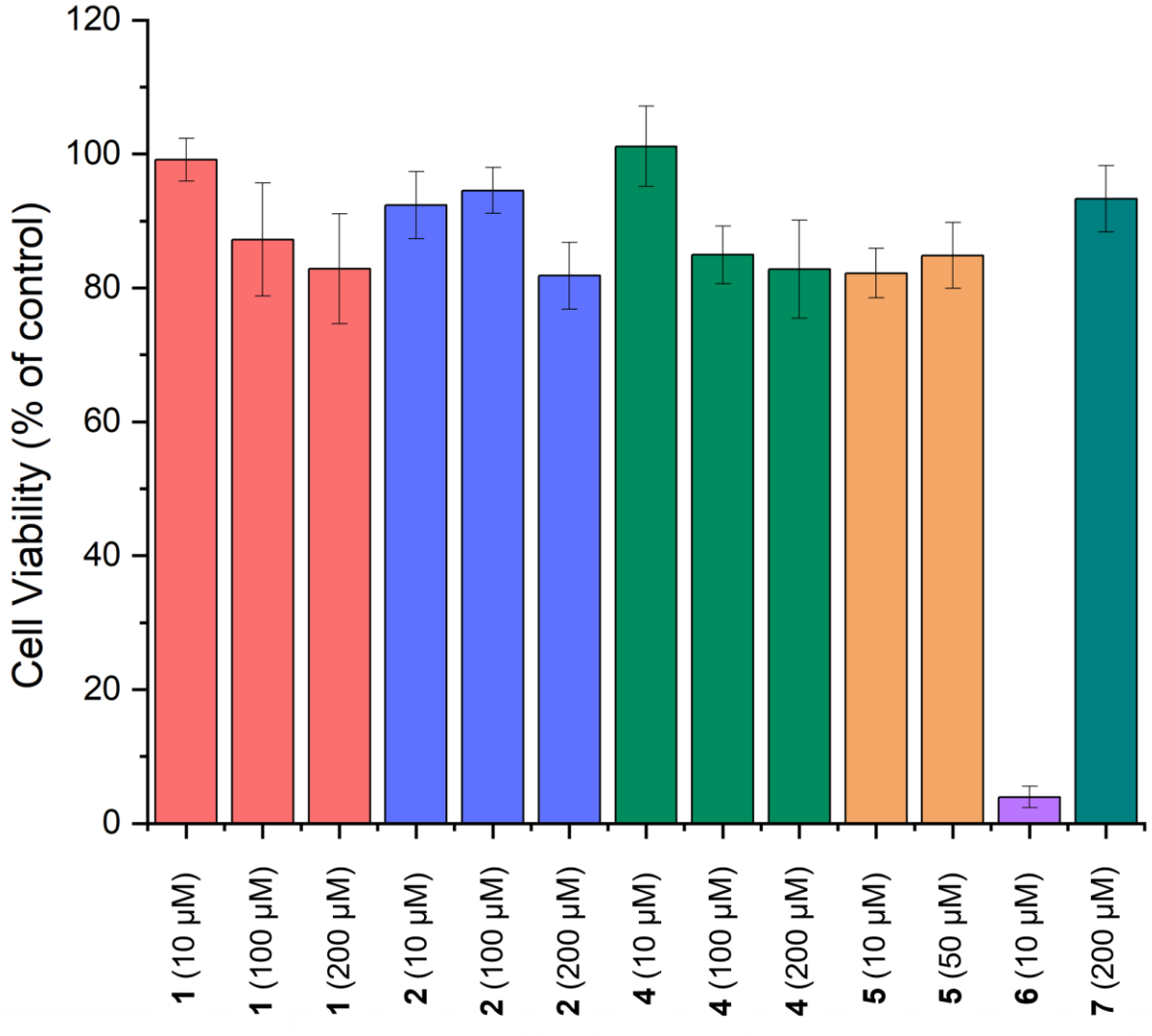

Figure S102. The % of viable MDA-MB-231 cells as a function of formazan absorbance (λ_{abs} = 490 nm) in the MTS assay after treatment with compounds **1**–**7** for 72 h. Results were repeated in triplicate across three 96-well plates, with error bars representing the SEM (Standard error of the mean) of the readings. Data normalised to DMSO vehicle control.

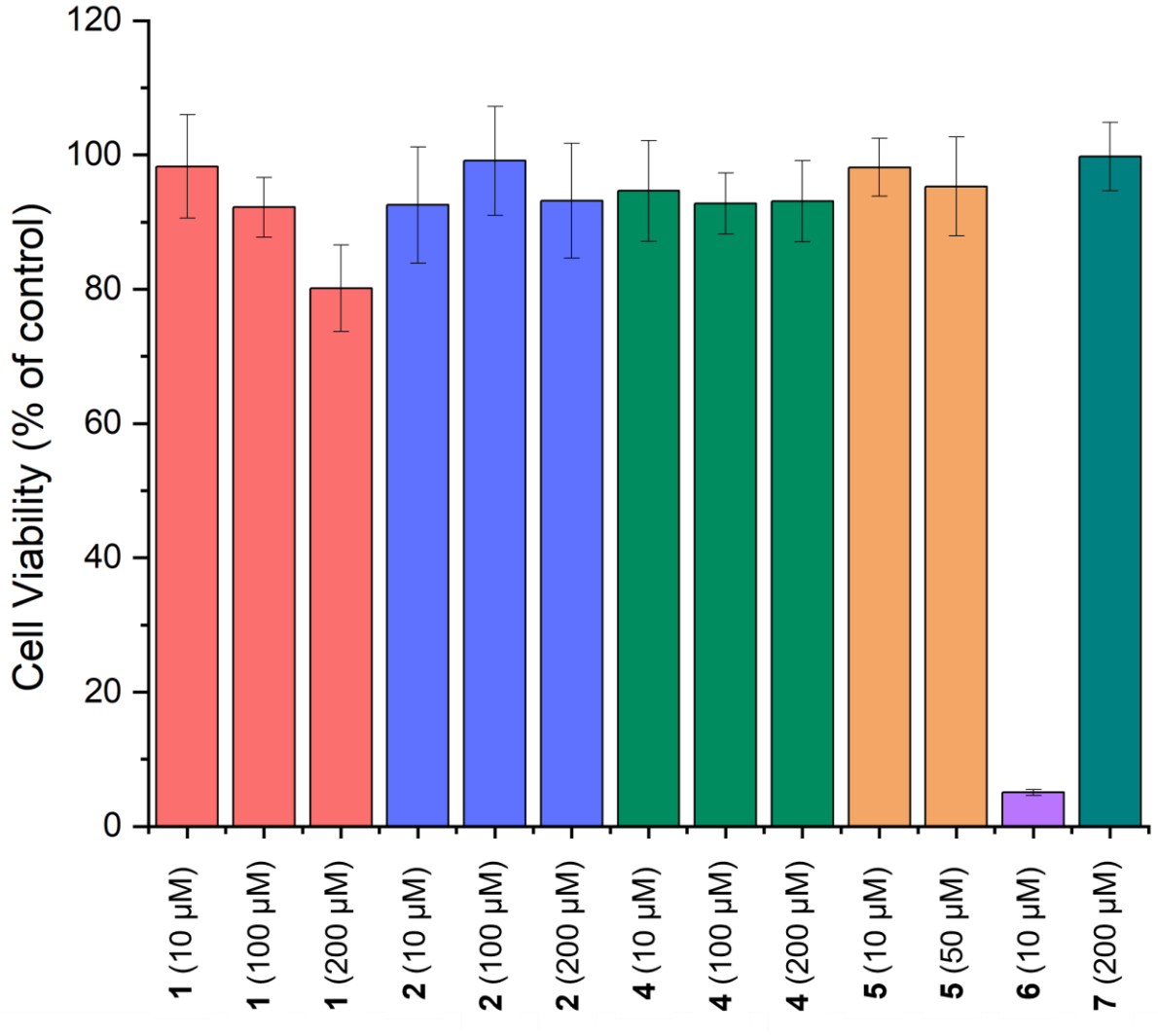

Figure S103. The % of viable A549 cells as a function of formazan absorbance (λ_{abs} = 490 nm) in the MTS assay after treatment with compounds **1**–**7** for 72 h. Results were repeated in triplicate across three 96-well plates, with error bars representing the SEM of the readings. Data normalised to DMSO vehicle control.

12. References

1. M. Arimura, K. Tanaka, M. Kanda, K. Urushibara, S. Fujii, K. Katagiri, I. Azumaya, H. Kagechika, and A. Tanatani, *ChemPlusChem*, 2021, **86**, 198.
2. R. S. Muthyala, G. Subramaniam and L. Todaro, *Org. Lett.*, 2004, **6**, 4663-4665.
3. L. M. Jackman and S. Sternhell, Applications of Nuclear Magnetic Resonance Spectroscopy in Organic Chemistry, 2nd ed.; *Pergamon Press*: Oxford, UK, 1969.
4. (*a*) D. B. Hibbert and P. Thordarson, *Chem. Commun.*, 2016, **52**, 12792–12805; (*b*) http://supramolecular.org.
5. I. V.Tetko and V. Y.Tanchuk, ALOGPS 2.1 (http://www.vcclab.org) is a Free on-line Program to Predict logP and logS of Chemical Compounds.
6. I. V. Tetko and V. Y. Tanchuk, *J. Chem. Inf. Comput. Sci.*, 2002, **42**, 1136-1145.
7. L. A. Jowett and P. A. Gale, *Supramol. Chem.*, 2019, **31** (5), 297-312.
8. A. M. Gilchrist, P. Wang, I. Carreira-Barral, D. Alonso-Carrillo, X. Wu, R. Quesada and P. A. Gale, *Supramol. Chem.*, 2021, **33** (7), 325-344.
9. X. Wu and P. A. Gale, *Chem. Commun.*, 2021, **57**, 3979-3982.
10. N. Busschaert, S. Park, K. Baek, Y. P. Choi, J. Park, E. N. W. Howe, J. R. Hiscock, L. E. Karagiannidis, I. Marques, V. Félix, W. Namkung, J. L. Sessler, P. A. Gale and I. Shin, *Nat. Chem.*, 2017, **9**, 667-675.